CARBOTHERMIC REDUCTION OF COMPLEX SULPHIDES

BY

UWAGBOE OSAMEDE IGIEHON

A thesis submitted for the degree of Doctor of Philosophy of the University of London and for the Diploma of Imperial College

Department of Materials,
Royal School of Mines,
Imperial College of Science,
Technology and Medicine

NOVEMBER 1989

ABSTRACT

The carbothermic reduction of antimony sulphides, iron-arsenic-, copper-arsenic- and copper-antimony sulphides has been carried out using graphite/collie coal and lime as reducing and exchange agents respectively. Significant reactions involved during the carbothermic reduction of lead and zinc sulphides were also investigated.

The reduction mechanisms were determined by analysis of rate data and X-ray diffraction results. Optical and scanning electron microscopy were used to determine the morphology of the reaction products and to characterise the conditions necessary for the efficient production of metallic species from natural concentrates.

Complete reduction of antimony sulphide (Sb_2S_3) with collie coal was attained after 30 minutes reaction at 700^{o}C forming liquid antimony (Sb) and calcium sulphide (CaS). The presence of the calcium antimonate ($Ca_2Sb_2O_5$) intermediate compound during the graphite reduction of Sb_2S_3 indicates that the rate of graphite carbothermic reduction is controlled by the carbon reduction of the intermediate oxide phase. The collie coal reduction proceeds at a much faster rate and is not controlled by the carbon reduction of the oxide intermediate.

Activation energies of 114 KJ mol^{-1} and 94 KJ mol^{-1} were determined for the coal reduction of Sb_2S_3 and Sb_2O_3 respectively. The formation of droplets of liquid antimony on the pellet surface as a result of carbothermic reduction of Sb_2S_3 at 700^{o}C is unique and enhances the effective separation and recovery of antimony from the reaction product.

Carbothermic reduction of natural and synthesised arsenopyrite (FeAsS) with collie coal occurs rapidly in the temperature range 800^{o}-1000^{o}C resulting in the formation of stable iron arsenides (Fe_2As, FeAs, $FeAs_2$) and calcium sulphide (CaS). Reduction is incomplete at 800^{o}C. Complete reduction of synthetic FeAsS is attained after 45 minutes reaction at 1000^{o}C. Iron-calcium oxysulphide [(1.33) CaS.FeO] is present in the reaction product when reduction is incomplete.

The lime-enhanced carbothermic reduction of synthesised enargite (Cu_3AsS_4) and tennantite ($Cu_{12}As_4S_{13}$) results in the formation of the stable copper arsenide (Cu_3As) and metallic copper (Cu). Reduction is complete after 40 minutes reaction at 1000°C; and incomplete at lower temperatures. $Cu_{12}As_4S_{13}$ reduction proceeds at a more rapid rate than Cu_3AsS_4 reduction. The lattice parameter of the metallic copper phase obtained by carbothermic reduction of the complex copper-arsenic sulphides is 3.641A° indicating a dissolution of 7.8 wt % As in the metallic copper product. This represents the maximum level of arsenic solubility in copper.

The complete reduction of synthesised famatinite (Cu_3SbS_4) and tetrahedrite ($Cu_{12}Sb_4S_{13}$) with collie coal requires 45 minutes reaction at 1000°C with the formation of copper antimonides (Cu_2Sb, $Cu_{4.5}Sb$) and calcium sulphide (CaS) as the reaction products. $Ca_2Sb_2O_5$ is present in the incomplete reaction products.

The greater affinity of antimony for copper and of arsenic for iron evident in the selective formation of copper antimonide and iron arsenide during the carbothermic reduction of a complex tetrahedrite concentrate (containing $[Cu, Fe]_{12}As_4S_{13}$ and Cu_3SbS_4 as the major phases), could be significant with regard to the separation of the various metallic species present in complex sulphide systems.

In all cases, the carbothermic reduction of the various iron-arsenic-, copper-arsenic- and copper-antimony- complex sulphides were found to be much more rapid than the reduction of the corresponding single phase iron and copper sulphides. These observations have been explained in terms of the favourable thermodynamic effects resulting from the formation of stable intermetallic compounds and the increased reaction surface area arising from the formation of liquid oxysulphide (intermediate) phases.

A limited number of experiments were carried out on the carbothermic reduction of zinc and lead sulphides. The diffraction pattern of the zinc calcium oxysulphide (ZnCaOS) compound has been determined and an idealised crystallographic structure (simple hexagonal) is presented.

Established thermodynamic relationships and experimental observations indicate that the carbothermic reduction of lead sulphide (PbS) proceeds via a mechanism involving the formation of basic lead sulphates. Direct production of lead by the lime-exchange reaction of lead sulphide has also been observed. It is suggested that further investigations be conducted to establish the conditions necessary for the formation of lead (Pb) and calcium sulphate ($CaSO_4$) by reaction of lead suphide and lime, without generating SO_2.

ACKNOWLEDGEMENTS

I wish to express my sincere gratitude to my supervisors Professor P. Grieveson and Dr. B.S. Terry for their constant encouragement and support throughout this study.

I would like to thank Mr. R. Sweeney, Mr. G. Hicks, Mr. J. Wright, Mr. M. Haddon, Mr. N. Salpadoru and Mr. J. Tipple for their technical assistance. I am particularly grateful to Mrs. G. Hopkins for her patience and care in typing the thesis and to Ms. R. O'Driscoll for the excellent production of the photographic plates.

My thanks are also due to Dr. A. Jha, Dr. A. Chrysanthou, Dr. D. Azubike, Dr. N. Machingawuta, R. Asjadi, M. Lee, Ms.S. De Souza and other members of the group for their continual friendship and stimulating discussions.

Finally, I am indebted to my family to whom I owe so much.

CONTENTS

LIST OF FIGURES

LIST OF TABLES

LIST OF PLATES

CHAPTER 1

INTRODUCTION

CHAPTER 1

INTRODUCTION

Conventional methods of pyrometallurgical sulphide smelting involve roasting and reduction processes during which large quantities of sulphur dioxide is emitted. These processes are coming under increasing threat due to the environmental problems created by the emission of toxic sulphur-bearing gases. Thus the development of a single-stage process which does not produce toxic sulphurous gases is of great industrial and environmental importance.

The single-stage carbothermic reduction of metal sulphides can be represented as:

$$2MS_{(s)} + C_{(gr)} = 2M_{(s)} + (CS_2)_{(g)} \qquad 1.1$$

For all sulphide compounds the thermodynamics of this reaction are unfavourable. The use of a basic oxide as sulphur sink splits the chemical equilibrium represented by equation 1.1 into two steps - the **exchange reaction** during which S^{2-} ions of the metal sulphide, **(MS)**, are exchanged with O^{2-} ions of the basic oxide **(XO)**; and the reduction step during which the metal oxide **(MO)** is reduced to metal **(M)**. These two steps can be represented as:

(i) **Exchange reaction** $MS_{(s)} + XO_{(s)} = MO_{(s)} + XS_{(s)}$ 1.2

(ii) **Reduction reaction** $MO_{(s)} + C_{(gr)} = M_{(s)} + (Co)_{(g)}$ 1.3

Carbon and lime are relatively cheap and readily available raw materials making them suitable choices as reducing and sulphide exchange agents in the direct reduction process.

Thus the development of a single stage carbothermic reduction process as an alternative to conventional roast-reduction sulphide smelting

techniques is desirable for the following reasons:

(i) Sulphur is tied up as calcium sulphide (CaS) preventing the emission of sulphur dioxide (SO_2) and eliminating the environmental threat. The calcium sulphide formed can be processed to produce H_2SO_4 or elemental sulphur.

(ii) Lime (exchange agent) and carbon (reducing agent) are relatively cheap and readily available.

(iii) The process possesses great potentials for the recovery of metallic species from complex sulphide minerals.

(iv) It is a single-stage process.

A scheme for the processing of sulphide concentrates by lime-enhanced carbon reduction would consist of three main steps:

a) lime-enhanced reduction by carbon (in the form of coal).

b) separation of the product metal from the slag [CaS + unreacted CaO] by mechanical separation, magnetic/gravity concentration or floatation techniques

c) melting and refining of the metal phase.

Complex sulphide minerals represent important resources of non-ferrous and precious metals. Their peculiar mineralogical associations present difficult problems during metallurgical processing. The presence of minor minerals, the economic importance of which could be significant in terms of their precious metal [gold, silver] content and their impact on metallurgical processing or on the environment [presence of arsenic, antimony, bismuth, mercury, cadmium etc.], are very important considerations in the development of complex sulphide extraction processes.

Minerals rich in gold and silver frequently contain antimony and arsenic as impurities. Gold commonly occurs in arsenous minerals, whereas silver is usually associated with complex antimonal deposits. Since copper, gold and silver are either chemically bonded to these impurities or finely dispersed in the material, they cannot be separated by beneficiation processes [1]. In addition, these minerals are often found intermingled with other sulphide minerals such as pyrite, pyrrhotite, chalcopyrite, galena, arsenopyrite, enargite and tetrahedrite and separation of the various sulphide phases present is usually extremely difficult.

The method employed in the extraction of a metal from its' sulphide depends on a number of factors, the most important consideration being its' affinity for sulphur . In the simple case where the metal has a low affinity for sulphur, simple thermal decomposition can be used to produce the metal - an example is the production of mercury from cinnabar (HgS). As the affinity of the metal for sulphur increases, and as the sulphide becomes more complex, other processes such as selective oxidation, reduction with another metal (possessing a higher affinity for sulphur), and/or the intermediate transformation of sulphide to sulphate or oxide may be used. The formation of water-soluble sulphates in some processes is usually a prelude to subsequent hydrometallurgical processing.

Arsenopyrite (FeAsS), enargite (Cu_3AsS_4) and tennantite ($Cu_{12}As_4S_{13}$) are the most common arsenic bearing minerals with which gold is frequently encountered. Gold associated with arsenopyrite can be extracted either by roasting and leaching or by roasting and smelting the concentrate. Gold associated with enargite and tennantite is recovered only by roasting and smelting, since cyanide leaching is not feasible for concentrates that contain copper. Antimony contained in minerals that contain antimony species is more difficult to eliminate. This is due to the fact that both sulphidic and oxidic compounds of antimony have much lower vapour pressures than arsenic compounds, and minerals with high antimony contents often have low melting points. A low melting point can result in the sintering of calcines, which hinders further volatilisation. To avoid sintering, the roasting temperature must be restricted, making it

difficult to efficiently remove antimony by applying conventional roasting techniques.

The products of roasting can be readily predicted from the thermodynamic information available in predominance area diagrams. The volatile arsenic and antimony species produced by roasting operations present a serious environmental hazard. In addition, the generation of sulphur dioxide and other toxic gaseous sulphur compounds as well as the operational difficulties involved in carrying out the selective oxidation of the innumerate sulphide phases that may be present in a complex sulphide mineral, necessitates the development of a novel route for the pyrometallurgical processing of sulphide concentrates.

In this project, natural and analoguous synthetic simple and complex sulphides of antimony and arsenic have been reduced at various temperatures, with carbon (graphite and coal) using lime as the sulphide exchange. A detailed study of the various reduction kinetics has been carried out and the reaction products were identified by X-ray diffraction techniques. The morphology of the reaction products was investigated by optical and electron microscopy. The main objectives of the study were to:

i) understand the carbothermic reduction mechanism and,

ii) evaluate the conditions necessary for the complete recovery of valuable metallic species from complex mineral sulphides without creating an environmental hazard.

Neither the separation of metals from reduced pellets nor the details of the disposal of calcium sulphide or its reconversion to calcium oxide (lime) are considered in this investigation .

CHAPTER 2

LITERATURE SURVEY

CHAPTER 2

LITERATURE SURVEY

2.1 Production of Metals from Sulphides

The metal sulphides are one of the most important groups of ore minerals, constituting the raw materials for most of the world's supply of non-ferrous metals. Pure metal sulphides and those synthesised with carefully controlled impurity contents also have important industrial applications. Metal sulphides are dominated by binary and ternary compounds of sulphur with iron, nickel, copper, lead and zinc. These together with the sulphides of manganese, cobalt, molybdenum, antimony, arsenic, bismuth and mercury (although less abundant) are of considerable industrial importance either for their resource value or for their roles as impurities which must be eliminated in order to produce metallic species of high quality.

Conventional complex sulphide smelting usually involves the concentration of the metal in a matte phase and subsequent conversion to crude metal by selective oxidation of the unwanted components of the matte. In recent times, the need to conserve energy and limitations placed on SO_2 emissions by environmental control policies have triggered many new process developments and corresponding efforts to advance the knowledge of sulphide smelting technology. A great deal of complex sulphide smelting involve the processing of copper-iron sulphides such as chalcopyrite ($CuFeS_2$) and Bornite (Cu_5FeS_4). The pyrometallurgical processing of copper sulphide concentrates containing iron usually involve three separate operations:

Roasting

during which sulphur is partially eliminated as SO_2 by partial oxidation of the sulphides at 500-700^{o}C in air.

Matte Smelting

in which the product of roasting is melted with a flux (silica) at about 1200^{o}C forming matte (sulphide phase) - which retains the copper and a liquid slag containing silica, alumina, iron oxides and other metal oxides.

Conversion

whereby the liquid matte containing copper and iron sulphide is oxidised in air; two sequential conversion reactions occur as:

(i) FeS elimination:

$$2FeS + 3O_2 + SiO_2(flux) \rightarrow 2FeO.SiO_2(slag) + 2SO_2 \qquad [2.1]$$

(ii) Blister copper formation:

$$Cu_2S + O_2 \rightarrow 2Cu + SO_2 \qquad [2.2]$$

An important feature of these conversion reactions is the fact that the formation of blister copper does not being until the concentration of FeS in the matte has been reduced to very low levels (~ 1.00%). The roasting and conversion reactions generate great quantities of toxic SO_2, the disposal of which is becoming increasingly difficult. Energy savings may be obtained in these smelting processes by oxygen enrichment of the reaction gases. However, the main effect of this gas enrichment is to increase the quantity of SO_2 generated, thus compounding the environmental problem. Most conventional complex sulphide smelting techniques are based on these (copper sulphide roasting) principles. Flash smelting which involves suspension and reaction of the concentrates in an oxidising gas stream and bath smelting where the concentrates are heated and reacted in contact with the slag/matte melt are the two broad classes of smelting systems currently used to carry out these roast-conversion operations.

Presently, conventional sulphide smelting processes recover SO_2 from flue gases and use this for sulphuric acid production. The revenue derived from the sale of the sulphuric acid by-product is significant in

terms of the operating cost of such processes. Thus, the current over production of sulphuric acid will have an adverse effect on its marketability, and hence on the economics of the overall process.

In nature, minerals rich in precious metals (gold and silver) usually contain antimony and arsenic as impurities. Gold is normally found in arsenous minerals while silver is associated with complex antimonal deposits. In addition, these sulphide minerals frequently contain appreciable quantities of base metals such as copper. The removal of impurities by beneficiation processes is difficult since the precious metals are usually finely disseminated in the mineral while the base metals may be chemically bonded to the impurity phases.

The commercially and metallurgically important complex minerals of arsenic are arsenopyrite (FeAsS), enargite (Cu_3AsS_4) and tennantite ($Cu_{12}As_4S_{13}$) while antimony occurs mainly in tetrahedrite ($Cu_{12}Sb_4S_{13}$). Arsenic is normally removed by conventional oxidising roasting whereas for concentrates rich in antimony, only a low degree of impurity removal is normally attained unless very long roasting times are applied. Both arsenic and antimony have low activities in copper matte and copper metal making it difficult to obtain a high degree of removal during copper smelting and concentration operations. The volatilistion of toxic arsenic and antimony species during the roasting of concentrates that contain these sulphides, constitutes a great hazard to the environment.

Holmstrom [2] has investigated the removal of arsenic by volatilisation roasting from arsenic-bearing sulphide concentrates. The influence of roasting temperature, time, type of arsenic-bearing minerals in the charge and its' initial arsenic content on the extent of arsenic removal was determined. Roasting tests were conducted in a laboratory scale furnace [50g batches] as well as in a pilot plant fluidised bed (20 kg/hr). It was reported that calcines containing between 0.15-0.30 wt% As could be produced from concentrates containing up to 26.0 wt% As in the form of arsenopyrite (FeAsS), enargite (Cu_3AsS_4) and tennantite ($Cu_{12}As_4S_{13}$). The report concluded that to achieve a high degree of arsenic removal, the roasting operation should be carried out above 700^{o}C. The roasting of

concentrates which contain arsenic in the form of metal arsenides produced calcines with high arsenic contents at all the roasting temperatures studied (550-850^{o}C). By comparing the removal rates of arsenic during the roasting of concentrates containing arsenopyrite (FeAsS) with those containing enargite (Cu_3AsS_4) and tennantite ($Cu_{12}As_4S_{13}$), Holstrom [2] reports that the arsenic removal from tennantite/enargite is considerably less rapid. The observed difference in arsenic removal rate is due to a higher transport rate for the gaseous diffusion of arsenic through the porous layer of pyrrhotite ($Fe_{1-x}S$) formed during the roasting of arsenopyrite compared with the solid state diffusion of arsenic and sulphur through the non-porous layer of chalcocite (Cu_2S) formed during the roasting of enargite and tennantite.

The removal of antimony from a tetrahedrite concentrate [25.4 wt% Cu, 21.5 wt% Fe, 20.5 wt% S, 13.8 wt% Sb] by roasting has been investigated by Jokilaakso et al [3]. Their results indicate that the elimination of antimony is not related to the removal of sulphur. Sulphur elimination is favoured by high oxygen concentrations [21-50% O_2] and high temperatures [900-1100^{o}C] whereas the removal of antimony requires low oxygen concentrations in the reaction gas, and as high temperatures as possible.

Chlorine based pyrometallurgical processes possess some advantages over conventional oxidising processes. The main advantage is that metal chlorides are easier to volatilize due to their higher vapour pressures compared with the metal oxides. This property is used to refine molten gold bullion by the injection of chlorine into liquid gold resulting in the chlorination of iron, zinc, lead and other metallic species present. The metal chlorides generated are easily eliminated by volatilisation. Holstrom [4-6] has carried out extensive studies on the removal of antimony, arsenic and bismuth from copper-, silver- and gold-rich concentrates by selective chloridisation roasting. The study determined the influence of roasting temperture, roasting time, gas composition, types of chloridising agent and the chemical composition of the concentrate on the removal of impurities. By roasting at 600^{o}C in an SO_2-rich atmosphere with the addition of calcium chloride, calcines

containing 0.1-0.2 wt% As, < 1.0 wt% Sb and < 0.05 wt% Bi were made from concentrates containing 2.0-5.0 wt% As, 5.0-10.0 wt% Sb and 0.1-0.2 wt% Bi. This study was conducted as part of the development of a process by which impurity rich copper, silver and gold concentrates can be treated to produce clean calcines suitable for smelting in a conventional copper plant. Pilot plant tests of this selective chloridisation process have been carried out in a rotary kiln and in a fluidised bed roaster [6]. The most efficient volatilisation of antimony was achieved in the rotary kiln with the addition of calcium chloride. The commercialisation of such chloridisation processes has been limited by the operational problems associated with corrosion of equipment, formation of liquid chlorides and the regeneration of chlorine .

The vacuum refinement of copper matte contaminated with arsenic, antimony and bismuth has been studied by several workers [7-10]. The copper content in the matte should be lower than 65.0 wt%, otherwise the activity of the impurities will be too low resulting in poor levels of elimination. No industrial application of the vacuum treatment of matte has so far been reported.

Hydrometallurgical processes that remove antimony from copper concentrates containing tetrahedrite have been developed [11,12]. The concentrates are leached in highly alkaline solutions producing leach residues with compositions similar to that of clean high-grade copper concentrates. The operation of such leach processes has been hampered by high operating costs which has led to severe economic problems in some plants.

Antimony and arsenic (to a less extent) are sometimes the main focus of the processing of sulphide concentrates. Important antimony-bearing minerals with high commercial and metallurgical importance include tetrahedrite, stibnite, bournonite, boulangerite, jamesonite and pyroargyrite. In table 2.1, the chemical formulae, melting points and major sources of important antimony bearing minerals have been listed.

World reserves of antimony are estimated at over 4.6 million tons, approximately 80% of which is located in Bolivia, China, Mexico, South

Mineral	Chemical Formula	Melting point (°C)	Mining Countries	Extracted Metals
Pyroagyrite	Ag_3SbS_3	485	Canada, Peru	Ag
Tetrahedrite	$Cu_{12}Sb_4S_{13}$	588	Canada, Peru	Cu, Ag
Bournonite	$CuPbSSbS_3$		Peru	Cu
Jamesonite	$FePb_4Sb_6S_{11}$		China, Mexico	Pb, Sb
Boulangerite	$Pb_5Sb_4S_{11}$	580	Mexico, Peru	Pb, Sb
Stibnite	Sb_2S_3	556	China, Bolivia, South Africa	Sb, Au
Bertierite	$FeSb_2S_4$	563	*	
Gudmundite	FeSbS	620		

* usually combined with other antimony bearing minerals

TABLE 2.1

Chemical Composition of Some Important Antimony Bearing Minerals [5]

	%
metal products	14
flame retardants	64
ceramic and glass	10
plastics	9
others	3

TABLE 2.2

Antimony End Use Pattern (USA), 1984 [14]

Africa, Thailand and the U.S.S.R., the largest reserves being located in China [13]. Besides antimony, silver and copper are produced from pyroargyrite and tetrahedrite whereas jamesonite and boulangerite are mainly used for the production of antimonal lead. Gold is often found in stibnite ores.

Antimony is commonly alloyed with lead to increase its strength for use in accumulator plates, sheets and pipes. It is also an important alloying element in bearing metals. The flame retardant properties of the oxide (Sb_2O_3) is applied in textiles, fibres and other materials that require flame retardant characteristics. Table 2.2 shows a typical end use pattern for antimony.

The demand for antimony by the transportation industry has been on the decline in recent years due to the development of low maintenance battery systems which use very little quantities of antimony as an alloying agent for lead. The development of electric vehicles which could utilise high antimony batteries for deep-cycling characteristics could reverse this trend. The cost advantage of some antimony substitutes such as tin, calcium and copper which can replace antimony in the hardening of lead, has also led to the decline in the industrial demand for antimony at a time when accessible antimony deposits are becoming smaller and less economic to mine. Thus the development of new methods for the beneficiation and recovery of antimony from low grade deposits is essential.

The industrial applications of arsenic are extremely limited, and mostly restricted to the use of arsenic trioxide (As_2O_3) in industrial chemicals. World reserves of arsenic are currently estimated at 1 million tonnes with half of this located in Chile, USA, Canada, Mexico, Peru and the Phillipines [15]. AsS (realgar) and As_2S_3 (orpiment) usually associate in mineral veins in minor amounts while FeAsS (arsenopyrite) is widely distributed in mineral veins with tin, tungsten, gold, silver, spharelite and pyrite.

	%
Industrial chemicals (wood preservatives, mineral floatation reagents)	57
Agricultural chemicals (herbicides α plant dessicants)	32
Glass and ceramics	6
Non-ferrous alloys (metallic form)	3
Others (animal feed additives, pharmaceuticals etc.)	2

TABLE 2.3

Arsenic (As_2O_3) End Use Pattern (USA), 1984 [15]

Small amounts of arsenic are alloyed with copper and lead to toughen the metals. In the oxide form (As_2O_3), it finds applications in the preparation of insecticides and in glass and ceramic products. Table 2.3 shows a typical arsenic end use pattern.

The replacement of silicon by gallium arsenide in semi-conductors is a technical development which could result in the growth of arsenic industrial use.

2.2 Phases and Phase Relations in the System Cu-Sb-S-O

2.2.1 Binary Systems

Antimony-Sulphur - The Sb-S system has been reviewed by Hansen and Andenko [16] and the phase diagram is illustrated in Figure 2.1. In the S-rich range, the monotectic temperature of 530^{o}C is observed only up to 80 at% S with the boiling of sulphur inferred at higher sulphur compositions. The solidus temperature of 110^{o}C in this composition range, is very close to the melting point of sulphur. Sb_2S_5 is metastable, does not crystallise from the melt and can only be prepared by wet chemical reactions.

For the partial system Sb-Sb_2S_3, a monotectic occurs at 615^{o}C while the eutectic is at 520^{o}C.

Sb_2S_3 (stibnite) is the only established mineral on the Sb-S binary, it melts at 546^{o}C and is generally uncomplicated by solid solutions. A second mineral metastibnite, with the approximate composition Sb_2S_3 has been reported from certain mines in Bolivia and Chile, and usually contains other metals in small quantities. Metastibnite is probably a metastable amorphous mineral stabilised by the presence of impurities such as Pb, Bi and As.

Anitmony-Oxygen The SbO-O system is shown in Figure 2.2 [17] and it includes the melting, boiling or decomposition temperaturates of compositions from SbO (50 at % O) to Sb_2O_5 (71.43 at % O). The intermediate phases include Sb_2O_3 and Sb_2O_4. The existence of Sb_6O_{13} was reported by Elliot [18] but has been disputed by Shunk [19] in a subsequent review of this system.

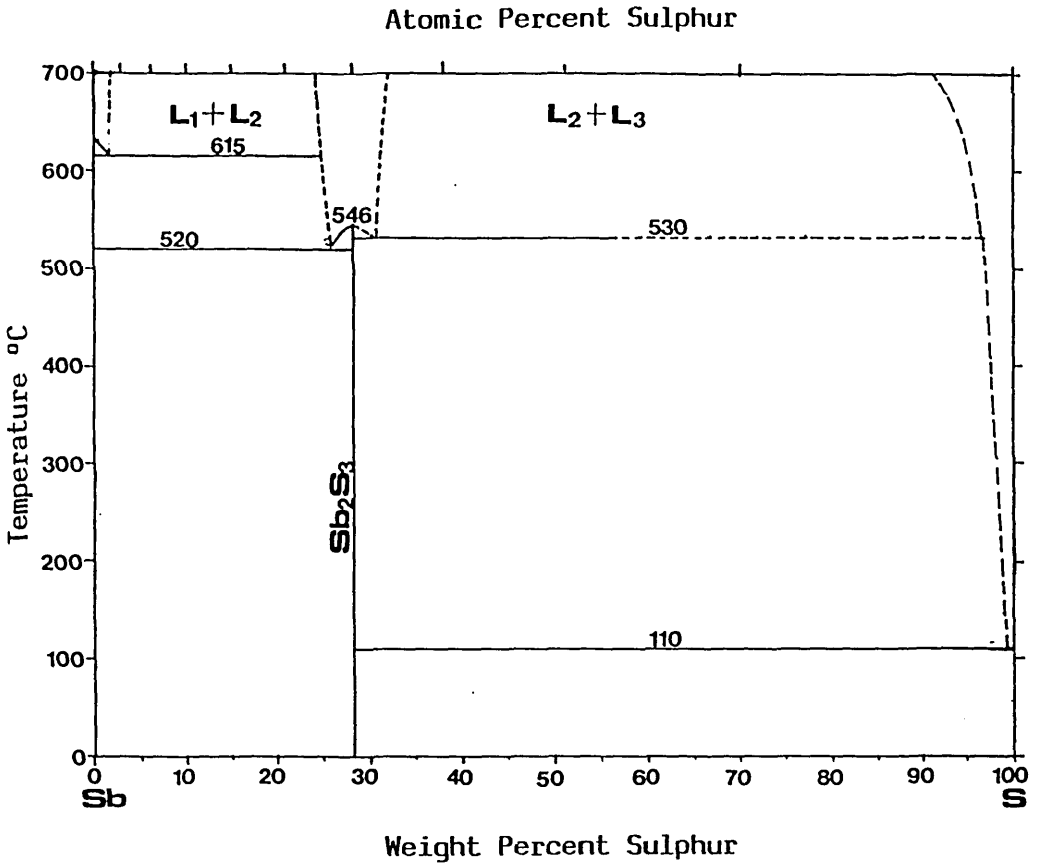

FIGURE 2.1

The Sb-S System [16]

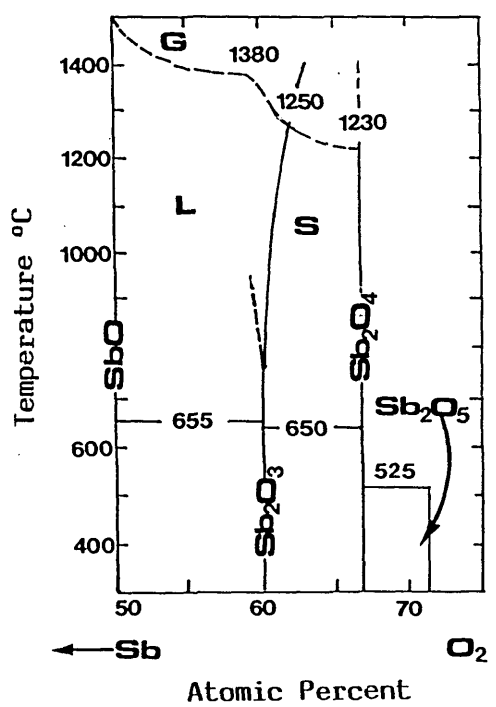

FIGURE 2.2

The SbO-O System [17]

Sb_2O_3 melts at 655°C and has no definite boiling point, but begins to decompose at approximately 1380°C. Sb_2O_4 decomposes completely at 1230°C, forming Sb_2O_3 and O_2 while Sb_2O_5 decomposes into Sb_2O_4 and O_2 at 525°C.

Copper-Sulphur - The Cu-S binary system has been investigated by Chakraborti and Laughlin [20] and is shown in Figure 2.3. The diagram shows the existence of a eutectic (1067°C) and a monotectic (1105°C) equilibrum between Cu and Cu_2S. Another eutectic exists between CuS and S at 813°C. Cu_2S undergoes a transformation at 103.5°C from the high temperature ζ-Cu_2S (hexagonal) to α-Cu_2S (orthorhombic). The existence of intermediate phases with approximate compositions $Cu_{1.96}S$ and Cu_9S_5 in the composition range Cu_2S-CuS has been established by various workers [18].

Mineral phases on the Cu-S binary are covellite (CuS); anilite ($Cu_{1.75}S$); digenite ($Cu_{1.76}S$ - $Cu_{1.79}S$); djurleite ($Cu_{1.97}S$) and chalcocite (Cu_2S). Anilite, djurleite and digenite all break down or invert to other phases at or above 93°C, leaving covellite, high digenite and the high temperature forms of Cu_2S as the only stable phases at higher temperatures [21].

Copper-Oxygen - Figure 2.4 shows the Cu-O phase diagram [22]. Eutectic reactions exist in the Cu-Cu_2O range at 1066°C and in the Cu_2O-CuO range at 1091°C. The decomposition reaction $4CuO \rightleftharpoons 2Cu_2O + O_2$ is considerable even in the solid state and Roberts and Smyth [23] have recorded the equilibrium partial pressure of O_2 as 402 mm Hg at the Cu_2O-CuO eutectic point. The same authors have also shown that the thermal equilibrium of mixtures of Cu_2O and CuO is dependent on the O_2 pressure that exists over the mixture.

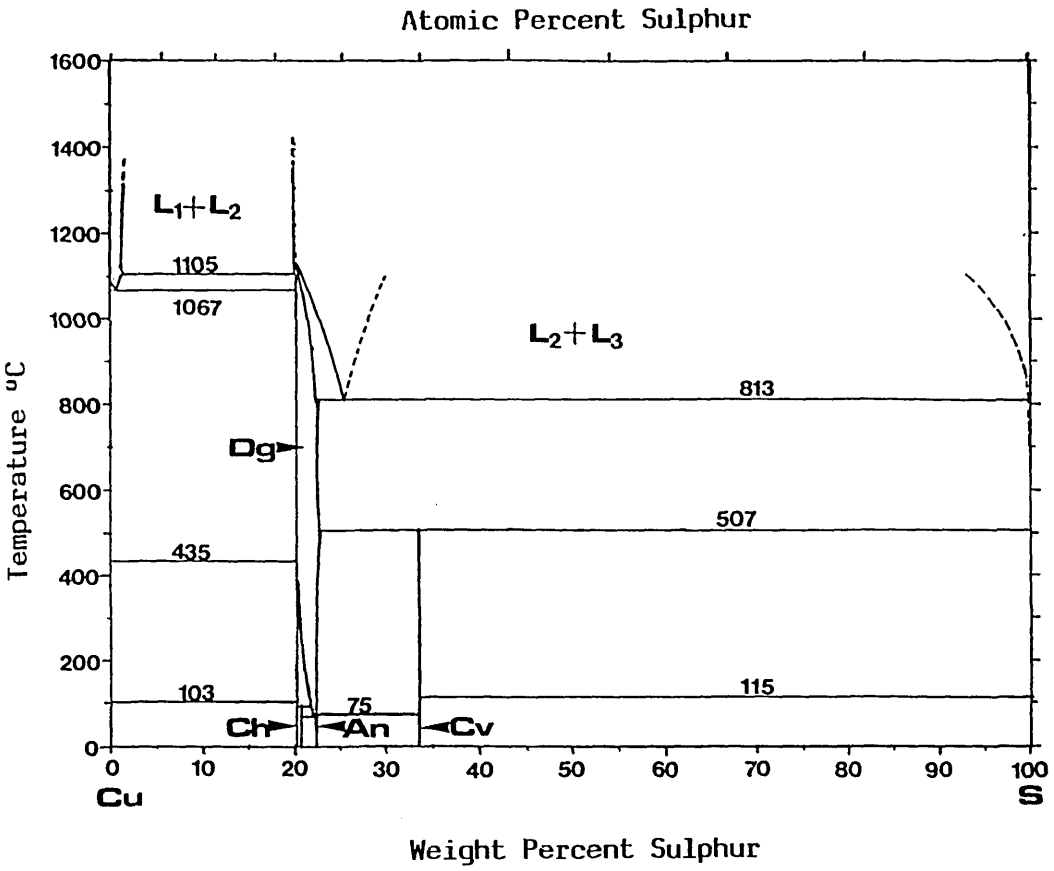

FIGURE 2.3

The Cu-S System [20]

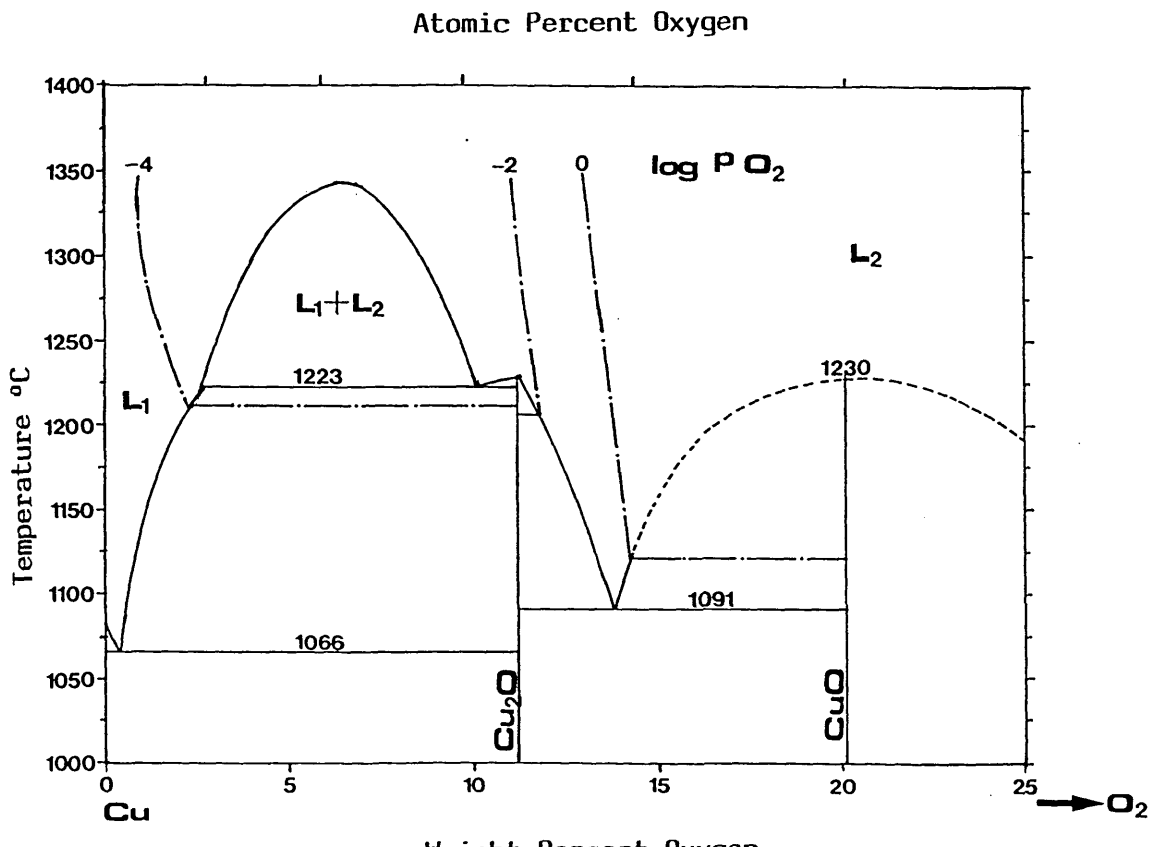

FIGURE 2.4

The Cu-O System [22]

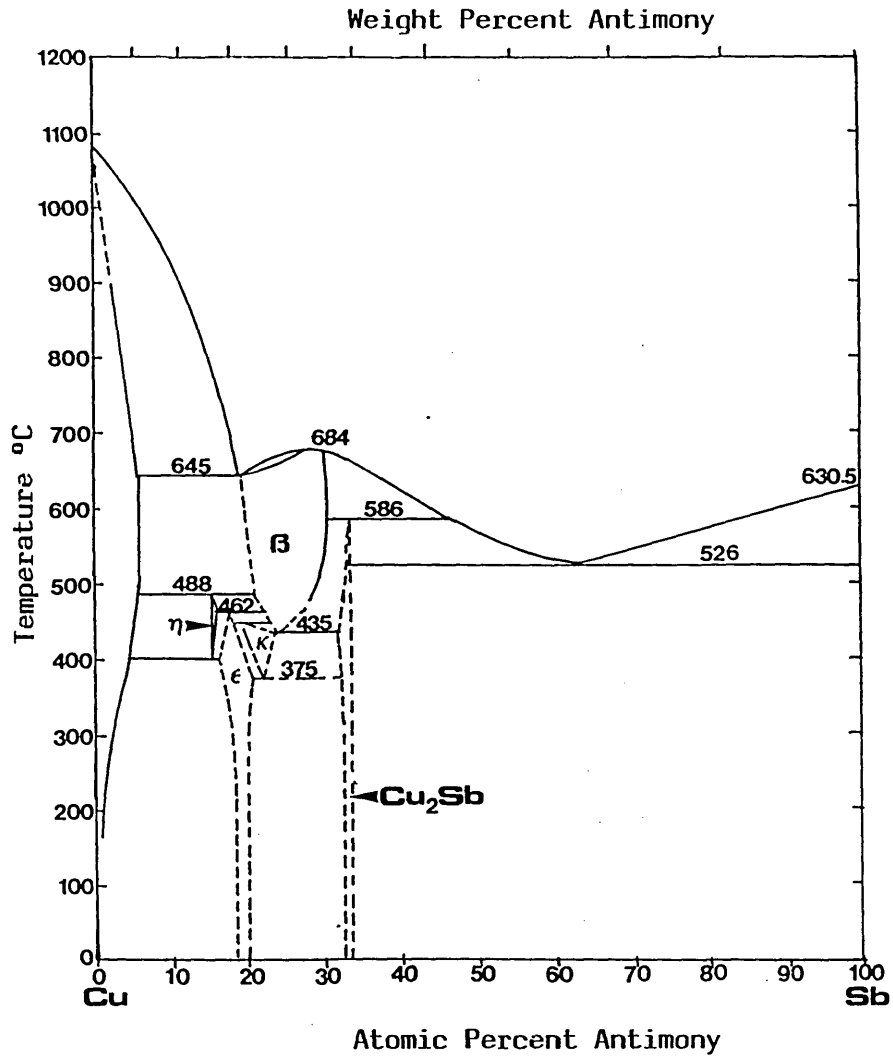

FIGURE 2.5

The Cu-Sb System [16]

Copper-Antimony - The Cu-Sb binary system has been extensively reviewed by Hansen and Andenko [16] and the phase diagram is illustrated in Figure 2.5. The liquidus exhibits a maximum at 684^{o}C, a peritectic at 586^{o}C and two eutectic points - Cu + β $\rightleftarrows$ L at 645^{o}C and Cu_2Sb + Sb $\rightleftarrows$ L at 526^{o}C.

In a series of investigations of the Cu-Sb system, Osawa and Shibata [24] deduced the existence of five intermetallic compounds - $Cu_{11}Sb_2$(η), Cu_9Sb_2(ε), Cu_5Sb_2(β), $Cu_{11}Sb_4$(Θ) and Cu_2Sb(γ) (the ε-phase has been referred to as δ by Japanese authors). The phases ε, Θ and γ exist at room temperatures while η and β are high temperature phases. Subsequent investigation by Schubert and Ilschner [25] could not confirm the existence of Θ but led to the discovery of an additional intermediate phase K stable between 450^{o}C and 375^{o}C.

Cu_2Sb, the intermeidate phase richest in antimony has a narrow homogeneity range between 48.0-49.0 wt % Sb. Osawa and Shibata [24] also indicated that the solubility of antimony in copper is comparatively large at high temperatures and decreases with temperature i.e. the lattice parameter of Cu is increased by the addition of Sb while the solubility of copper in antimony is negligible; thus the addition of copper does not alter the lattice dimensions of antimony. The existence of Cu_2Sb as the mineral cuprostibnite has been reported by Sorensen et al [26].

2.2.2 Ternary Systems

Copper-Antimony-Oxygen - Solid state reactions in the system Cu-Sb-O have been investigated by Shimada and Mackenzie [27] using thermogravimetric techniques. The phases formed were identified using X-ray diffraction, X-ray fluorescence and atomic absorption analysis.

$CuSb_2O_6$ has been synthesised from equimolar mixtures of CuO and Sb_2O_3 by slowly heating thinly-spread samples in air at temperatures up to 1000^{o}C. This process involves the oxidation of Sb_2O_3 to Sb_2O_4 (380-500^{o}C) followed by further oxidation of Sb_2O_4 to Sb_2O_5, and then the formation of $CuSb_2O_6$ in the temperature range 500-1000^{o}C.

The thermal decomposition of $CuSb_2O_6$ in a stream of oxygen free nitrogen at 980°C leads to the evolution of Sb_2O_3 vapour and oxygen, with the formation of $Cu_4SbO_{4.5}$

$$4CuSb_2O_{6(s)} \longrightarrow Cu_4SbO_{4.5(s)} + 7/2Sb_2O_{3(g)} + 9/2\ O_{2(g)} \qquad [2.3]$$

The kinetics of this reaction follow a linear rate with an activation energy of 356 kJ $mole^{-1}$. $Cu_4SbO_{4.5}$ can be further decomposed in nitrogen at higher temperatures; the kinetics of this decomposition reaction again follow a linear rate with an activation energy of 230 kJ $mole^{-1}$.

$$2Cu_4SbO_{4.5(s)} \longrightarrow 4Cu_2O_{(s)} + Sb_2O_{3(g)} + O_{2(g)} \qquad [2.4]$$

$$4Cu_2O_{(s)} \xrightarrow{>1120°C} 8Cu_{(s)} + 2O_{2(g)} \qquad [2.5]$$

$Cu_4SbO_{4.5}$ can also be synthesised by the reaction of CuO and $CuSb_2O_6$ in air at 1120-1150°C. The synthesised $Cu_4SbO_{4.5}$ compound has a structure of lower symmetry compared with that formed by thermal decomposition of $CuSb_2O_6$; this leads to the splitting of some of the X-ray diffraction peaks in the powder patterns.

Further investigations of this ternary system by Shimada et al [28] led to the formation of a new ternary phase $Cu_9Sb_4O_{19}$ prepared by the solid-state reaction between CuO and $CuSb_2O_6$ (3.5:1 mole ratio) at 1000-1100°C and 10K bar pressure. $Cu_9Sb_4O_{19}$ which is not stable at atmospheric pressure, decomposes to $Cu_4SbO_{4.5}$ + $CuSb_2O_6$ with the evolution of oxygen, when heated to 950-990°C in air.

Copper-Antimony-Sulphur - Skinner et al [29] have carried out extensive studies of the phases and phase relations in the ternary Cu-Sb-S system at temperatures down to 300°C. The experiments were performed in evacuated silica capsules with all the phases and assemblages co-existing with vapour. The ternary phases present in this system are Cu_3SbS_4

(famatinite), $Cu_{12+x}S_{4+y}S_{13}$ (tetrahedrite), CuSbS2 (chalcostibnite) and Cu_3SbS_3.

(i) **Cu_3SbS_4 (Famatinite)** is tetragonal with a structure derived from spharelite in which the S atoms lie at the nodes of a face centred cubic lattice with the Cu and Sb atoms ordered in the tetrahedral sites. Sb is present in the pentavalent state and Cu_3SbS_4 melts congruently at 627 ± 2^oC. Famatinite is the antimonoan isotype of Cu_3AsS_4 (enargite) with which it forms an extensive solid solution.

(ii) **$Cu_{12+x}Sb_{4+y}S_{13}$ (tetrahedrite)** is cubic and like Cu_3SbS_4 is derived from the spharelite structure with the S atoms distributed at the nodes of a spharelite type lattice and some Cu in tetrahedral co-ordination. Unlike Cu_3SbS_4 however, Cu occurs in both monovalent and divalent states while the Sb atoms are trivalent and bonded to three sulphur atoms forming the $[SbS_3]$ group. Tetrahedrite has a wide composition field and Skinner et al [29] reported that the phase tends to contain more Cu than is indicated by the ideal formula $Cu_{12}Sb_4S_{13}$; the general formula $Cu_{12+x}Sb_{4+y}S_{13}$ ($0 < x$ 1.92; $-0.02 < y < 0.27$) has been suggested for the observed composition field. Tetrahedrite breaks down at 543 ± 2^oC. It forms a continuous solid solution with its' arsenoan isotype tennantite ($Cu_{12}As_4S_{13}$).

(iii) **$CuSbS_2$ (chalcostibnite)** has an orthorhombic structure in which the Sb atoms also form the $[SbS_3]$ pyramid.

(iv) **Cu_3SbS_3** is a phase unknown as a mineral and was first elucidated by Skinner et al [29]. It is only stable above 359 ± 2^oC and disappears at high temperatures melting congruently at 607.5 ± 3^oC.

The phase relations in the ternary system are well described by the isothermal phase relations at 300^oC, 400^oC, 500^oC, 540^oC, and 600^oC derived by Skinner et al [29] and shown in Figures 2.6(a) and 2.6(b). Two features dominate the phase relations - the join between fcc and Sb, stable down to room temperature, precludes the stable co-existence of Cu-Sb

Abbreviation	Name
B	New Compound
β	Cu-Sb Alloy
cstb	Chalcostibnite
Cu_{ss}	Copper Solid Solution
Cv	Covellite
fcc	Face Centred Cubic
fm	Famatinite
L	Liquid
td	Tetrahedrite

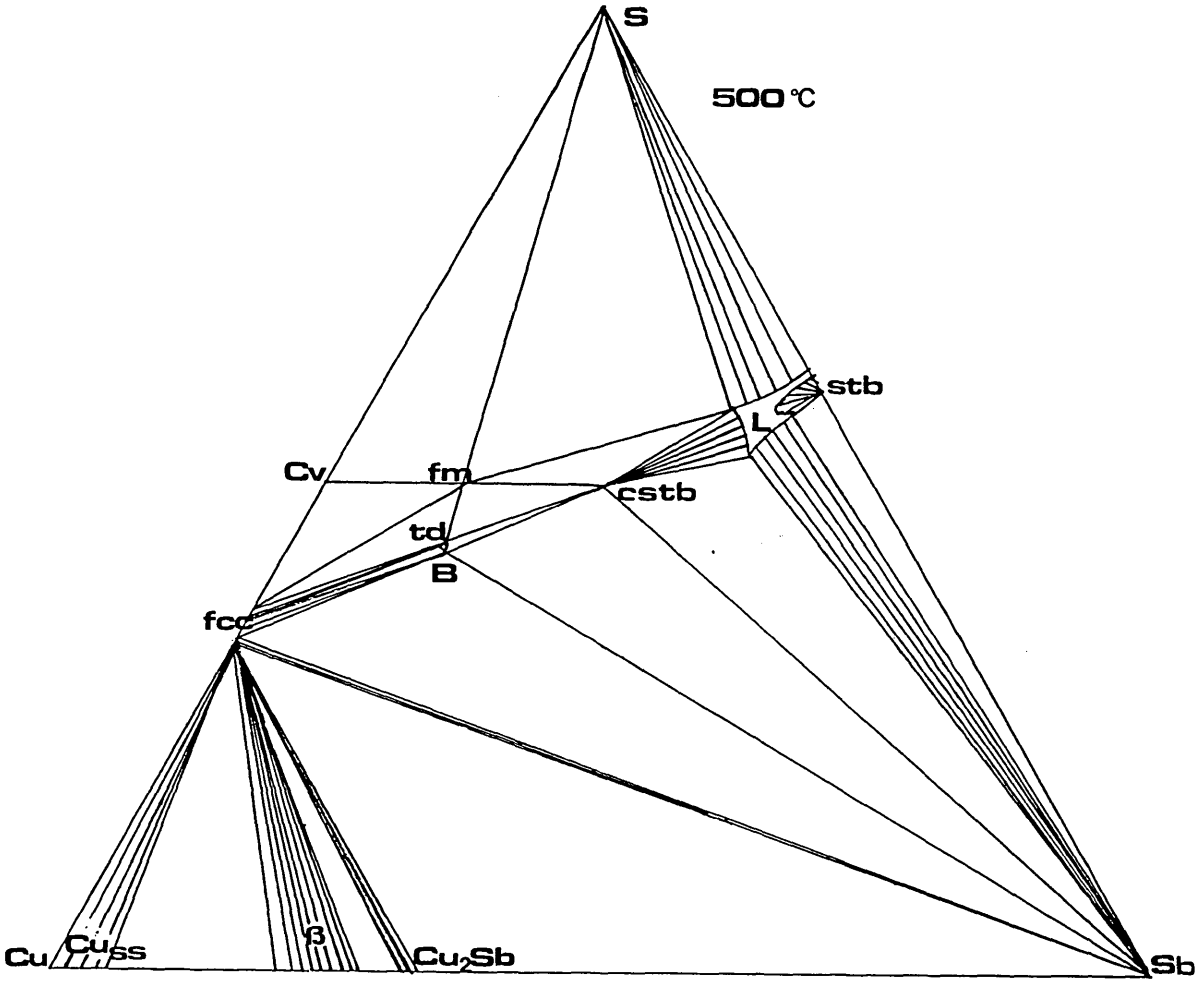

FIGURE 2.6(a)

Phase Relations in the Cu-Sb-S System at 500°C [29]

[Compositions are plotted in atom percent. One-phase fields appear as points or are stippled, two-phase fields are shaded by tie lines and three-phase fields are open]

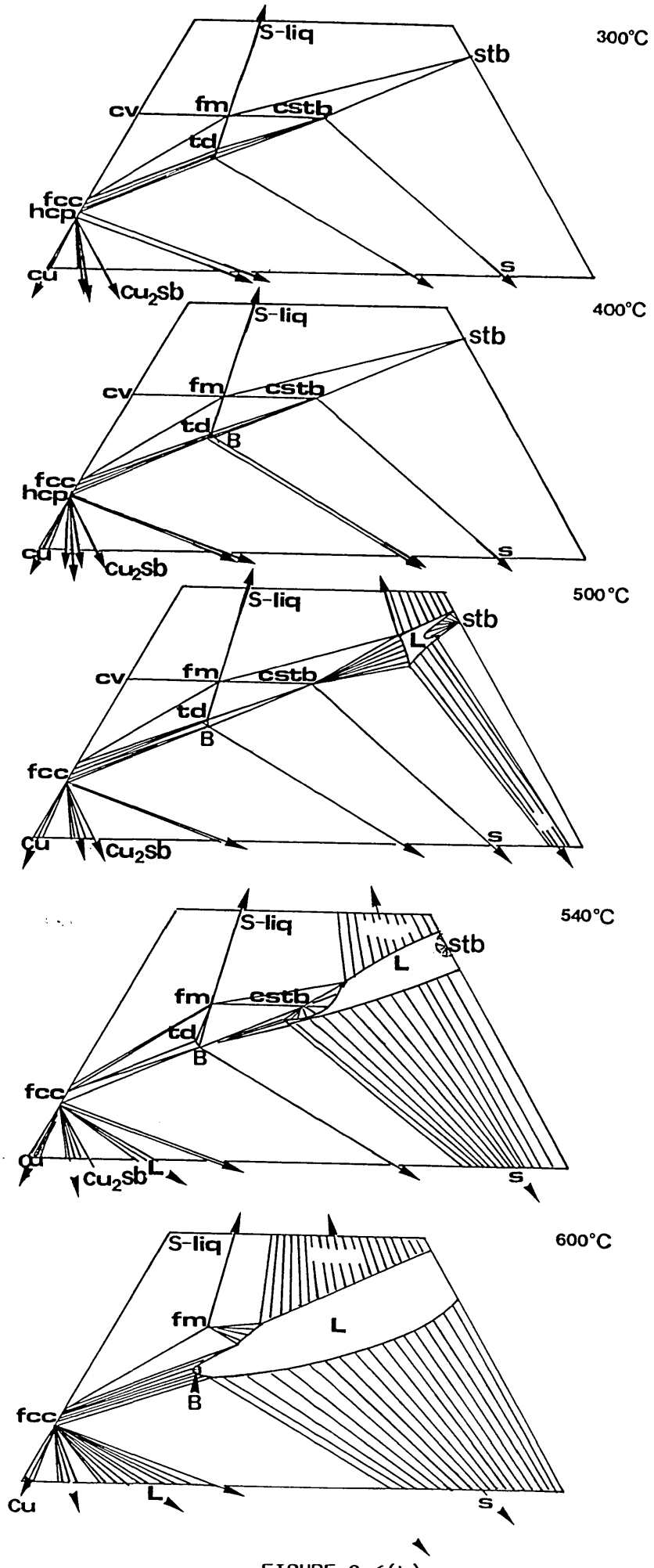

FIGURE 2.6(b)

Phase Relations in the Cu-Sb-S System at Various Temperatures [29]

alloys with any of the ternary phases; secondly, all the ternary phases are confined within a narrow composition band bounded by Sb_2S_3, Cu_2S and CuS. The main reaction points in the Cu-Sb-S system are:

REACTION	TEMP (^oC)
B' → B	122±3
cstb + td + Sb → B	359±2
td + Sb → B + fcc	436±2
fm + Stb + S → L	472±2
fm + Stb → cstb + L	476.5±2
cstb + stb → sb + L	476.5±2
cv + fm → fcc + $S_{(L)}$	507±3
td + cstb → fm + B	522±2
cstb + sb → B + L	531±2
td → fcc + fm + B	543±2
B + cstb → fm + L	543±2
fm + cstb → L + $S_{(L)}$	546.6±2.5
cstb → L	553±2
B + Sb → fcc + L	588±2.5
B + fm → fcc + L	588±2
B → L	607.5±3
fcc + fm → L + $S_{(L)}$	627±2
fm → L	627±2

Copper-Sulphur-Oxygen - Most investigations of this system have been aimed at understanding the phase relationships that occur during copper smelting and conversion processes that involve equilibria between copper, matte and slag.

Schmeidl et al [30] have studied the equilibrium between Cu and liquid Cu_2S at temperatures between 1100^oC and 1250^oC. On the basis of experimental results, they developed empirical relationships that establish the dependence of sulphur, oxygen and copper concentrations of

both liquids on the partial pressure of SO_2

Metal Phase:

$$\text{wt \% O} = 86.61 \times 10^{[-1.37084 - 1277.67/T]} \times P_{SO_2}^{\frac{1}{2}}$$

$$\text{wt \% Cu} = 10^{[1.97893 + 23.8886/T]}$$

$$\text{wt \% S} = 100 - \text{wt \% O} - \text{wt \% Cu}$$

Sulphide Phase:

$$\text{wt \% O} = 86.61 \times 10^{[-1.95989 + 1013.2/T]} \times P_{SO_2}^{\frac{1}{2}}$$

$$\text{wt \% Cu} = 79.605 + 0.26042 \times 10^{-12} \times T^4$$

$$\text{wt \% S} = 100 - \text{wt \% O} - \text{wt \% Cu}$$

Kullerud [31] has determined that the $Cu-Cu_2O-Cu_2S$ assemblage is stable over a wide temperature range. A liquid field transects the system, prohibiting lines between the ternary and binary phases even at as low a temperature as 250°C. The ternary phases present in this system are $CuSO_4$ (chalcocyanite), $Cu_2(SO_4)O$ (dolerophanite) and Cu_2SO_4.

2.3 Phases and Phase Relations in the System Cu-As-S-O

2.3.1 Binary Systems

Arsenic-Sulphur - The As-S phase diagram is shown in Figure 2.7. Phases present in the system are AsS (realgar) which melts congruently at 321°C and As_2S_3 (orpiment) which also melts congruently, at 310°C. As_2S_5 can only be preapred by precipitation from aqueous solutions of H_3AsO_4 with H_2S.

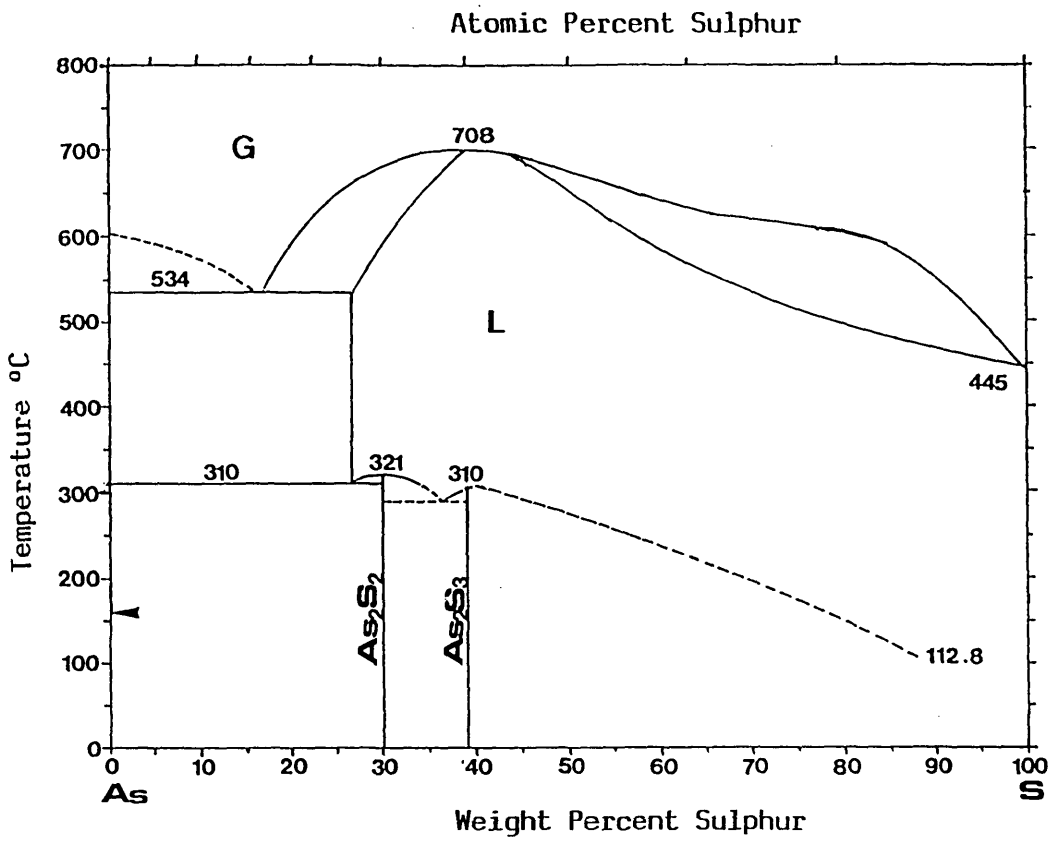

FIGURE 2.7

The As-S System [16]

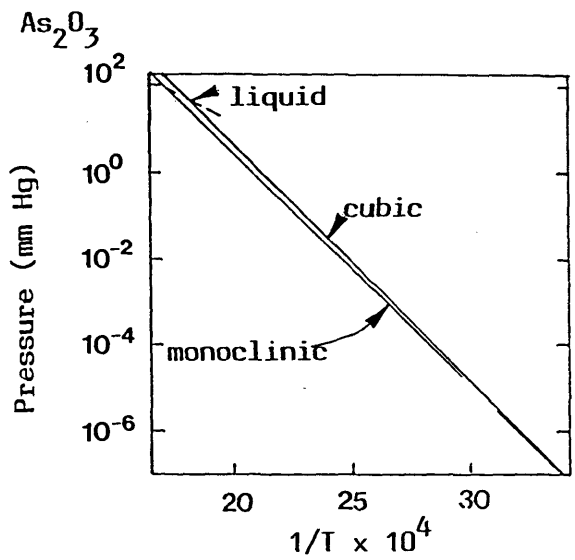

FIGURE 2.8

Vapour Pressures of Arsenolite (As_2O_3-cubic) and Claudetite (As_2O_3-monoclinic) [32]

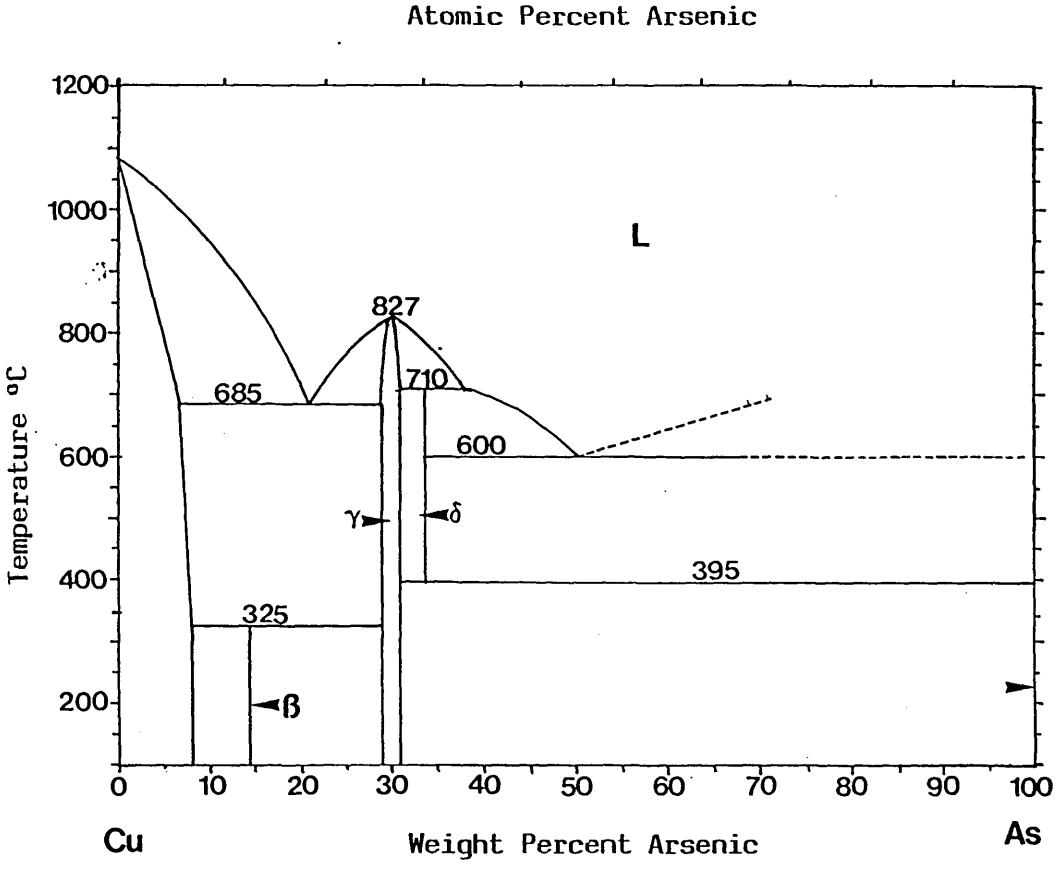

FIGURE 2.9

Cu-As System [16]

Arsenic-Oxygen - The compound As_2O_3 exists as both arsenolite (fcc) with a melting point of 278°C and claudetite (monoclinic). As_2O_5 decomposes at 315°C [19]. Vapour pressure data for As_2O_3 have been determined by Karutz and Stranski [32] and is shown in Figure 2.8.

Copper-Arsenic - The phase system Cu-As has been redrawn by Kullerud [31] from data by Hansen and Andenko [16] and by Heyding and Despault [33]. Known compounds in this system are $Cu_{5-x}As_2$ ($0 < x < 0.1$), Cu_3As (β-domeykite) which forms a solid solution from 28.2-30.4 wt% As at 560°C, and Cu_8As (algodonite) which is stable below about 340°C. The compound $Cu_{15}As_4$ is reported to be stable at pressures above 200 bars and below about 225°C. Figure 2.9 [16] illustrates the phase relations in the Cu-As system.

2.3.2 Ternary Systems

Copper-Arsenic-Sulphur - The Cu-As-S system has been investigated by Maske and Skinner [34] at temperatures down to 300°C, with slow reaction rates hindering studies at lower temperatures. The experiments were carried out in evacuated silica tubes and the resulting phases and assemblages all co-existed with vapour. Figure 2.10a is a schematic diagram showing the synthetic and natural phases present in the Cu-As-S system. The ternary phases are Cu_3AsS_4 (enargite, luzonite), $Cu_{12+x}As_{4+y}S_{13}$; $0 < x < 1.72$; $0 < y < 0.08$ (tennantite); CuAsS (lautite); $Cu_6As_4S_9$ (sinnerite) and $Cu_{24}S_{12}S_{31}$.

i) Cu_3AsS_4 - This represents the ideal formula of **enargite** and its low temperature polymorph **luzonite**. The inversion from luzonite to enargite occurs just below 300°C. Enargite is orthorhombic with a structure derived from wurtzite in which the S atoms lie at the nodes of a hexagonal packed lattice while luzonite is tetragonal with a structure derived from spharelite with the S atoms located at the nodes of a face centred cubic lattice. In both, the Cu and As atoms are ordered in tetrahedral sites and As is pentavalent.

ii) $Cu_{12+x}As_{4+y}S_{13}$ - $0 < x < 1.72$; $0 < y < 0.08$ - This formula corresponds to **tennantite**, the arsenoan isotype of tetrahedrite ($Cu_{12+x}Sb_{4+y}S_{13}$)

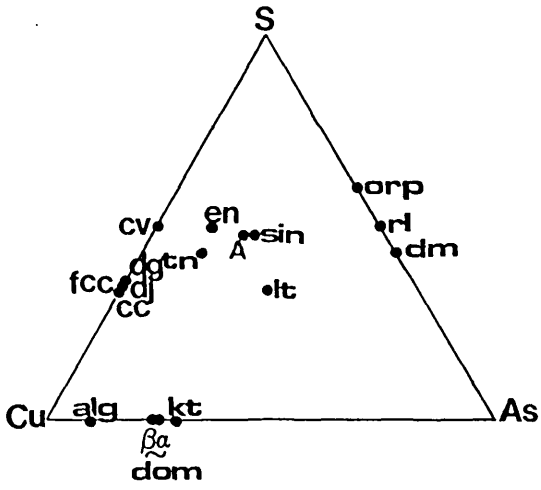

FIGURE 2.10(a)

Synthetic and Natural Phases in the Cu-As-S System (at. %)

Abbreviation	Name
A	New Compound
alg	Algodonite
cc	Chalcocite
Cu_{ss}	Copper Solid Solution
cv	Covellite
dg	Digneite
dj	Djurleite
dm	Dimorphite
α-dom	α-Domeykite
β-dom	β-Domeykite
en	Enargite
fcc	Face Centred Cubic
hcp	Hexagonal Close Packed
Kt	Koutekite
lt	Lautite
orp	Orpiment
rl	Realgar
sin	Sinnerite
tn	tennantite

FIGURE 2.10(b)

Phase Relations in the Cu-As-S System (at. %) [34]

[All phase fields appear solid or stippled, two-phase fields are shaded by tie lines and three phase fields are open]

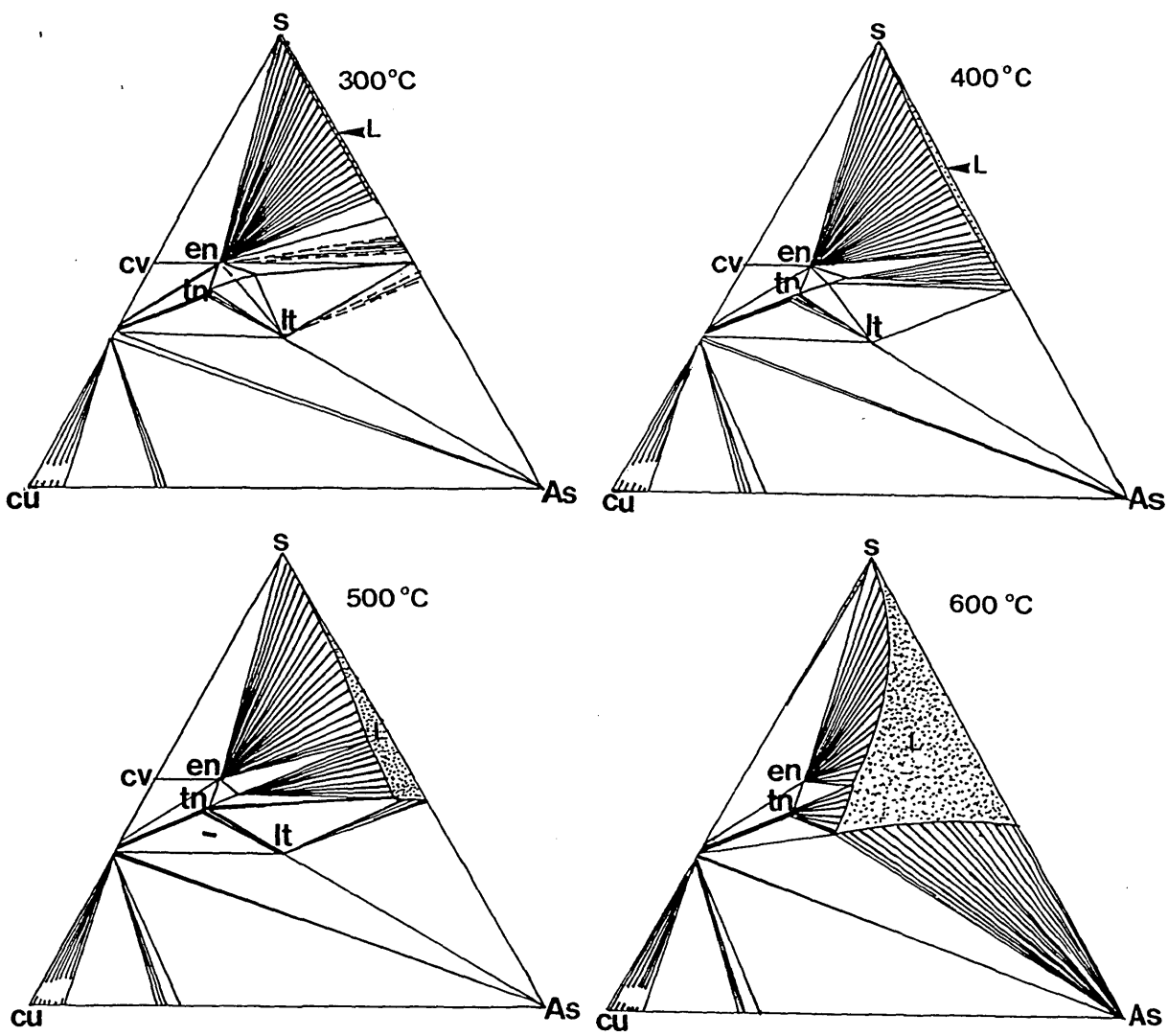

with which it forms a continuous solid solution. Tennantite is cubic and has some Cu atoms in tetrahedral co-ordination. Cu occurs in both the divalent and monovalent states while the As atoms are trivalent and form pyramidal [AsS_3] groups. Tennantite has an extensive composition range and usually has slightly more Cu than is indicated by the ideal formula $Cu_{12}As_4S_{13}$. The composition range varies with temperature. Down to 300°C, the ideal composition $Cu_{12}As_4S_{13}$ does not fall within the observed composition field. However, the composition field closely approaches $Cu_{12}As_4S_{13}$ at 300°C and it is thought that the ideal composition could become included in the field at lower temperatures.

iii) **$Cu_6As_4S_9$** - **Sinnerite** has a spharelite-type packing of S atoms like tennantite. The composition falls on the join Cu_2S-As_2S_3 being equivalent to $3Cu_2S.2As_2S_3$ with all the Cu atoms in the monovalent state.

iv) **$Cu_{24}As_{12}S_{31}$** - The existence of this compound was first reported by Maske and Skinner [34] who suggested that it might have been mistaken for tennantite by earlier investigators. The structure is again derived from a spharelite-type packing of the S atoms which relates it to the structure of tennantite. The composition formula $Cu_{24}As_{12}S_{31}$ corresponds to $11Cu_2S.2CuS.6As_2S_3$ while tennantite corresponds to $10Cu_2S.4CuS.4As_2S_3$. This compositional relationship indicates that their structure might be determined by similar crystallographic principles.

v) **CuAsS** - This ternary compound corresponds to **lautite**, a relatively rare sulphide mineral. The structure is unlike that of the other ternary compounds and although it is again derived from spharelite, both the Zn and S sites are occupied by Cu, As and S atoms in an ordered array. The relationship is simply that of geometry and does not involve the kind of substitution present in enargite and tennantite.

Maske and Skinner [34] determined the phase relations in the Cu-As-S ternary at 300°C, 400°C, 500°C and 650°C and these have been illustrated in

Figure 2.10(b). The main feature of the phase relations is the persistence of the Cu_2S-As join, prohibiting the copper arsenides from co-existing with the ternary sulphide compounds.

The reactions involving ternary compounds in the system Cu-As-S are

REACTION	TEMP ^oC
sin + Lt → A + L	379
en + sin → A + L	456
A + Lt → tn + L	474
sin → A + L	489
en + cv → fcc + L	507
fcc + Lt → tn + As	571
en + A → tn + L	573
lt → As + tn + L	574
A → tn + L	578
tn + As → fcc + L	598
tn + fcc → en + L	654
$tn_{(Cu_{12.31}As_4S_{13})}$ → L	665
Cu_3AsS_4 → As-deficient en + L	666

The replacement of copper by iron and zinc, and of arsenic by antimony in the common minerals of this ternary sulphide system will affect these reactions in a manner that cannot be readily predicted.

2.4 Phases and Phase Relations in the System Fe-As-S-O

2.4.1 Binary systems

Iron-Sulphur - The Fe-S phase diagram is shown in Figure 2.11. FeS_2 is shown to be stoichiometric melting incongruently at 743 ± 3^oC. The upper stability curve of this phase corresponds to the univariant curve which defines the conditions at which the reaction $FeS_2 \rightleftarrows Fe_{1-x}S + L$ takes place. A two-liquid field exists between $Fe_{1-x}S$ and S above 1082^oC. Slow reaction rates have hindered studies at low temperatures and the phase relations in this system at low temperatures are thought to be complicated.

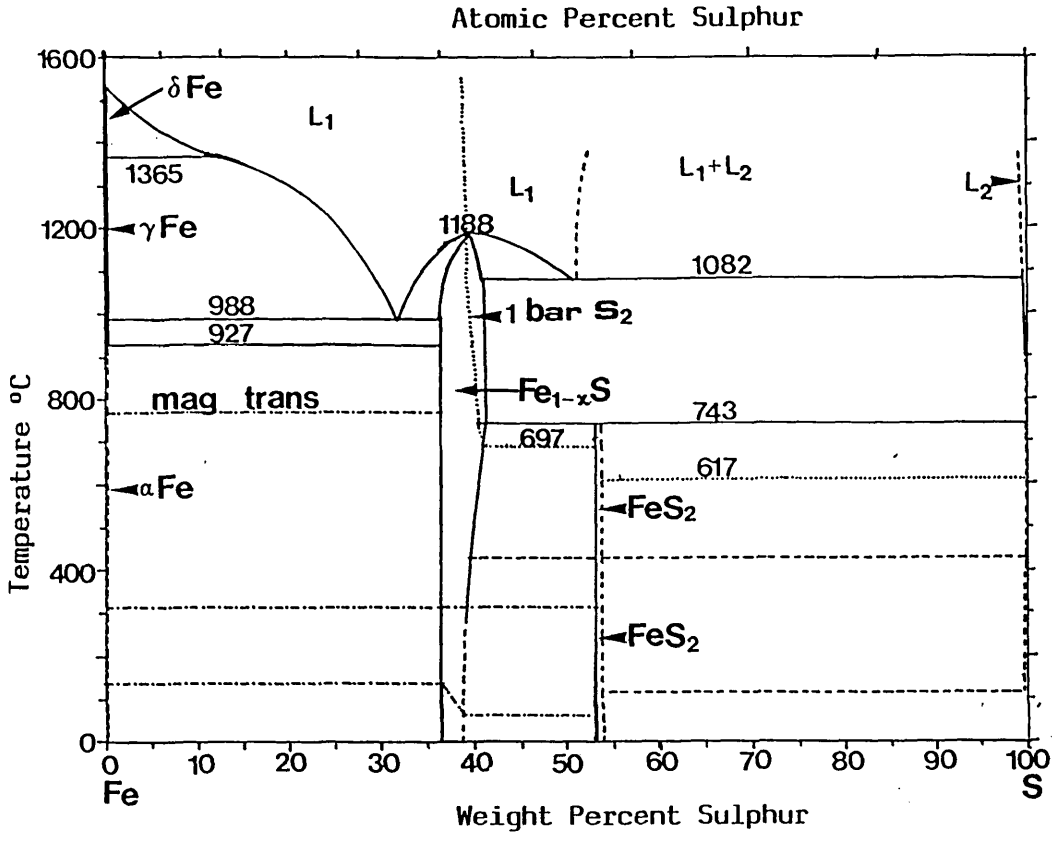

FIGURE 2.11

The Fe-S System [35]

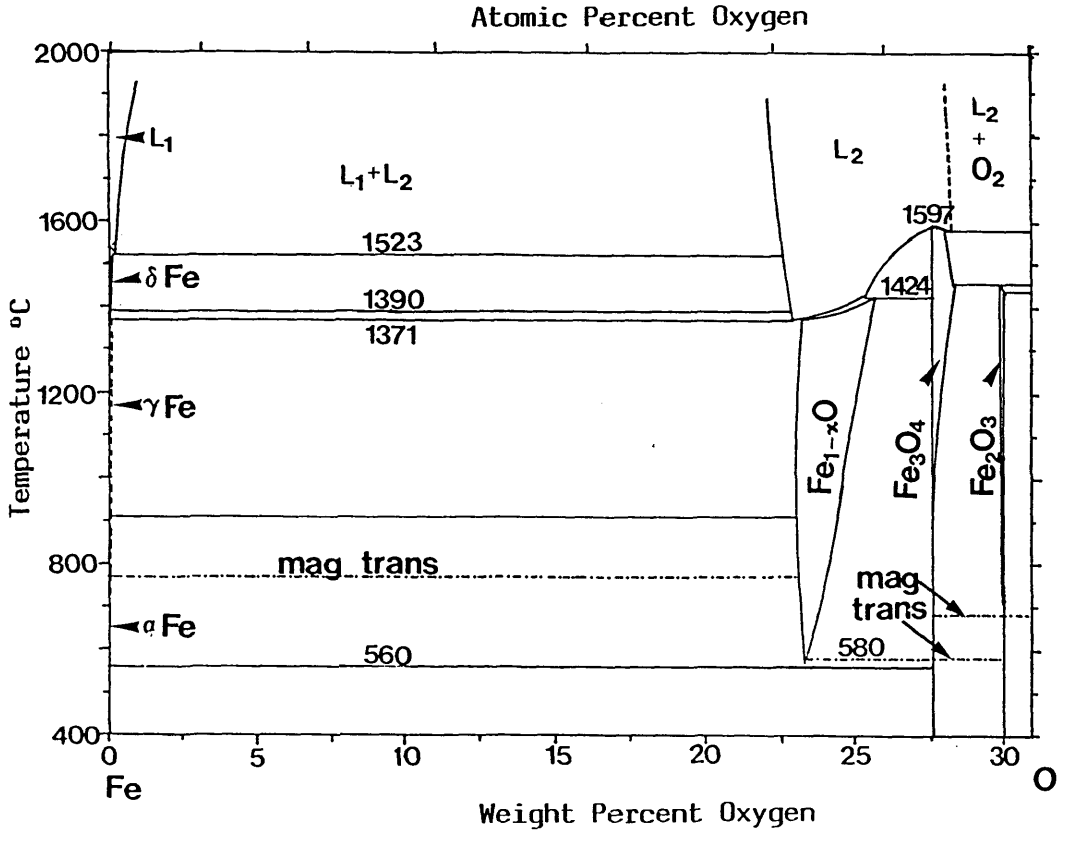

FIGURE 2.12

The Fe-O System [35]

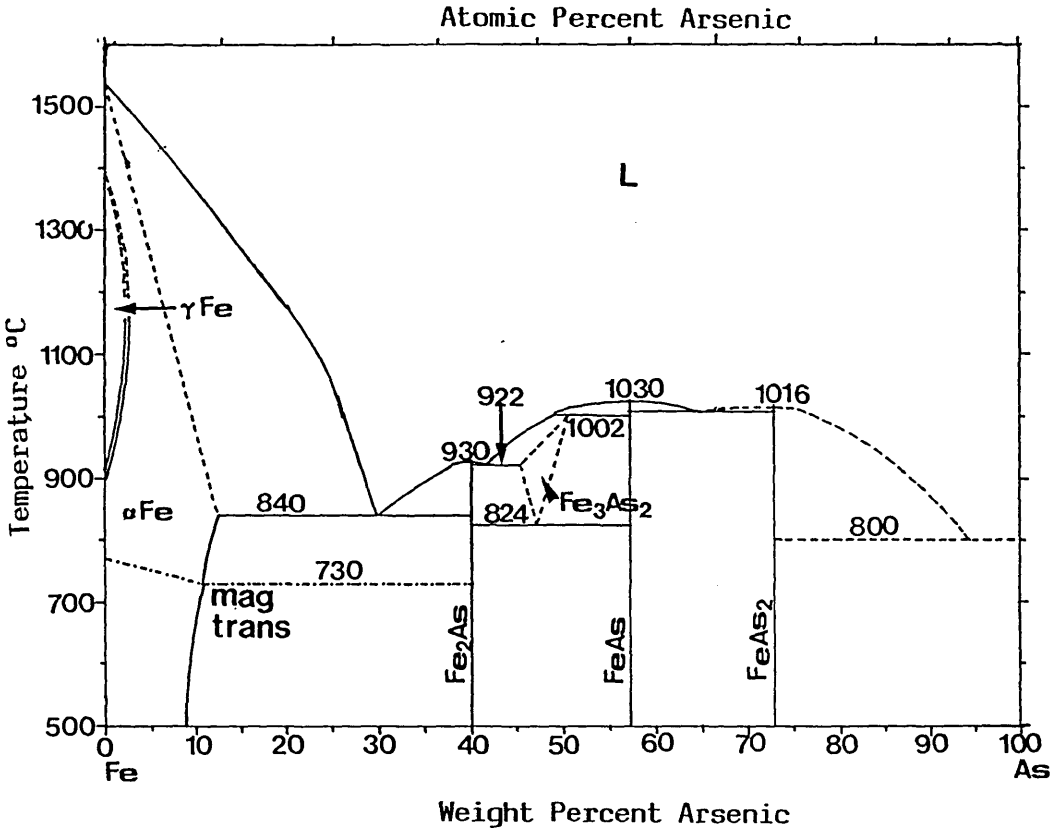

FIGURE 2.13

The Fe-As System [23]

Marcasite, the orthorhombic modification of FeS_2 is stable in this region.

$Fe_{1-x}S$ (pyrrhotite) is a non-stoichiometric compound with a solid solution due to the omission of Fe from the FeS structure. The iron-rich limit of the solid-solution field closely corresponds to the FeS composition at all temperatures up to the Fe-FeS eutectic at 988°C. Pyrrhotite melts congruently in the presence of a saturated vapour at a maximum of 1188°C for a composition containing 52 at % S; and this is the unique pyrrhotite phase that melts to a liquid of the same composition.

Iron-Oxygen - The Fe-O phase diagram is reproduced from Kubaschewski [35] (Figure 2.12). Most of the phases and reaction points are reasonably well established due to the extreme importance of this system in ferrous extractive metallurgy. Binary phases present include FeO_{1-x} (wustite), Fe_3O_4 (magnetite) and Fe_2O_3 (haematite).

Iron-Arsenic - The Fe-As binary phase diagram is shown in Figure 2.13 [35]. The phases present are Fe_2As (tetragonal), FeAs (orthorhombic) and $FeAs_2$ (orthorhombic) which has a mineral equivalent-loellingite. The existence of an additional intermediate phase (Fe_3As_2) has been suggested [36] and subsequent investigations by Haag [37] confirmed the existence of such a phase between Fe_2As and FeAs. He also reported the existence of an additional high temperature intermediate phase which cannot be retained by quenching since its eutectoid decomposition at about 800°C cannot be suppressed.

FeAs (loellinigite) melts congruently at 1030±8°C and the $FeAs_2$-As; $FeAs_2$-FeAs; Fe_2As-αFe eutectics occur at 800±10°C; 1008±5°C and 840°C respectively. It is not clear whether Fe_2As has a maximal melting point or is formed by a peritectic reaction.

2.4.2 Ternary Systems

Iron-Sulphur-Oxygen

The phase relations below 560°C and between 560-675°C in the Fe-S-O ternary system have been determined by Kullerud [38] and are illustrated in

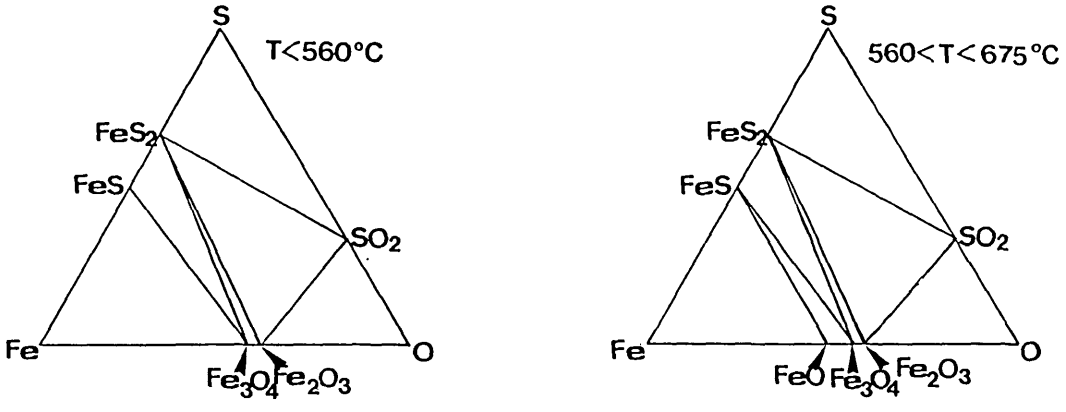

FIGURE 2.14

Phase Relations in the Fe-O-S System [38]

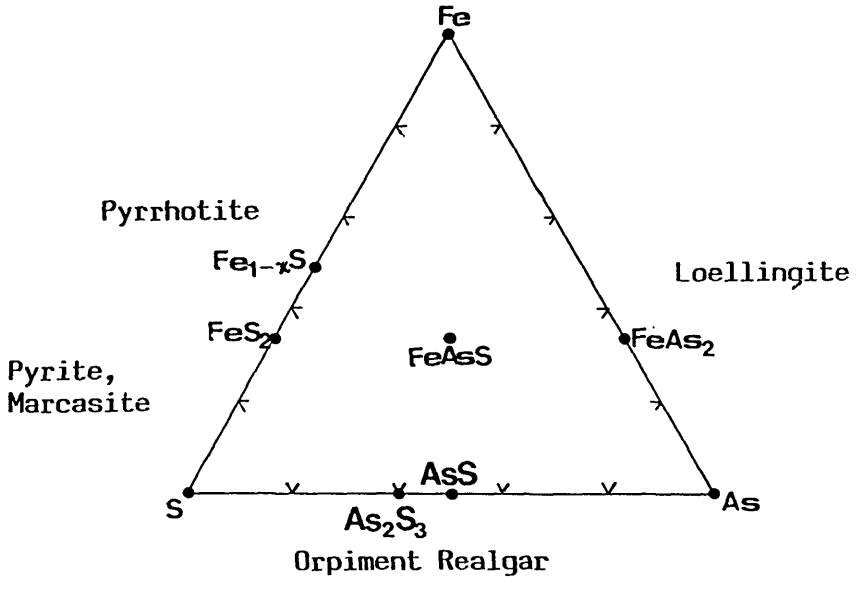

FIGURE 2.15(a)

Minerals in the Fe-As-S System

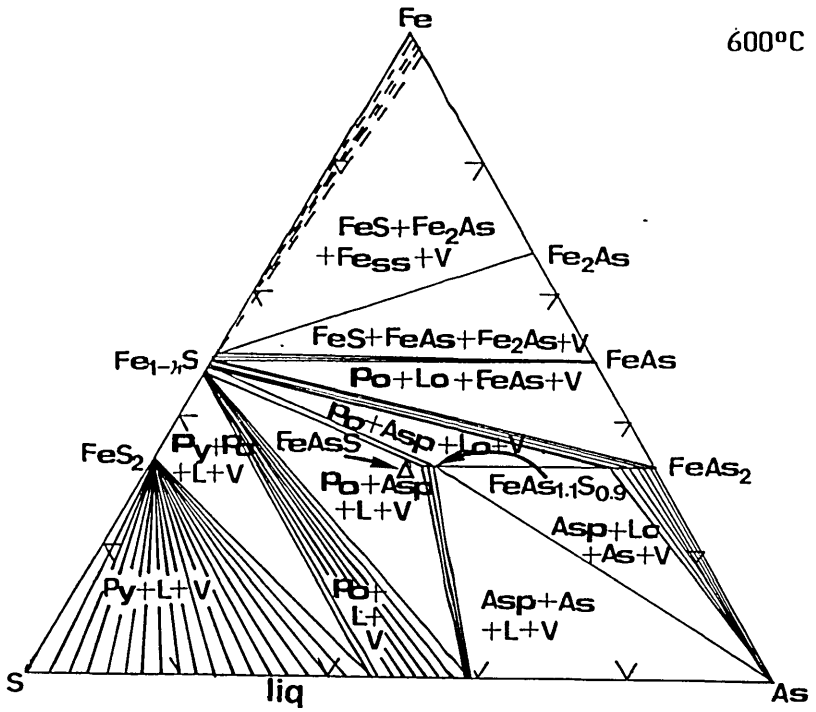

FIGURE 2.15(b)

The Fe-As-S System at 600°C [39]

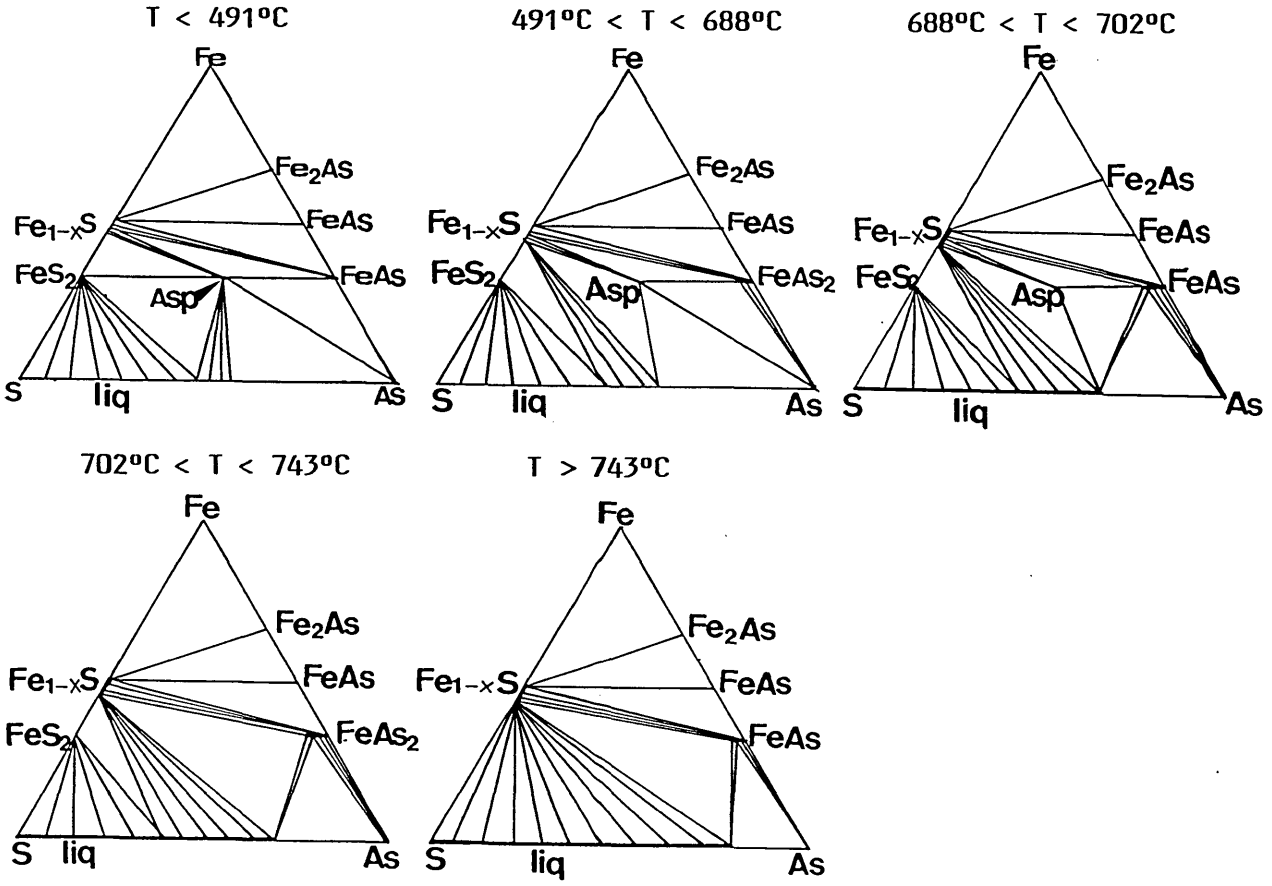

FIGURE 2.15(c)

Phase Assemblages in the Fe-As-S
System in Specified Temperature Ranges [39]

Figure 2.14. The system contains no ternary phases at elevated temperatures. Below 560°C, FeO does not exist as a phase. The tie line Fe_3O_4-FeS_2 is replaced by Fe_2O_3-FeS at about 675°C. At about 700°C, the Fe_2O_3-FeS_2 tie line breaks and FeS+$SO_{2(gas)}$ co-exist. FeS_2(Pyrite) disappears at 743°C. Eutectic conditions exist along the FeS-FeO join at 940°C (~40% FeS).

Iron-Arsenic-Sulphur

The Fe-As-S equilbrium phase relations in the 400°C to 800°C temperature range were determined by Clark [39]. Figure 2.15(a) shows the minerals that have been reported in the ternary system while Figure 2.15(b) shows the ternary system at 600°C. The phase assemblages stable with vapour in the specified temperature ranges are illustrated in Figure 2.15(c).

FeAsS (arsenopyrite) which is monoclinic, is the only ternary compound present in this system. It has a small field of solid solution with the approximate limits of $FeAs_{1.08}S_{0.92}$ and $FeAs_{1.05}S_{0.95}$ and does not encompass the ideal composition FeAsS. At 600°C, synthetic arsenopyrite has the approximate composition $FeAs_{1.1}S_{0.9}$. Compositions that are sulphur rich relative to the ideal FeAsS become stable at lower temperatures and under high confining pressures.

At 600°C, a narrow liquid field along the As-S side line and tie lines connect this liquid field to arsenopyrite as well as to pyrite and pyrrhotite. A vapour phase is always present in all these assemblages, and by consideration of the Gibb's phase rule, the vapour pressure is fixed at constant temperature, in the 4-phase assemblages whereas it varies over the 3-phase and 2-phase assemblages.

Invariant temperatures in the phase assemblages shown in Figure 15(c) include -491$\pm$12°C - FeS_2 + FeAsS tie line is replaced by $Fe_{1-x}S$+L. -688 $\pm$3°C - $FeAs_2$ + L tie line replaces the FeAsS + As line. -702 $\pm$ 3°C - FeAsS melts incongruently producing $Fe_{1-x}S$ + $FeAs_2$ + L. The reactions all take place in the presence of vapour.

Equilibrium	lnK	Temp. Range K
Elemental		
$As_{4(g)} = 4As_{(s)}$	16,116/T - 18.3	< 853
$As_{4(g)} = 2As_{2(g)}$	-33,960/T + 17.3	900-1200
$As_{2(g)} = 2As_{(g)}$	-46,500/T + 13.7	400-1200
$3As_{4(g)} = 4As_{3(g)}$	-69,040/T + 31.4	900-1200
Sulphides		
$4As_{(s)} + 2S_{2(g)} = As_4S_{4(s)}$	47,510/T - 42.03	298-554
$As_4S_{4(s)} = As_4S_{4(g)}$	-14,251/T + 18.47	452-534
$As_4S_{4(l)} = As_4S_{4(g)}$	-11,000/T + 12.9	452-534
$4As_{(s)} + 3S_{2(g)} = 2As_2S_{3(s)}$	69,336/T - 59.76	~ 448-573
$As_{4(g)} + 3S_{2(g)} = 2As_2S_{3(g)}$	58,714/T - 46.18	727-966
$2S_{2(g)} + As_{4(g)} = 4AsS_{(g)}$	-47,964/T + 17.4	798-973

(continued ...)

TABLE 2.4

Thermodynamic Data for the Fe-As-S-O System [43]

Equilibrium	lnK	Temp. Range K
Oxides		
$4As_{(s)} + 3O_{2(g)} = 2As_2O_3$ (s, arsenolite)	$155,850/T - 29.72 \log T + 0.021T + 30,190/T^2 + 8.88$	298-548
$4As_{(s)} + 3O_{2(g)} = 2As_2O_3$ (s, claudetite)	$151,720/T - 29.72 \log T + 0.021T + 30,190/T^2 + 17.1$	298-586
$4As_{(s)} + 3O_{2(g)} = As_4O_{6(g)}$	$144,229/T - 41.74$	700-1000
$2As_2O_{5(s)} = As_4O_{6(g)} + 2O_{2(g)}$	$-69,940/T + 67.72$	810-1013
Arsenides		
$2Fe_{(s)} + As_{(s)} = Fe_2As_{(s)}$	$559/T + 6.55$	673-1073
$Fe_{(s)} + As_{(s)} = FeAs_{(s)}$	$2100/T + 4.2$	673-1073
$Fe_{(s)} + 2As_{(s)} = FeAs_{2(s)}$	$5211/T + 3.6$	773-1123
Arsenopyrite		
$2Fe_{(s)} + 2As_{(s)} + S_{2(g)} = 2FeAsS_{(s)}$	$40,756/T - 16.4$	773-975
Arsenate		
$3As_4O_{6(g)} + 7O_2 + 4Fe_3O_{4(s)} = 12FeAsO_{4(s)}$	$-188.04 + 27.6\times10^{-4}T + 3.898\times10^{5}/T - 27.9 \log T$	

TABLE 2.4: Thermodynamic Data for the Fe-As-S-O System [43] (continuation..)

Iron-Arsenic-Oxygen

The system Fe-As-O is of major interest in the roasting of arsenoyrite and other arsenic-bearing concentrates. Phases reported in the system Fe-As-O include $Fe_2As_4O_{12}$, $FeAsO_4$, $Fe_4As_2O_{11}$, $Fe_2As_4O_9$ and $Fe_4As_2O_{11}$. Two of these have been found existing as natural minerals - $Fe_4As_2O_{11}$ - Angelesite [40], $Fe_4As_2O_{11}$-Karibitite [41].

Skaeff [42] has determined the thermochemical properties of $FeAsO_4$ by studying the $FeAsO_4$-Fe_2O_3 equilibrium in the temperature range 317-536^oC using electrochemical technqiues. The thermodynamically stable form of $FeAsO_4$ above 452^oC (725 K) is the high temperature β-phase modification and the α-β transformation occurs with an associated enthalpy of 34.3 KJ/mol.

Iron-Arsenic-Sulphur-Oxygen

No phases belonging to the quartenary Fe-As-S-O system has been reported in the literature. The thermodynanmic data available for the various phases that exist in this system have been compiled by Chakraborti and Lynch [43] and these are shown in Table 2.4.

2.5 Direct Reduction of Sulphides

2.5.1 Thermodynamics of the direct reduction of sulphides

The free energy of formation of some metal sulphides have been plotted in Figure 2.16 [44] and it can be seen that the affinity of metals for sulphur decreases with temperature, a significant decrease in entropy occurs on the formation of metal sulphide. CS_2 is one of the least stable sulphides and carbon cannot be directly used to reduce sulphides in the same manner as it is used for oxides. The relative affinities of some metals for oxygen and sulphur can be deduced from Figure 2.17 [45] in which the standard free energy for the reaction:

$$2MS_{(s)} + O_{2(g)} = 2MO_{(s)} + S_{2(g)} \qquad [2.6]$$

has been plotted against temperature for various metals, carbon and hydrogen. The relatively high affinity of manganese, the alkali and alkaline earth metals for sulphur is of great importance in the removal of sulphur from iron and steel.

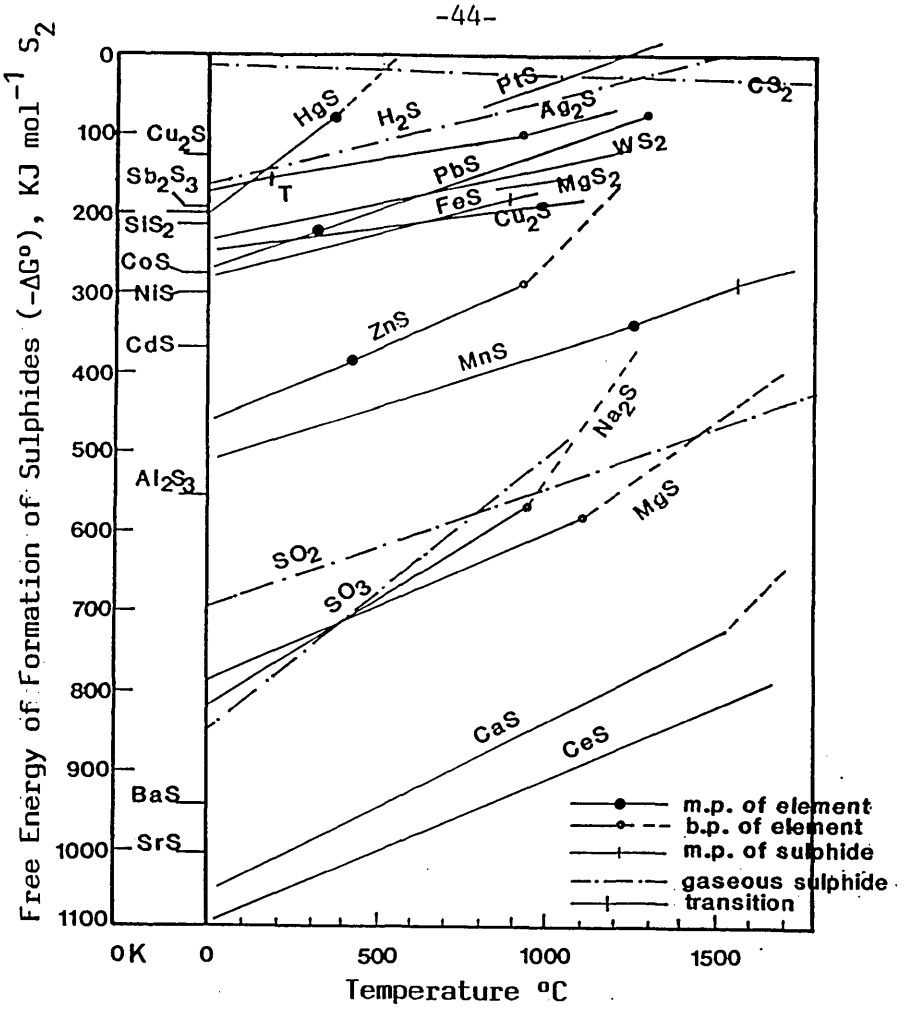

FIGURE 2.16: The Standard Free Energy of Formation of Sulphides [44]

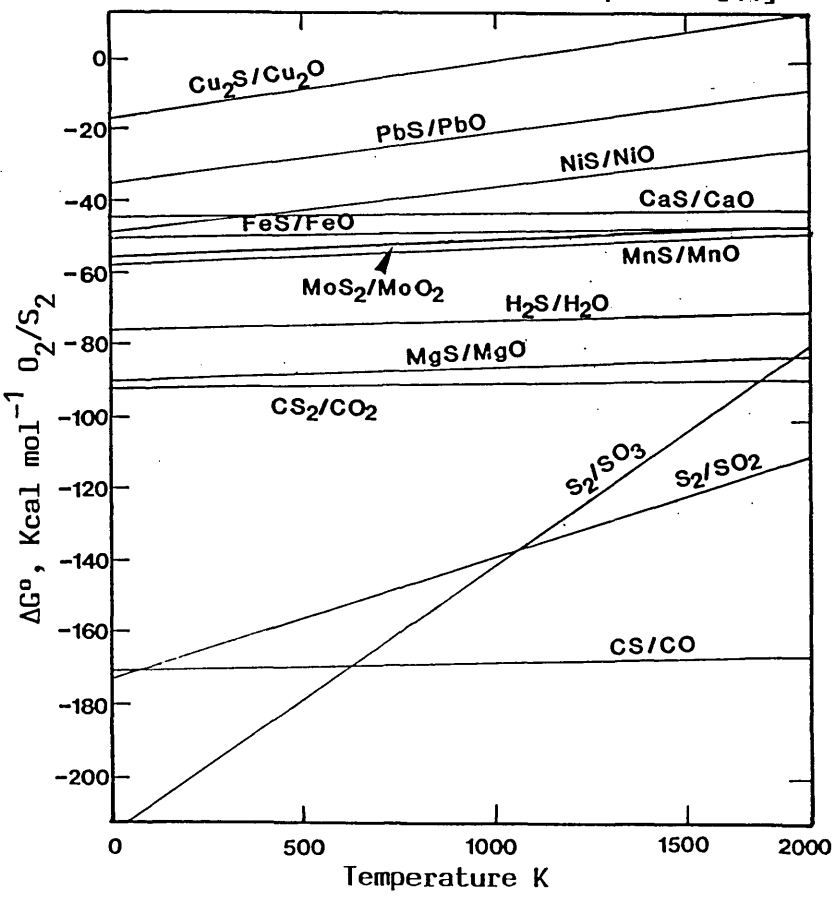

FIGURE 2.17: Relative Affinities of Some Elements for Sulphur and Oxygen [45]

In most cases, the entropy change in the reaction represented by equation 2.6 is small indicating that the relative affinity of metals for oxygen and sulphur does not change significantly with temperature for most metals the major exceptions being lead, copper and nickel. The affinities of oxygen for sulphur in SO_2 and SO_3 have also been included. Below 1073K, SO_3 is more stable than SO_2 which becomes more stable at higher temperatures. The affinities of hydrogen and carbon for sulphur are lower than their affinity for oxygen. These are so low that sulphides can neither be directly reduced by hydrogen nor by carbon at temperatures normally attainable in practice.

The single stage direct reduction of metal sulphide can be represented as:

$$2MS_{(s)} + C_{(gr)} = 2M_{(s)} + CS_{2(g)} \qquad [2.7]$$

$$MS_{(s)} + CO_{(g)} = M_{(s)} + COS_{(g)} \qquad [2.8]$$

$$MS_{(s)} + H_{2(g)} = M_{(s)} + H_2S_{(g)} \qquad [2.9]$$

Thermodynamically, these reactions are unfavourable at reasonably high temperatures because of a higher chemical potential of sulphur in the gaseous products. This is evident from the very low equilibrium constant values for such direct reduction reactions (Table 2.5).

In order to alter the equilibrium, it is necessary to provide a sink for the sulphur thereby decreasing the P_{CS_2}, P_{H_2S} or P_{COS} values and this is usually achieved by the use of basic oxides such as CaO, MgO, BaO and Na_2O. When carbonates are used, they can act as both sulphur fixing and reducing agents. For example, sodium carbonate can be used as:

$$4MS_{(s)} + 4Na_2CO_{3(s)} = 4M_{(s)} + 3Na_2S_{(s)} + Na_2SO_{4(s)} + 4CO_{2(g)} \qquad [2.10]$$

The use of calcium carbide provides another example of a compound acting as both exchange and reducing agents. The use of CaC_2 could lead to

Sulphide	I	Ia	II	IIa	III	IIIa
Bi_2S_3	4.39	8.23×10^{3}	2.04×10^{-1}	1.17×10^{4}	9.19×10^{-2}	2.02×10^{4}
Ag_2S	2.52×10^{-1}	1.27×10^{2}	1.10×10^{-2}	9.13×10	2.94×10^{-2}	4.64×10^{3}
Sb_2S_3	1.77×10^{-1}	3.29×10^{2}	8.16×10^{-3}	4.68×10^{2}	3.67×10^{-3}	8.08×10^{2}
PbS	7.36×10^{-2}	3.74×10	3.22×10^{-3}	2.68×10	8.60×10^{-3}	1.35×10^{3}
Co_9S_8	3.57×10^{-2}	1.82×10	1.57×10^{-4}	1.30×10	4.18×10^{-3}	6.58×10^{2}
Ni_3S_2	6.50×10^{-3}	3.30	3.45×10^{-4}	2.87	2.54×10^{-3}	4.00×10^{2}
FeS	4.90×10^{-3}	2.45	2.13×10^{-4}	1.77	5.68×10^{-4}	8.95×10
CdS	4.48×10^{-3}	2.42	2.09×10^{-4}	1.73	5.58×10^{-4}	8.81×10
MoS_2	2.76×10^{-3}	1.40	1.21×10^{-4}	1.01	4.91×10^{-3}	7.70×10^{2}
Cu_2S	1.13×10^{-3}	6.58×10^{-1}	5.71×10^{-5}	4.76×10^{-1}	1.53×10^{-4}	2.41×10
ZnS	8.10×10^{-6}	4.07×10^{-3}	3.55×10^{-7}	2.95×10^{-3}	9.44×10^{-7}	1.49×10^{-1}

* data at 1000K

Direct H_2 reduction $MS + H_2 = M + H_2S$ (I)

Lime-enhanced H_2 reduction $MS + CaO + H_2 = M + CaS + H_2O$ (Ia)

Direct CO reduction $MS + CO = M + COS$ (II)

Lime-enhanced CO reduction $MS + CaO + CO = M + CaS + CO_2$ (IIa)

Direct carbon reduction $MS + \frac{1}{2}C = M + \frac{1}{2}CS_2$ (III)

Lime-enhanced carbon reduction $MS + CaO + C = M + CaS + CO$ (IIIa)

TABLE 2.5: Equilibrium Constants for the Direct Reduction of Metal Sulphides by H_2, CO and Carbon [46,47,48]

(continued ...)

Lime-Sulphidation Reactions

Sulphidation Reaction	Equilibrium constants		ΔH^o Kcal mol^{-1}s	
	1000K	1200K	1000K	1200K
$CaO + H_2S = CaS + H_2O$	1.88×10^3	5.08×10^2	-15.5	-15.7
$CaO + COS = CaS + CO_2$	5.74×10^4	8.30×10^3	-23.0	-23.1
$CaO + \frac{1}{2}CS_2 = CaS + \frac{1}{2}CO_2$	1.69×10^5	2.27×10^4	-23.8	-24.0

TABLE 2.5 (continued)

Equilibrium Constants for the Direct Reduction of Metal Sulphides by H_2, CO and Carbon [46,47,48]

high energy costs since to produce CaC_2, lime and carbon have to be mixed and heated to very high temperatures (2000^oC). However, its' use avoids the formation of undesirable oxysuphide intermediate compounds.

Carbon, carbon monoxide and hydrogen are the most common reducing agents usually employed in practise. But the use of CO and H_2 are not always feasible due to the possible occurence of back reactions involving the CO_2 and H_2O product gases.

The effectiveness, low cost and relative abundance of lime and carbon (in the form of coal) make them the prime choice as exchange and reducing agents for the direct reduction of metal sulphides.

The use of lime as an exchange medium for S^{2-} and O^{2-} ions, and carbon as reductant can be represented as:

$$MS_{(s)} + CaO_{(s)} = MO_{(s)} + CaS_{(s)} \qquad [2.11]$$

$$MO_{(s)} + C_{(gr)} = M_{(s)} + CO_{(g)} \qquad [2.12]$$

and the overall carbothermic reduction reaction can be written as:

$$MS_{(s)} + CaO_{(s)} + C_{(gr)} = M_{(s)} + CaS_{(s)} + CO_{(g)} \qquad [2.13]$$

Lime-metal sulphide interaction data for various sulphides have been compiled in Table 2.6.

Except in the case of ZnS, all other lime-enhanced sulphide reduction reactions considered (Table 2.5), are thermodynamically feasible. The exothermic nature of the lime-sulphidation reactions result in favourable heats of reaction for the direct reduction of most sulphides.

The quantity of lime required to contain sulphur emission during the direct reduction of various sulphides depends on the nature of the

$\Delta G^o = A + BT$ (cal $mol^{-1}s$)

		A	B
	$\langle FeS \rangle + \langle CaO \rangle = \langle FeO \rangle + \langle CaS \rangle$	-4000	0.66
††	$\langle COS \rangle + \langle CaO \rangle = \langle CoO \rangle + \langle CaS \rangle$	-1644	11.16
	$\langle ZnS \rangle + \langle CaO \rangle = \langle ZnO \rangle + \langle CaS \rangle$	6630	-3.49
	$\langle Ni_3S_2 \rangle + 2\langle CaO \rangle = 2\langle NiO \rangle + 2\langle CaS \rangle + \langle Ni \rangle$	10620	-0.13
	$\langle PbS \rangle + \langle CaO \rangle = \langle PbO \rangle + \langle CaS \rangle$	11130	-0.24
	$\langle Cu_2S \rangle + \langle CaO \rangle = \langle Cu_2O \rangle + \langle CaS \rangle$	13250	-8.54
	$\langle MoS_2 \rangle + 2\langle CaO \rangle = \langle MoO_2 \rangle + 2\langle CaS \rangle$	800	-5.96
	$\langle CuFeS_2 \rangle + 2\langle CaO \rangle = \frac{1}{2}\langle Cu_2O \rangle + \langle FeO \rangle + 2\langle CaS \rangle + \frac{1}{4}(O_2)$	27435	-5.93
	$\langle Sb_2S_3 \rangle + 3\langle CaO \rangle = \langle Sb_2O_3 \rangle + 3\langle CaS \rangle$	-5400	-2.79
	$\langle As_2S_3 \rangle + 3\langle CaO \rangle = \langle As_2O_3 \rangle + 3\langle CaS \rangle$	-2580	-2.86

†† for the free energy of CoS, the data for $CoS_{(1+x)}$ has been taken, $x = 0.04$ [48]

TABLE 2.6

Lime-Metal Sulphide Interaction Data

sulphide, the reduction temperature, relative particle sizes of the sulphide/lime mixtures (in solid-solid reduction reactions) and on the flow rate of reducing gas in situations where a gaseous reducing agent is used.

2.5.2 Mechanism of Direct Sulphide Reduction

Two different mechanisms have been proposed for the direct reduction of metal sulphides. One mechanism suggests that the reaction occurs in two steps - the conversion of metal sulphide into oxide followed by the reaction of oxide.

$$MS_{(s)} + CaO_{(s)} = MO_{(s)} + CaS_{(s)} \qquad [2.11]$$

$$MO_{(s)} + C_{(gr)} = M_{(s)} + CO_{(g)} \qquad [2.12]$$

$$MO_{(s)} + CO_{(g)} = M_{(s)} \quad CO_{2(g)} \qquad [2.14]$$

$$MO_{(s)} + H_{2(g)} = M_{(s)} \quad H_2O_{(g)} \qquad [2.15]$$

Such an 'oxide intermediate' mechanism has been suggested by various workers [50,51,52] who have reported the formation of metal oxides during direct reduction reactions.

An alternative mechanism involving solid-solid reactions occurring through gaseous intermediates, has been suggested by Abramowitz and Rao [53] in their study of the direct reduction of zinc sulphide. The reaction sequence invovles the production of gaseous sulphur species which then react with the sulphur acceptor. The relevant reactions can be represented as:

$$MS_{(s)} + CO_{(g)} = M_{(s)} + COS_{(g)} \qquad [2.8]$$

$$MS_{(s)} + H_{2(g)} = M_{(s)} + H_2S_{(g)} \qquad [2.9]$$

$$COS_{(g)} + CaO_{(s)} = CaS_{(s)} + CO_{2(g)} \qquad [2.16]$$

$$H_2S_{(g)} + CaO_{(s)} = CaS_{(s)} + H_2O_{(g)} \qquad [2.17]$$

When carbon is used as the reducing agent, the CO is generated by the Boudouard reaction

$$C_{(gr)} + CO_{2(g)} = 2CO_{(g)} \qquad [2.18]$$

2.5.3 Carbothermic Reduction of Sulphides

A number of studies have been carried out on the carbothermic reduction of metal sulphides. Jha [52] has investigated the reduction mechanism of copper sulphides, iron sulphides and chalcopyrite with lime and carbon as exchange and reducing agents. Reaction with lime led to the formation of compounds and solid solutions during the reduction process. Temporary cessation of reaction was observed in some cases and conditions necessary for the complete reduction of sulphide within an hour at temperatures less than 1000^{o}C was established.

During the reduction of copper sulphide (Cu_2S), the formation of a pseudo-ternary Cu_2 S-Cu_2O-CaS liquid saturated with CaS was reported and the overall reaction rate was determined by the carbon gasification reaction. Under conditions where the rate of reduction is less than the rate of exchange reaction, oxygen concentration builds up near the lime-oxysulphide liquid interface resulting in an oxygen activity sufficient to oxidise CaS to $CaSO_4$ at which stage the transport of O^{2-} ions is towards the CaS-$CaSO_4$ interface and CO evolution ceases. Such a reversion of oxygen transport does not occur when graphite is replaced by coal or CO, leading to faster reaction rates without temporary cessations.

In the reduction of iron sulphide, the formation of a quarternary liquid belonging to the Fe-Ca-S-O system was observed. The presence of this liquid above 850^{o}C, enhances the rate of reduction. Apart from the quarternary liquid, the formation of two oxy-sulphide intermediate compounds [1:33 CaS:FeO and FeS.CaO], was also reported. Their exact composition and crystal structures was not determined.

The intermediate compounds 1.33CaS.FeO and FeS.CaO were also formed during the carbothermic reduction of chalcopyrite ($CuFeS_2$) and their presence again enhances the rate of reaction. The nucleation of copper occurs first, followed by the reduction of iron calcium oxysulphide to iron.

The possibility of the extraction of nickel from nickel sulphide by carbothermic reduction was investigated by Machingawuta and Jha [54] in the temperature range, 800-950^{o}C. They reported that the reduction is assisted by the presence of liquid Ni_3S_2 above 800^{o}C. A high lime and carbon to sulphide ratio was necessary to obtain complete reduction. Complete reduction of nickel sulphide was achieved in 20 mins at 950^{o}C.

The reaction system ZnS-CaO-C has been investigated by Abramowitz [55] who studied the direct reduction of zinc sulphide with carbon and lime producing zinc vapour, carbon monoxide and a solid calcium sulphide residue. He reported that temperature history curves displayed arrests and that the overall process is limited by heat transfer. The reaction rate was described by two expressions, a third order equation (first order with respect to each reactant concentration) below 945^{o}C; and by a first order rate equation with respect to zinc sulphide concentration above 945^{o}C.

Rao and El-Rahaiby [56] have investigated the carbothermic reduction of lead sulphide between 795^{o}C and 989^{o}C. Samples of PbS:4CaO:4C mixtures were reacted isothermally in inert (nitrogen) atmospheres. The kinetics of reduction were determined for both the catalysed and the uncatalysed reduction processes by thermogravimetry.

The extent of catalysis was significant and 10-fold rate increases were obtained with some catalysts. The following ranking was developed for the various catalysts;

Li_2CO_3 > Rb_2CO_3 > ternary $(K, Li, Na)_2CO_3$ eutectic = NaF = K_2CO_3 > Na_2CO_3 > Na_2SO_4.

The gas evolved was reported to be virtually free of SO_2 and chemical analysis confirmed that virtually all the sulphur in the reactant is

retained as calcium sulphide in the final product.

Panfilov [57] has studied the direct reduction of various metal sulphides with CaC_2. The reactions can be represented by the general equation

$$MS_{(s)} + CaC_{2(s)} = M_{(s)} + CaS_{(s)} + 2C_{(gr)} \qquad [2.19]$$

The reduction of Cu_2S starts at 600°C and proceeds slowly reaching a maximum of 71.8% completion after 60 mins at 1200°C. PbS reduction begins at 600°C and nears completion (97.4%) in 60 mins at 1200°C. ZnS reduction is complete in 30 mins at 1200°C. The reaction of FeS with CaC_2 starts at 300°C and is 80% complete in 90 mins at 1200°C. After 5 mins reduction at 1200°C, 94.0, 90.0, 69.0, 50.0% of the ZnS; PbS; FeS and Cu_2S respectively were reduced by CaC_2.

2.5.4 Hydrogen reduction of sulphides

Several studies have been carried out on the hydrogen reduction of metal sulphides both in the presence and absence of basic oxides. The thermodynamic feasibility of the reduction of metal sulphides using hydrogen can be deduced from Table 2.5.

The values of the equilibrium constants show that the hydrogen reduction of metal sulphides is thermodynamically less feasible compared with carbothermic reduction at similar temperatures.

Habashi and Dugdale [51] studied the kinetics of the hydrogen reduction of copper and iron based sulphide minerals and their observations were consistent with the results of an earlier investigation by Cech and Tieman [58]. In the absence of CaO, approximately 80% of iron contained in bornite (Cu_3FeS_2) was recovered by hydrogen reduction at 800°C. When the hydrogen reduction of bornite was carried out using lime as an exchange agent, the removal of iron was found to decrease when the lime:sulphide ratio was higher than 1.25:1.

The hydrogen reduction of stibnite (Sb_2S_3) in the absence and presence of sulphur acceptors has been investigated by Torma and Inal [59] between 200°C and 600°C. The activation energy of these processes were found to be 17.4 kcal mol^{-1} (~$7.2x10^4$J), 20.4 $Kcalmol^{-1}$ (~$8.5x10^4$J) and 27.7$Kcalmol^{-1}$ (~11.6 x 10^4J) in the absence of sulphur acceptors, with calcium oxide and with magnesium oxide respectively. The purity of the antimony metal produced varied between 98.0% and 99.5%.

Prasad and Mankhand [60] have surveyed the available literature on the hydrogen reduction of sulphides and summarised the kinetic data obtained by several authors.

During the hydrogen reduction of sulphides, the possibility exists that the moisture formed might render the atmosphere sufficiently oxidising as to favour the formation of oxide rather than metal.

CHAPTER 3

EXPERIMENTAL

CHAPTER 3

EXPERIMENTAL

Thermogravimetric techniques were used to study the reaction kinetics while X-ray diffraction, optical and electron microscopy were used to identify and study the phases present in the reaction product.

3.1 Apparatus

A schematic diagram of the experimental apparatus is shown in Figure 3.1. It consists of a furnace (1), quartz reaction tube (2) and a load cell (3) for continuous monitoring of weight changes of the sample (4). Gas flow rates were measured using a flowmeter (8) and a rotameter (10).

3.1.1 Furnace and Reaction Tube

Figure 3.2 shows a schematic illustration of the furnace and reaction tube. The furnace tube (M) is made of mullite, 65mm outside diameter and 350mm long wound with Kanthal A-1 wire of 60 ohm resistance. A layer of Kaowool (K), 115 mm thick serves as insulation. The furnace is mounted on a guide system (G) which facilitates the raising and lowering of the furnace around the reaction tube. The whole assembly is supported on a frame (F). The furnace temperature is controlled by a eurotherm controller activated by a Pt/Pt-13% Rh thermocouple placed adjacent to the furnace windings.

Figure 3.3 shows a plot of temperature profile along the furnace length.

A constant temperature zone ($\pm$ 2^{o}C) about 40mm long was obtained and this was adequate for the experimental investigations. Typical temperature profiles in the furnace with the reaction tube in position are shown in Figure 3.4.

The quartz reaction tube (R) is made of two parts. The upper section is connected by a cone and socket joint (J) to the load cell while the lower

1 Furnace
2 Quartz reaction tube
3 Load cell
4 Sample
5 Thermocouple
6 Refractory plug
7 Needle valve
8 Flowmeter
9 Drying column
10 Rotameter
11 Deoxidising furnace
12 Valve
13 Stopcock
14 Gas cylinder
15 Two pen chart recorder (wt. loss α temp)
16 Power supply unit and temperature controller

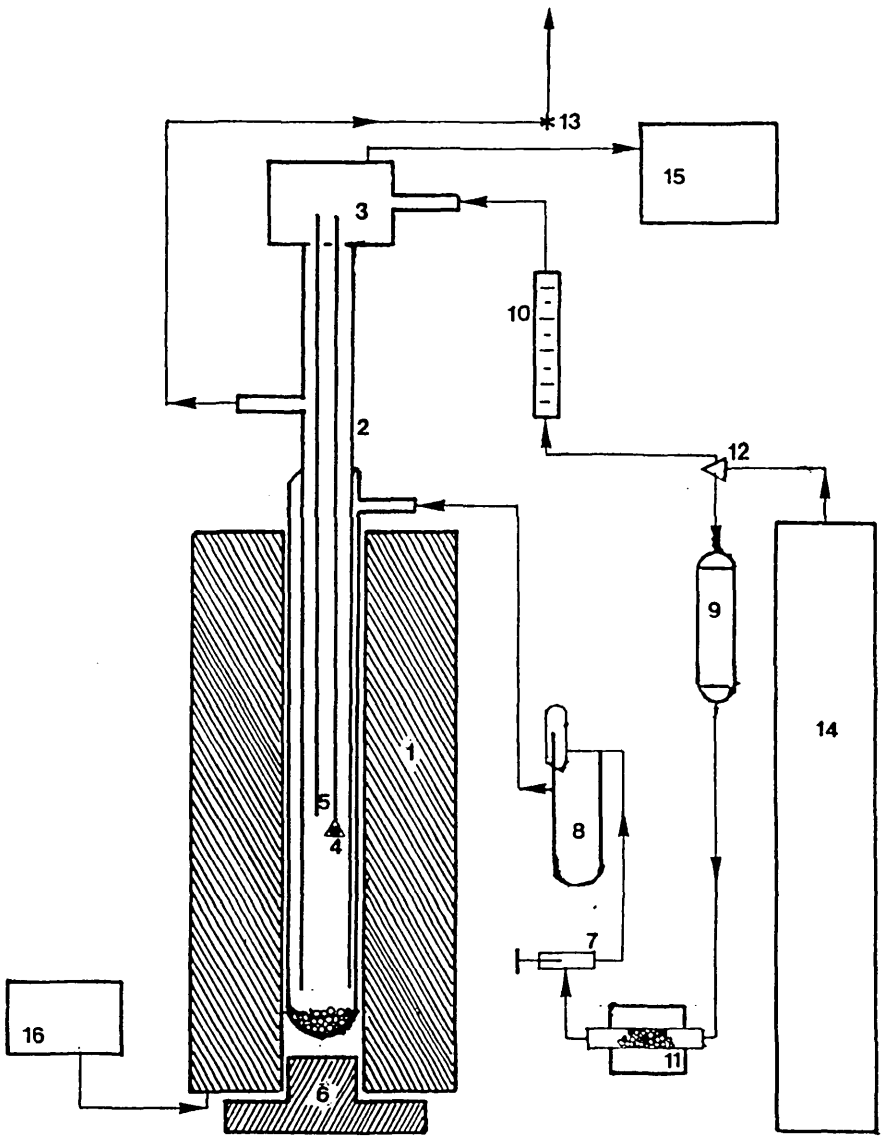

FIGURE 3.1: Schematic diagram of apparatus

A Sample thermocouple
B Split sleeve
C Alumina chips
D Quartz tube
E Water cooled housing
F Angle-iron frame
G Guide line
H Counter weight
I Gas inlet
J Cone and socket joint
K Kaowool packing
L Sample suspension chain
M Mullite tube
O Gas outlet
P Plug
R Quartz reaction tube
S Sample
Z Power supply

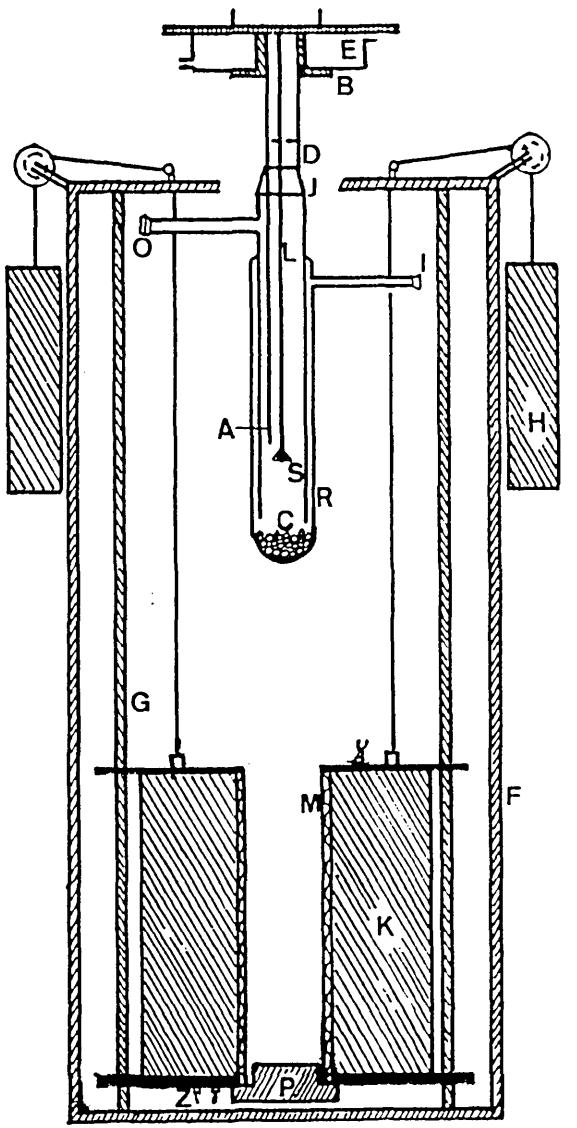

FIGURE 3.2: Schematic diagram of furnace and reaction tube

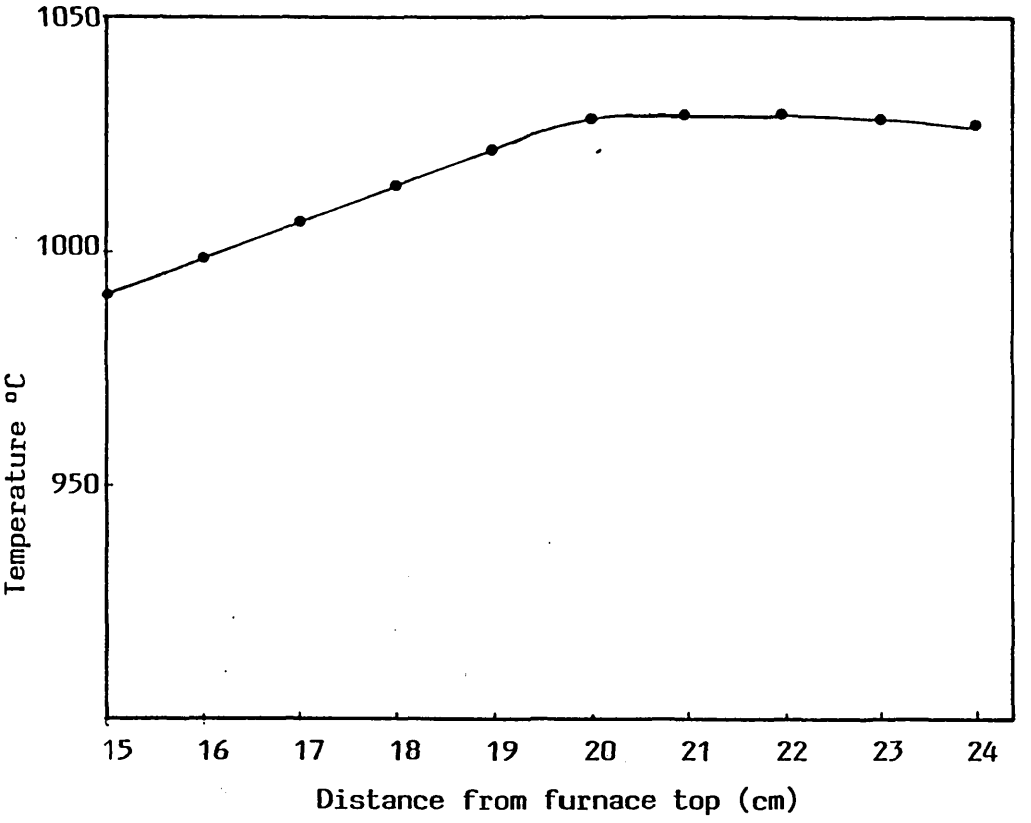

FIGURE 3.3: Temperature profile along furnace length

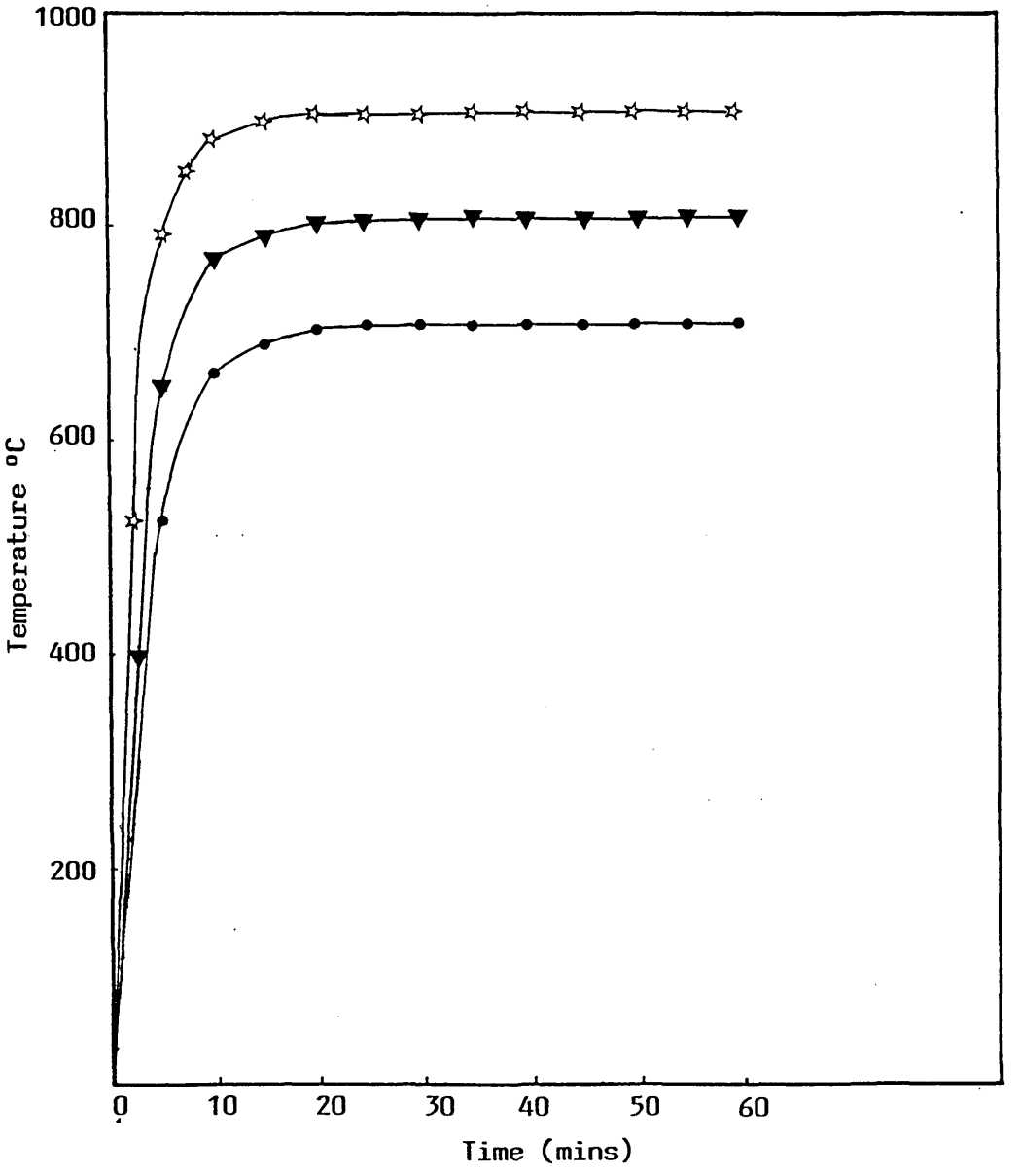

FIGURE 3.4: Typical temperature curves with reaction tube in position

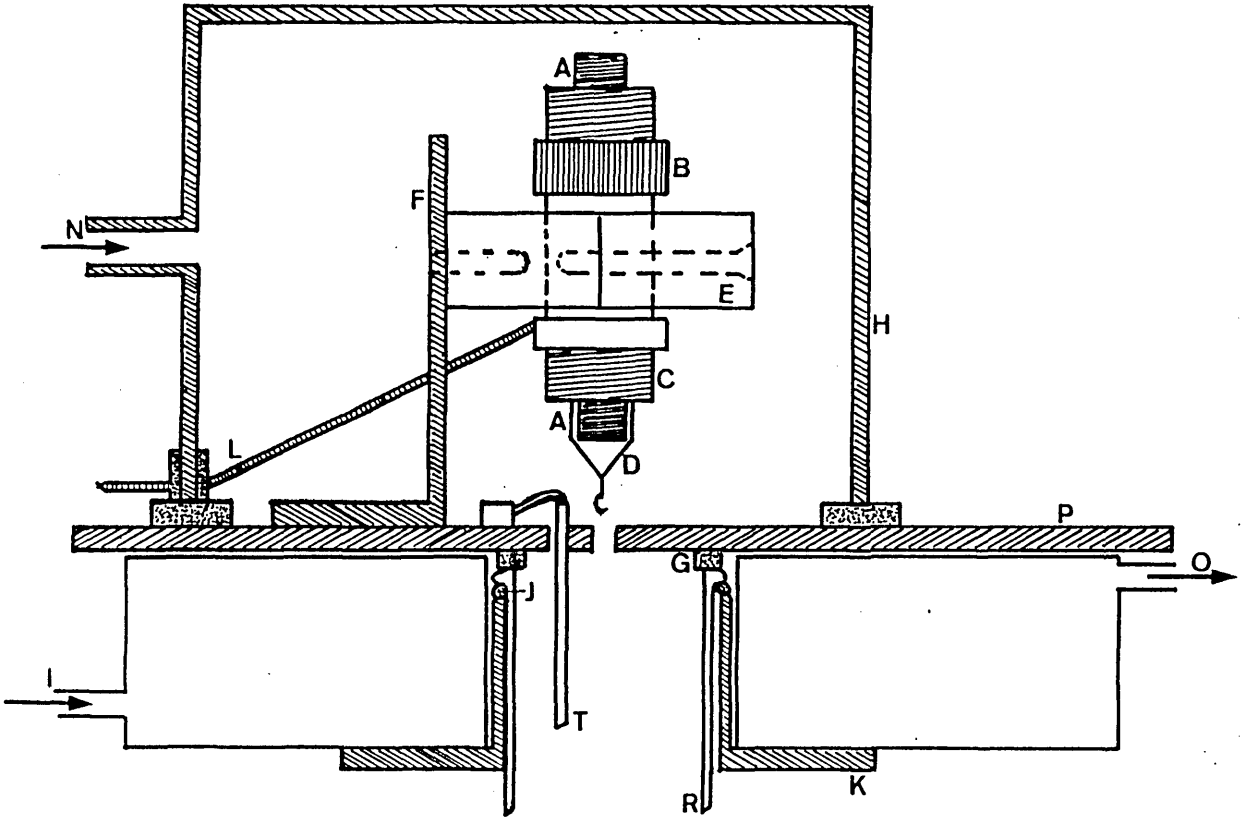

A Armature of load cell
B Zero adjustment
C Alumina adapter
D Platinum wire and hook
E Perspex holder
F Load cell support
G Rubber pad
H Load cell housing
I Water inlet
J Rubber 'O' ring
K Split brass sleeve
L Electrical leads
N Argon gas inlet
O Water outlet
P Mild steel plate
R Quartz reaction tube
T Thermocouple

FIGURE 3.5: Schematic diagram of load cell and mounting

section consists of two concentric tubes 35mm and 50mm internal diameter with gas inlet (I) and outlet (O) tubes. A bed of alumina chips (C), 30mm deep ensures adequate gas pre-heating and uniform distribution. The inert gas is initially deoxidised and preheated by passing it through a mullite tube furnace filled with titanium granules and maintained at 700^{o}C.

The upper section of the reaction tube contains a disc with two holes, 5mm and 3mm diameter which allow entry for the suspension wire (L) and thermocouple (A). The disc prevents the exit gas from entering the load cell housing. This section of the reaction tube which is held in position by a split brass sleeve (B) is water cooled (E). The thermocouple tip was sheathed with an alumina sleeve. The sample crucibles were made from silica tubes (9mm internal diameter).

3.1.2 Load cell and sample suspension

The weight of the sample undergoing reaction was determined from the voltage output of the load cell which was connected to a chart recorder, which was also set up to record the sample temperature in mV. Thus a continuous recording of weight changes and temperature was made by the chart recorder. The load cell (Figure 3.5) is enclosed in a box (H) and mounted on a water-cooled mild steel plate (P).

A constant flow of argon gas through the load cell housing maintains it at a constant temperature and prevents the entry of hot gases from the reaction chamber. The load cell was calibrated by measuring the voltage output for a series of known weights suspended from it.

3.2 Materials

3.2.1 Solid Reactants

The chemical composition of antimony sulphide concentrates used in this investigation are shown in Table 3.1. This was supplied by Cookson Ceramics and Antimony Limited. The arsenopyrite concentrate

	Bolivian (wt %)	Canadian (wt %)	South African (wt %)	Sb_2S_3 (wt %)
Sb	63.90	67.60	55.10	71.70
S	27.80	24.90	21.40	28.30
As	0.06	0.17	0.20	
Pb	0.13	0.16	0.15	
Cu	0.08	0.02	0.13	
Ni	0.02	0.02	0.02	
Fe	3.00	0.72	2.25	
HCl insoluble gangue	1.40	4.20	13.30	
H_2SO_4 insoluble gangue	1.10	3.70	12.40	

TABLE 3.1

Chemical Analysis of Antimony Sulphide Concentrates

Tetrahedrite	wt %
Cu	27.15
Fe	6.29
Zn	6.42
Pb	1.06
Sb	6.99
As	8.95
S	26.52
SiO_2	5.99

Arsenopyrite	wt %
As	25.60
Fe	31.00
S	18.60
Cu	0.09
Sb	<0.50
SiO_2	12.62
Al_2O_3	2.55

TABLE 3.2

Chemical Analysis of Arsenopyrite and Tetrahedrite Concentrates

	Weight %
Total carbon	59.50
Fixed carbon	48.40
Hydrogen	3.60
Sulphur	0.34
Ash	2.65
Loss at 105°C	23.30

TABLE 3.3

Chemical Analysis of Collie Coal

		Impurity content in ppm						
Gas	Content %	O_2	H_2	N_2	CH_4	CO_2	H_2O	Others
Ar	99.90	4	1	15	1	-	-	20

TABLE 3.4

Impurity Content of Argon

investigated is from the Zimbabwe Bar 20 Goldmine, while the tetrahedrite is from Peru and the analysis of these are presented in Table 3.2. The analysis of the collie coal is presented in Table 3.3. The unmilled ores and collie coal were crushed and sieved using 106, 63 and 45 μm BS410 sieves. The specpure graphite was of pelletable grade with a total maximum impurity content of 5 ppm.

Reagent grade CaO, MgO, Sb_2O_3 have been used in the appropriate reduction reactions. Analar grade antimony, arsenic, iron, copper, sulphur, and iron sulphide were used in the preparation of various synthetic complex sulphides.

3.2.2 Gases

High purity Argon was obtained from BOC Limited. The impurity content quoted by the supplier is shown in Table 3.4.

3.3 Reduction Procedure

Appropriate quantities of sulphide were mixed with freshly calcined lime and graphite/coal in the required stoichiometric amounts, and mixed overnight on a roll mixer. The mixture was formed into a cylindrical pellet using a steel die of 6.25mm diameter under constant load.

The pellet was then placed in a silica crucible (15mm deep, 9mm internal diameter) which was suspended from the load cell. The quartz reaction tube was then put in place and the gas inlet and outlet tubes connected (Figure 3.2). Gas flow was started and maintained for 15 minutes to flush out the system and create an inert atmosphere. The furnace, at the appropriate reaction temperature was then rasied onto the reaction tube and the reaction started. The voltage output from the load cell (and thus the weight changes of the pellet), and the sample temperature were continously monitored and displayed on a chart recorder. At the completion of an experiment, the furnace was lowered and the sample allowed to cool in a flowing stream of argon. The weight of the pellet before and after the reaction was determined using an analytical balance.

Weight changes obtained were always in good agreement with that indicated by the chart recorder (±5%).

A representative portion of the sample was subjected to X-ray diffraction analysis. The remainder was mounted and examined microscopically.

The particle size of the pellets in the reduction experiments was within the range -106 + 45 μm. In the reduction experiments, liquid phases formed hence the relative particle sizes had a negligible effect on the rate of reduction.

3.4 Synthesis of Complex Sulphides

Complex sulphides were prepared by the reaction of their elemental components in sealed evacuated silica glass capsules.

Reaction samples of the desired composition were prepared from pure elements. Cylindrical pellets of this mixture were kept in a silica tube which was evacuated and sealed off.

The silica capsules were then placed in a horizontal muffle furnace. Temperatures in the furnace were measured with a NiCr/NiAl thermocouple.

At the completion of the run, the capsules were withdrawn and quenched in water. The reacted samples were then analysed using X-ray diffraction techniques.

In all the complex sulphides synthesised, vapour and liquid phases co-existed with the sulphides at the reaction temperatures. Thus, towards the end of the heating period, the silica tubes were moved in the furnace so as to give a gradient of about $5^{o}C$ along its length. Within a relatively short time, the co-existing liquid collects at the cool end of the silica tube making it easy to separate it from the main sulphide phase after quenching.

3.5 Characterisation of Phases

3.5.1 X-ray diffraction (XRD)

The phases present in the reacted samples were determined by X-ray powder diffraction analysis of finely ground representative specimens using a Guinier focussing camera with a monochromatised CoK_{α} radiation. On this instrument, four patterns can be obtained simultaneously on the same piece of film, this allows a quick and easy comparison to be made. The exposure time was 4 hours using a voltage of 30 kV and a current of 20 mA. Quartz was used as an internal standard.

3.5.2 Optical Microscopy

After reaction, the samples were mounted in araldite which gives excellent impregnation. The surface of the mounted pellet was exposed by grinding on silicon carbide paper of grades 400, 600, 800 and 1200, followed by polishing with 14, 6, 3 and 1 μm hyprez diamond lapping compounds. The phases present and their morphology were identified from micrographs taken by a microscope mounted Nikon camera.

3.5.3 Scanning electron microscopy (SEM)

The JOEL T220 scanning electron microscope was used to examine polished specimens. The energy dispersive spectrum (EDS) gave a qualitative analysis of elements with atomic numbers greater than 10. The specimens were coated with a thin film of carbon, ~100 μm thick, before examination in order to improve specimen conductivity.

CHAPTER 4

RESULTS AND DISCUSSION

CHAPTER 4

RESULTS AND DISCUSSION

In this chapter, the results and discussion of the reactions of antimony sulphides, iron-arsenic sulphides, copper-arsenic sulphides and copper-antimony sulphides with lime and graphite/coal at various temperatures are presented.

The phases present at various stages of the reaction were determined by X-ray diffraction, while the rates of reaction were determined by a thermogravimetric technique. The percentage weight loss is defined as:

$$\%\text{wt. loss} = \frac{\Delta W}{W_o} \times 100$$

Where appropriate, the extent of reduction was determined from the weight loss curves by taking into account the volatile species present and relating this to the phases observed by X-ray diffraction analysis. The rate of reduction is defined as:

$$\%\ \text{reduction} = \frac{W_o - W}{W_o - W_{WC}} \times 100$$

where W_o = weight of original sample
W = weight of the sample at a given time
W_{WC} = theoretical weight of the sample after complete reduction.

4.1 The Carbothermic Reduction of Antimony Sulphides

4.1.1 Exchange reaction between antimony sulphide and lime

The reaction between antimony sulphide (Sb_2S_3) and lime (CaO) [exchange reaction] was studied at 700°C, 800°C, and 900°C. Figures 4.1 and 4.2 illustrate the weight losses obtained during reaction with stoichiometric and 100% excess quantitites of lime. Table 4.1 shows the X-ray diffraction analyses of the reaction products.

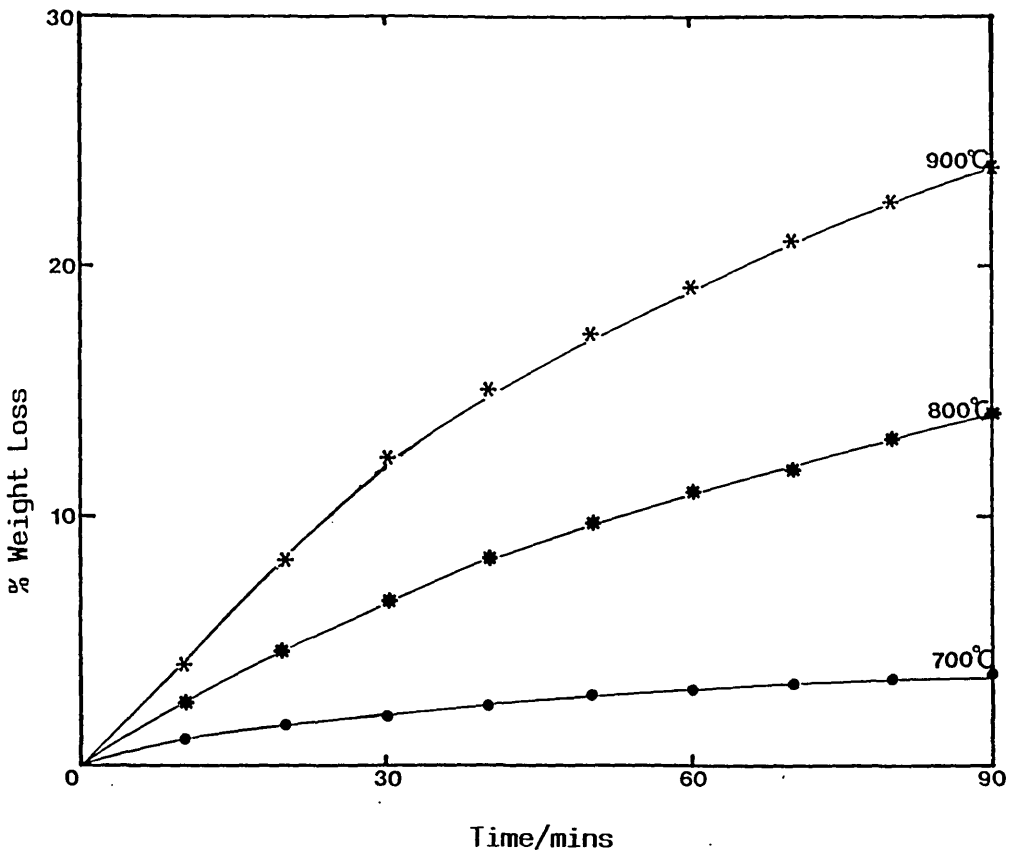

FIGURE 4.1

Rate of Weight Loss for the Exchange Reaction of Antimony Sulphide [Sb_2S_3:CaO (1:1)] at Various Temperatures

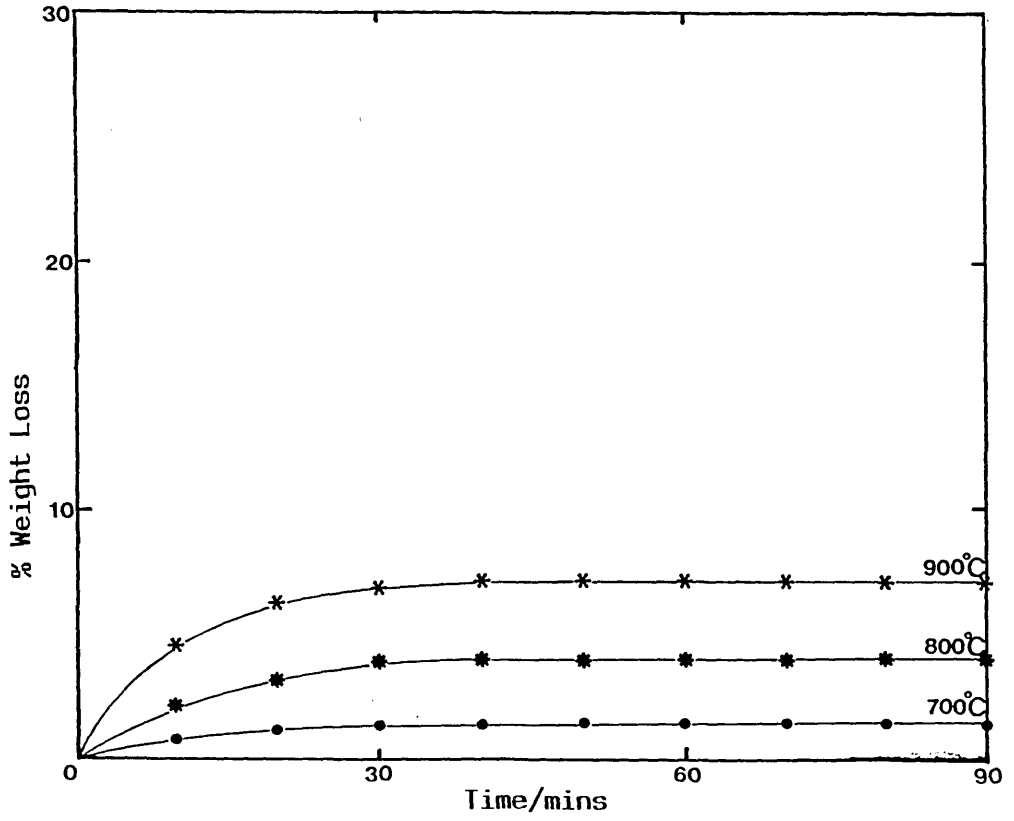

FIGURE 4.2

Rate of Weight Loss for the Exchange Reaction of Antimony Sulphide with Enhanced Lime [Sb_2S_3:CaO (1:2)] at Various Temperatures

Pellet Composition - Sb_2S_3:CaO (1:1)

Temp (°C)	Reaction Time (mins)	Mass Balance % wt Loss	Phase Analysis Sb_2S_3	CaO	$Ca_2Sb_2O_5$	CaS	Sb_2OS_2
700	90	3.8	W	MW	M	MW	M
800	90	14.0	W	-	S	S	-
800	30	6.6	W	-	S	S	-
800	15	3.6	W	-	MS	MS	-
900	90	24.0	VW	-	MS	MS	-

Pellet Composition - Sb_2S_3:CaO (1:2)

700	90	1.4	W	MW	S	S	-
800	90	4.0	W	MW	VS	VS	-
800	30	3.8	W	MW	VS	VS	-
800	10	2.0	W	MW	VS	VS	-
900	90	7.2	W	W	S	S	W

Phase Analysis intensity:

VS - Very Strong
VW - Very Weak
W - Weak
MS - Medium Strong
S - Strong
VVW - Very Very Weak
MW - Medium Weak
M - Medium

TABLE 4.1

Mass Balance and Phase Analysis of the Products of Antimony Sulphide-Lime Exchange Reaction

The weight losses observed during these reactions result mainly from the volatilisation of Sb_2S_3 with the rate of volatilisation increasing with temperature. X-ray diffraction analysis indicate the formation of calcium antimonate - $Ca_2Sb_2O_5$ ($2CaO.Sb_2O_3$) and calcium sulphide - CaS. The exchange reaction is incomplete at all temperatures. The use of excess lime (100%) leads to the formation of increased quantities of calcium antimonate and sulphide indicating more favourable reaction kinetic conditions. The antimonate phase - $Ca_3Sb_2O_6$ ($3CaO.Sb_2O_3$) richer in CaO is also present in the reaction product resulting from the use of excess lime at 900°C.

The results of the exchange reactions conducted at 800°C for short reaction times (30 mins, 15 mins, 10 mins) are included in Table 4.1. A comparison of these results with those obtained from 90 minute reaction times indicate that the exchange reactions occur rapidly at the early stages of the heat treatment periods and subsequent weight losses are due to the volatilisation of unreacted Sb_2S_3, as well as uncombined Sb_2O_3.

The reaction of stoichiometric quantities of antimony sulphide and lime at 700°C produced an antimony oxysulphide - Sb_2OS_2 [1/3 Sb_2O_3.2/3 Sb_2S_3] in addition to the formation of calcium antimonate [$Ca_2Sb_2O_5$]. The diffraction pattern obtained for this reaction product includes other reflexions which are relatively weak in intensity but do not correspond to any of the previously mentioned product phases they are probably due to the presence of an Sb-Ca-S-O quarternary oxysulphide. Available data on the phases present in this system is quite limited. These oxysulphides were absent in the reaction product of the lime-sulphide reaction using 100% excess lime at 700°C.

Plate 4.1 shows an electron micrograph of the reaction product obtained after the exchange reaction between sulphide and lime (stoichiometric ratio) at 800°C for 90 minutes. On the micrograph, calcium sulphide appears dark while the bright areas are calcium antimonates - ($Ca_2Sb_2O_5$). The two phases are evenly distributed throughout the pellet and there is no evidence of any melting of the calcium antimonate.

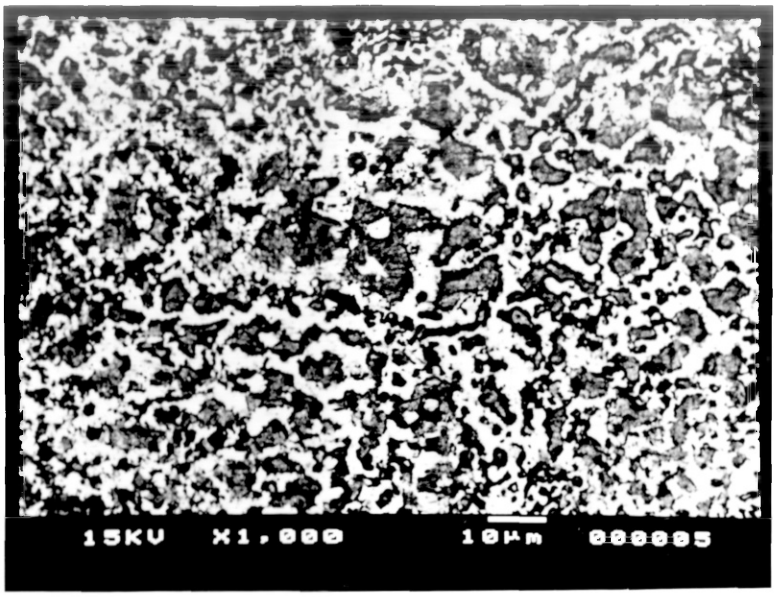

PLATE 4.1

Electron micrograph of antimony sulphide-lime exchange reaction [800°C] product [back scattered electron (BSE) image]

4.1.2 Reduction of antimony sulphide

Plots of % weight loss against time for the carbothermic reduction [with coal and lime as reductant and exchange reagent respectively], of synthetic antimony sulphide (Sb_2S_3) and the Canadian, Bolivian and South African antimony sulphide concentrates are shown in Figures 4.3, 4.4, 4.5 and 4.6 respectively. Figure 4.7 shows the result obtained on reduction with graphite while Figure 4.8 shows the weight loss curves obtained for the collie coal reduction of Sb_2O_3. The results of the X-ray diffraction analyses for these reduction reactions are shown in Table 4.2.

As expected, the reduction rates are dependent on temperature. The weight loss curves show a change in gradient at the completion of reaction due to the cessation of CO gas evolution. The subsequent weight loss is due to the volatilisation of antimony.

A comparison between the weight loss curves for the reduction of synthetic and natural antimony sulphides with coal indicates a similarity in their rate profiles. Figure 4.3 shows that the reduction of synthetic Sb_2S_3 is complete after 40 minutes reaction at 700^{o}C (weight loss = 15.0%). X-ray diffraction analysis of the reaction product shows the absence of Sb_2S_3 indicating complete reaction. The points of inflexion on the rate curves (corresponding to complete reduction) occur after about 10.0 minutes and 5.0 minutes at 800^{o}C and 900^{o}C respectively. Subsequent weight loss occurring beyond these points is due to the volatilisation of the antimony product and this is also dependent on temperature.

The rate of reduction of the antimony sulphide - Canadian concentrate is faster than that of the synthetic sulphide and the reaction is complete after about 30 minutes at 700^{o}C, 7.5 minutes at 800^{o}C and 2.5 minutes at 900^{o}C. This is due to a higher Sb:S ratio in the concentrate.

The Sb:S ratio in the Bolivian concentrate is much less than that of the synthetic sulphide while the value for the South African ore is slightly more. The rate of carbothermic reduction of the Bolivian concentrate (complete reduction takes up to 60 minutes at 700^{o}C) is much lower than for the synthetic sulphide while that for the South African ore is similar.

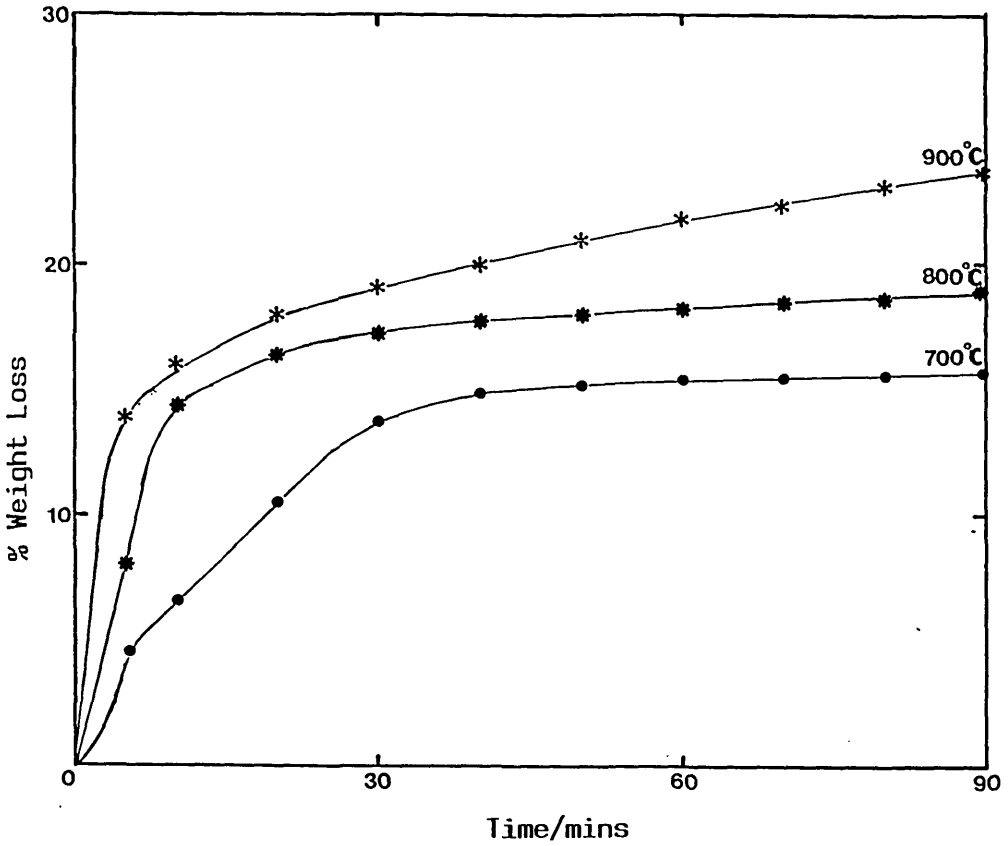

FIGURE 4.3

Rate Plot for the Carbothermic Reduction of Antimony Sulphide with Collie Coal at Various Temperatures

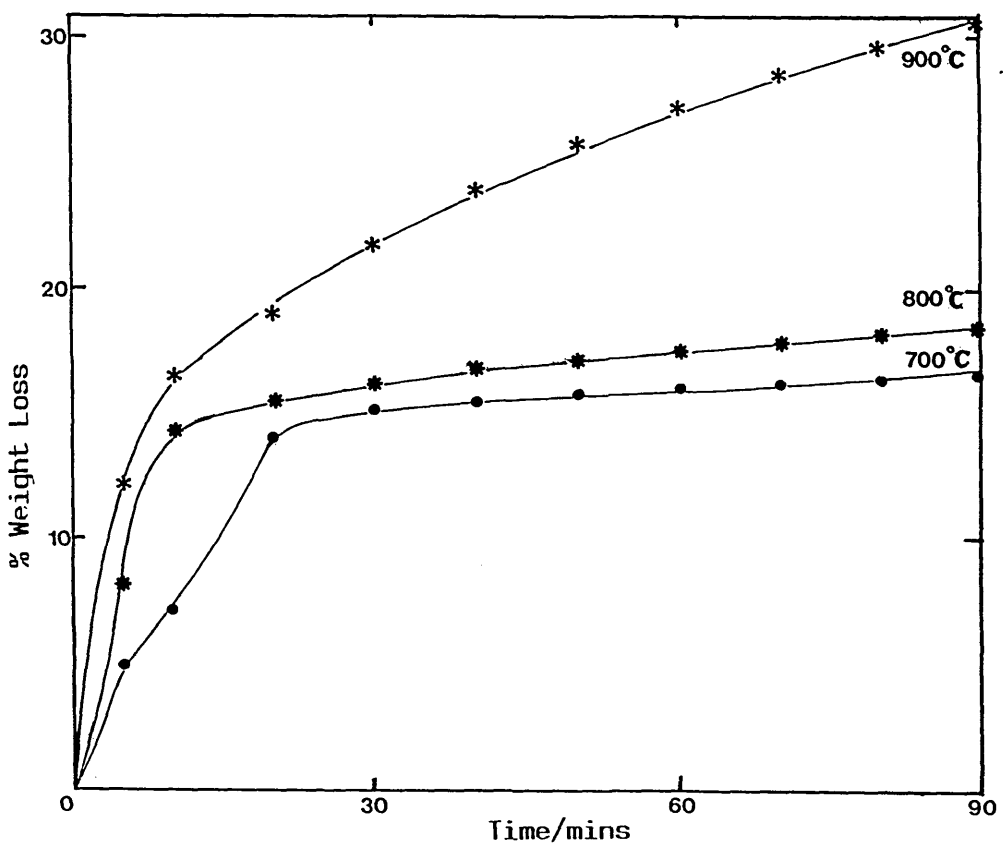

FIGURE 4.4

Rate Plot for the Carbothermic Reduction of Antimony Sulphide (Canadian Concentrate) with Collie Coal at Various Temperatures

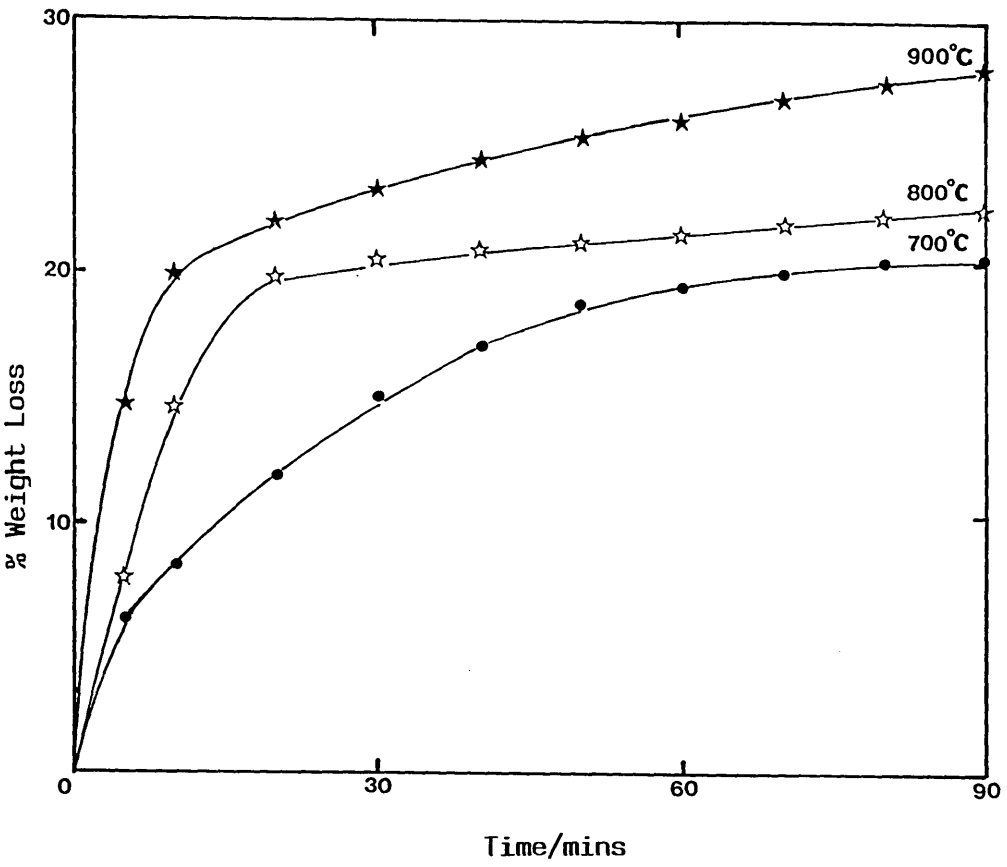

FIGURE 4.5

Rate Plot for the Carbothermic Reduction of Antimony Sulphide (Bolivian Concentrate) with Collie Coal at Various Temperatures

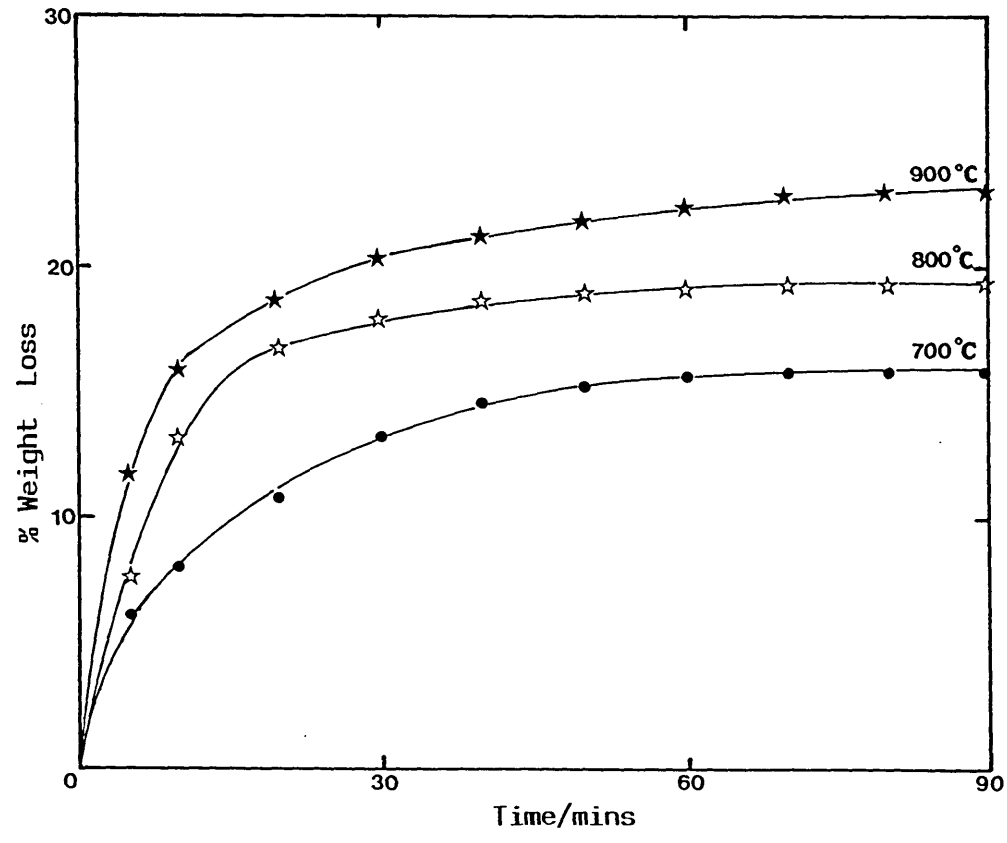

FIGURE 4.6

Rate Plot for the Carbothermic Reduction of Antimony Sulphide (South African Concentrate) with Collie Coal at Various Temperatures

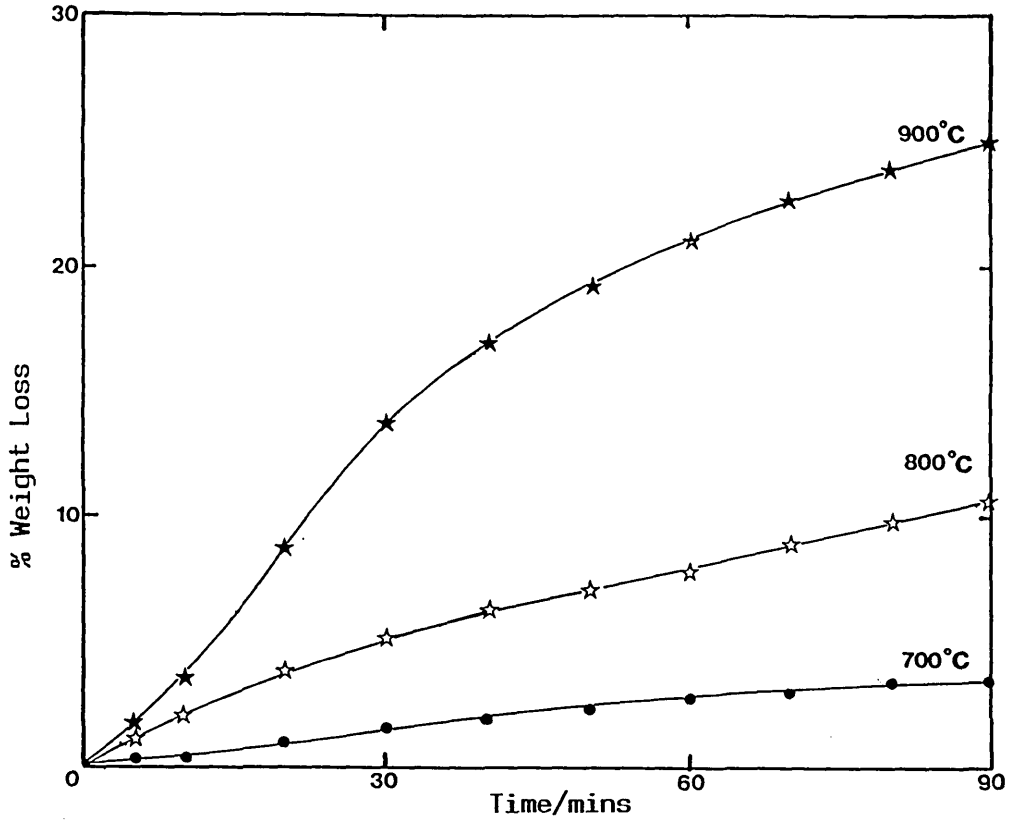

FIGURE 4.7

Rate Plot for the Carbothermic Reduction of Antimony Sulphide with Graphite at Various Temperatures

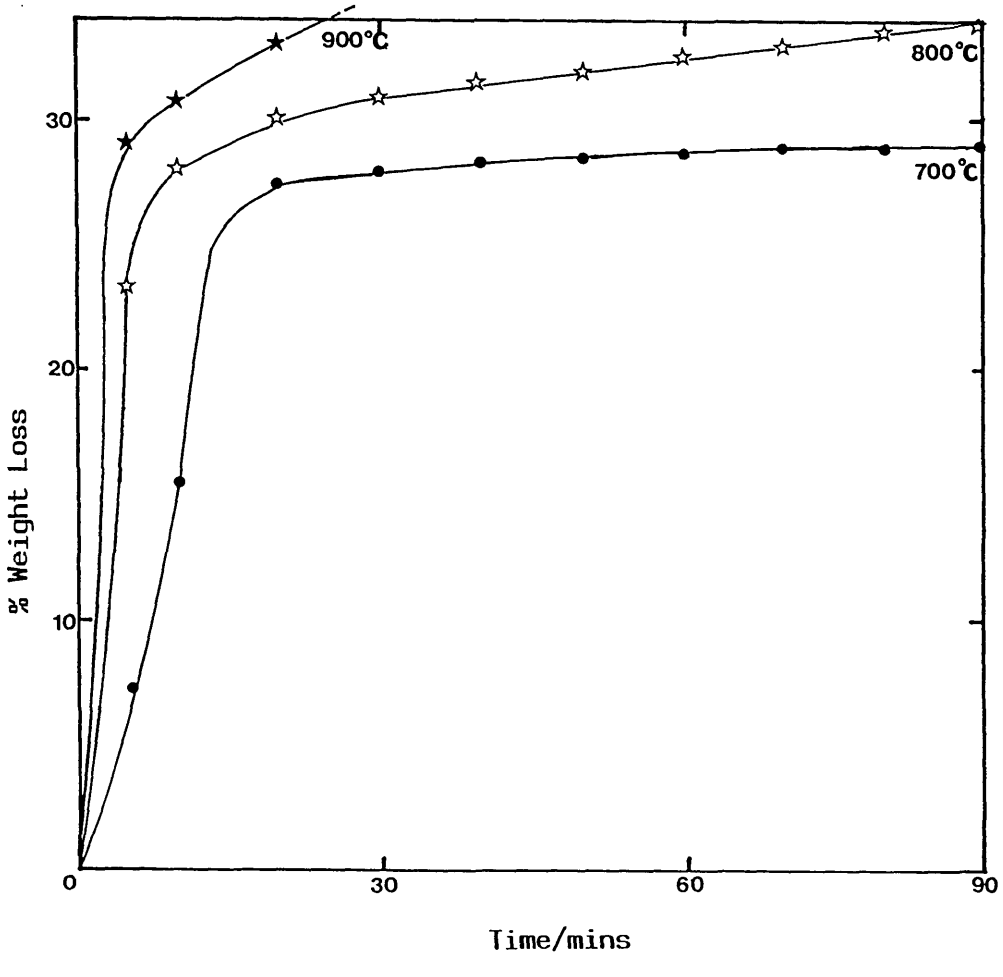

FIGURE 4.8

Rate Plot for the Reduction of Antimony Oxide with Collie Coal at Various Temperatures

Pellet Composition - Synthetic Sb_2S_3:CaO:C_{Coal} (1:1:1)

Temp (°C)	Mass Balance % wt Loss	Reaction Time (mins)	Phase Analysis Sb_2S_3	CaO	CaS	Sb	$Fe_{1-x}S$	Fe
700	10.2	20	W	VW	M	MS		
700	15.8	40	-	-	VS	VS		
700	16.8	90	-	-	VS	VS		
800	19.4	90	-	-	VS	VS		
900	25.0	90	-	-	S	S		
Pellet Composition - Sb_2S_3(Canadian Concentrate):CaO:C_{Coal} (1:1:1)								
700	14.2	20	VW	VVW	MS	S		
700	15.6	40	-	-	VS	VS		
700	16.7	90	-	-	VS	VS		
800	19.4	90	-	-	VS	VS		
900	30.6	90	-	-	S	VS		
Pellet Composition - Sb_2S_3(Bolivian Concentrate):CaO:C_{Coal} (1:1:1)								
700	20.5	90	-	-	VS	VS	VW	--
800	22.4	90	-	-	VS	VS	VW	--
900	28.1	90	--	-	VS	S	VVW	VW

TABLE 4.2

Mass Balance and Phase Analysis of the Products of the Carbothermic Reduction of Antimony Sulphides

(continued....)

Pellet Composition - $Sb_2S_{3(South\ African)}$:CaO:$C_{Coal}$ (1:1:1)

Temp (°C)	Mass Balance wt Loss %	Reaction Time (mins)	Phase Analysis					
			Sb_2S_3	CaO	CaS	Sb	$Fe_{1-x}S$	Fe
700	15.8	90	-	VW	VS	VS	VW	-
800	18.8	90	-	VW	VS	VS	VW	-
900	24.0	90	-	VW	VS	.S	VVW	VW

Pellet Composition - Synthetic Sb_2S_3:CaO:$C_{graphite}$ (1:1:1)

Temp (°C)	Mass Balance wt Loss %	Reaction Time (mins)	Phase Analysis					
			Sb_2S_3	CaO	Sb	CaS	$Ca_2Sb_2O_5$	Sb_2OS_2
700	3.6	90	W	MW	VW	W	MW	M
800	10.6	90	W	-	W	M	MS	-
900	25.0	90	VW	-	MW	S	W	-
900	18.1	45	VW	-	MW	MS	W	-

TABLE 4.2

Mass Balance and Phase Analysis of the Products of the Carbothermic Reduction of Antimony Sulphides

(continued...)

Pellet Composition - Sb_2O_3:C_{Coal} (1:1)

Temp (°C)	Mass Balance wt % Loss	Reaction Time (mins)	Phase Analysis Sb_2O_3	Phase Analysis Sb
700	10	16.8	MS	S
700	15	26.6	-	VS
700	90	28.8	-	VS
800	90	34.0	-	VS
900	90	37.6	-	VS

Phase Analysis Intensity:

VS - Very Strong
VW - Very Weak
W - Weak
MS - Medium Strong
S - Strong
MW - Medium Weak
M - Medium
VVW - Very Very Weak

TABLE 4.2

Mass Balance and Phase Analysis of the Products of the Carbothermic Reduction of Antimony Sulphides

Thus, the rate of reduction is dependent on the Sb:S ratio in the pellet. The increased weight losses obtained during the reduction of the Bolivian and South African concentrates is due to the volatilisation of impurities (e.g. As) which are present in larger amounts in these ores. X-ray diffraction analysis of the reaction products indicates that the partial reduction of $Fe_{1-x}S$ present in these concentrates occurs at 900°C resulting in the formation of some iron metal.

The isothermal weight loss curves determined at 700°C, 800°C and 900°C for the reduction of synthetic antimony sulphide by graphite, with lime, as sulphur acceptor, are shown in Figure 4.7. The weight loss obtained after 90 minutes reaction at 700°C and 800°C is less than the theoretically predicted value for complete reduction (15.4%) indicating that the reduction reaction is incomplete. However, the reduction is almost complete at 900°C and the inflexion point on the weight loss curve after 35 minutes reaction time suggests that no appreciable reduction occurs after this stage. This is confirmed by results of the X-ray diffraction analysis of the reaction product. Volatilisation of antimony accounts for the subsequent weight losses observed. Reduction with collie coal proceeds faster at all temperatures compared with graphite reduction and complete reduction is attained at temperatures as low as 700°C with coal.

In Figure 4.8, the weight loss curves determined for the isothermal reaction between antimony (III) oxide and coal are shown. Reduction of the oxide occurs rapidly at all temperatures leading to the formation of liquid antimony with the evolution of CO. The initial volatilisation of antimony oxide and the antimony product contributes to the weight losses resulting in total weight loses which are more than the theoretically expected value (22.9.%). The effect is more marked at higher temperatures as the antimony species become more volatile. The rapid rate of the coal reduction of antimony sulphide indicates that the reduction step is unlikely to be rate-controlling in the overall carbothermic reduction process.

Three distinct regions can be identified in the various isothermal weight loss curves. The first step (I) corresponding to the most rapid

weight losses involve the initial volatilisation of antimony sulphide and volatiles contained in coal (where coal is used as reductant). Reduction reactions begin at the later stages of this step as the crucible temperature rises. The second step (II) mainly involves the reduction reactions and this is followed by the third step (III) during which the volatilisation of the reaction product occurs. Reduction is usually complete at the end of the second step. The linear rates observed in step II can be identified with the carbothermic reduction reactions and can be described reasonably well by the linear rate law

$$\alpha = Kt \qquad [4.1]$$

α - rate of reduction
K - rate constant
t - time

The temperature dependence of reaction rates is best described by the Arrhenius relationship

$$K = A\exp-\frac{E}{RT} \qquad [4.2]$$

where K - rate constant
R - gas constant
E - activation energy
T - temperature

Figure 4.9 shows plots of lnK against 1/T for the antimony oxide and antimony sulphide reduction reactions.

The activation energies for the coal reduction of antimony sulphide and antimony oxide have been determined to be 114 KJ mol^{-1} and 94 KJ mol-1 respectively from the plot illustrating the temperature dependence of their rate constants (Figure 4.9).

Plate 4.2 shows an electron micrograph of the antimony sulphide pellet reduced with coal at 700^{o}C for 90 minutes with CaO acting as sulphur

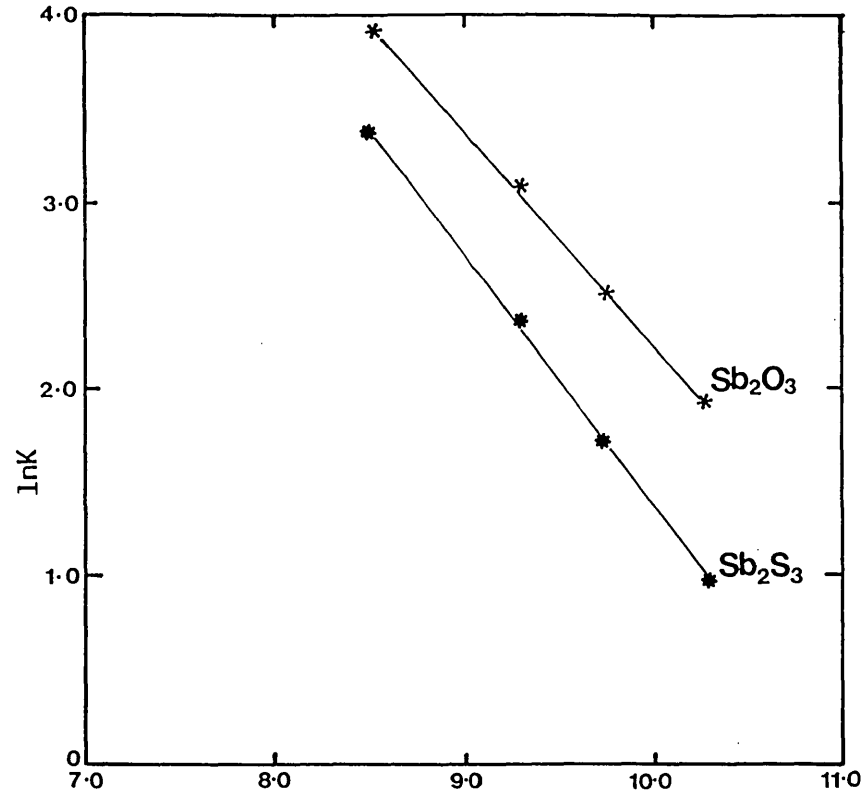

FIGURE 4.9

Temperature Dependance of Rate Constants for the Reduction of Antimony Sulphide and Antimony Oxide

acceptor. Liquid antimony (light phase) occurs throughout the pellet and solid calcium sulphide shows as the dark regions.

The formation of voids is due to the volume change resulting from the reduction of sulphide to metal (loss of CO). On cooling, the liquid antimony tends to agglomerate into large globules some of which exude and collect on the pellet surface. Plate 4.3 illustrates droplets of antimony formed on the pellet surface after carbothermic reduction of antimony sulphide at 700°C for 90 minutes. Droplet formation on the pellet surface was not observed after reduction at higher temperatures. Longer periods of heat treatment led to the enlargement of the antimony droplets indicating that they were probably being 'fed' through capillaries connected to 'pools' of liquid metal in the pellet.

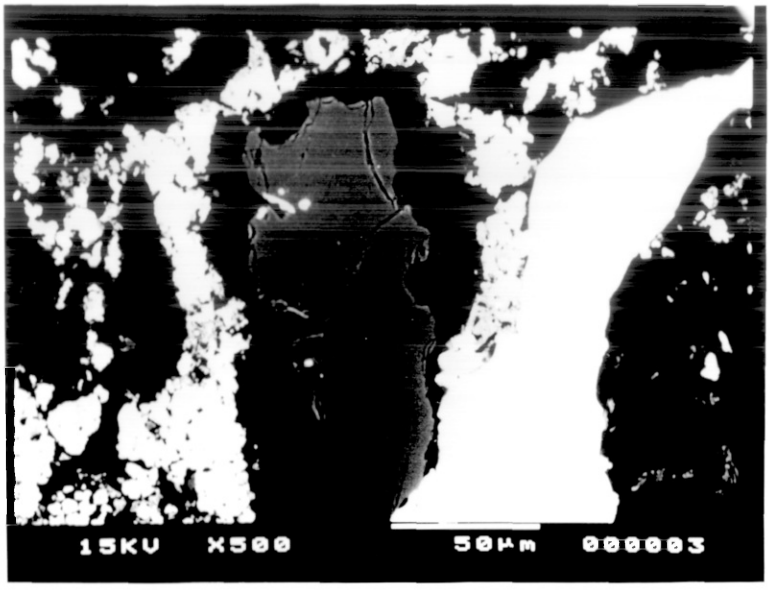

PLATE 4.2

Electron micrograph of antimony sulphide concentrate reduced with collie coal at 700°C for 90 mins [BSE image]

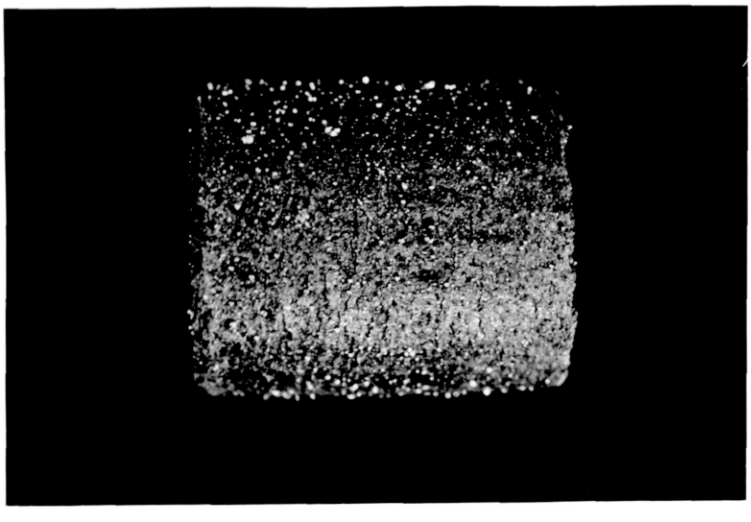

PLATE 4.3

Photograph of antimony sulphide concentrate pellet reduced with collie coal at 700°C for 90 mins - illustrating the formation of antimony globules on the pellet surface (x7)

In order to determine whether the reaction conditions contribute to the coalescence and formation of antimony droplets on the pellet surface, experiments in which pellets containing varying ratios of Sb:CaS were heat-treated in a flowing stream of argon at 700°C, were conducted. The formation of a few droplets occurred at high Sb:CaS ratios after long periods of heat treatment; no droplets were formed in pellets with an antimony concentration less than that of the Sb:CaS (1:1) sample. This indicates that the conditions present during the carbothermic reduction reactions enhance the formation of the antimony droplets.

4.1.3 Discussion of the carbothermic reduction of antimony sulphide

The rate of carbothermic reduction with graphite is much slower than with coal and X-ray diffraction analysis of the reaction products indicate the presence of unreacted antimony sulphide and oxide even after reaction at 900°C. At 700°C, two pseudo-binary compounds belonging to the $CaO-Sb_2O_3$ and $Sb_2O_3-Sb_2S_3$ systems are present in the reaction product. The presence of antimony oxide indicates that the exchange reaction represented by:

$$Sb_2S_{3(s)} + 3CaO_{(s)} = Sb_2O_{3(s)} + 3CaS_{(s)} \qquad [4.3]$$

is not the rate limiting step during the graphite carbothermic reduction of antimony sulphide. In the overall carbothermic reduction reaction represented by

$$Sb_2S_{3(s)} + 3CaO_{(s)} + 3C_{(gr)} = 2Sb_{(l)} + 3CaS_{(s)} + 3CO_{(g)} \qquad [4.4]$$

The graphite reduction of the intermediate oxide cannot keep up with the rate at which the exchange reaction generates the intermediate antimony oxide phase leading to the accumulation of antimony oxide which forms pseudo-binary compounds with CaO and Sb_2S_3. Wanmaker, Hoekstra and Verriet [61] have investigated the thermal stability of various calcium antimonates. On heating in inert (nitrogen) atmospheres, $Ca_3Sb_2O_6$ and $Ca_2Sb_2O_6$ were reported to be stable up to 1200°C while $CaSb_2O_4$ which is less stable begins to decompose at about 950°C. The relative stability of $Ca_2Sb_2O_5$ and the limited quantity of CaO present in the reacting pellet explains why this phase is formed in preference to the other calcium antimonates.

The limited information available on the ternary system makes it difficult to establish the thermodynamic stability of the antimony oxysulphide phase formed during the antimony sulphide-lime reactions. But the fact that $Sb_2OS_2[1/3Sb_2O_3.2/3Sb_2S_3]$ is a naturally occuring oxysulphide mineral - Kermesite [62] indicates that it is relatively stable at low temperatures.

The Sb_2O_3-Sb_2S_3 pseudo-binary phase diagram drawn by Quercigh [63] indicates the probable presence of a phase (80 mol % Sb_2S_3) stable up to about 525^{o}C. The Kermesite formula $Sb_2OS_2[1/3Sb_2O_3.2/3Sb_2S_3]$ indicate an Sb_2S_3 concentration of 67 mol % in this oxysulphide compound. X-ray diffraction analysis of the various reaction products containing this oxysulphide phase indicates that it is formed from the reaction of excess Sb_2O_3 (after the formation of calcium antimonate-$2CaO.Sb_2O_3$) with unreacted Sb_2S_3. The large quantities of unreacted Sb_2S_3 present after reaction at 700^{o}C enhances the formation of the antimony oxysulphide.

The absence of the antimony oxide intermediate compound in the partially reacted sample during the reduction of antimony sulphide with coal strongly suggests that the reduction of the oxide takes place much faster than the lime-sulphide exchange reaction can produce the antimony oxide intermediate. The faster rate of the reduction reaction indicates that the rate of reaction will be dependent on the rate at which the exchange reaction takes place.

In order that a reaction may proceed, reactants must be brought to the reaction site and the reaction products removed from it. Thus it is usual to find diffusion and other transport mechanisms to be the rate controlling factor in most reactions. However in the carbothermic reduction of antimony sulphide where one the reactants - Sb_2S_3 (m.p. 550^{o}C), the intermediate product - Sb_2O_3 (m.p. 650^{o}C) and two the reaction products - Sb (m.p. 630^{o}C) and CO (gas) are fluid at the reaction temperatures (700-900^{o}C); it is unlikely that solid diffusion governs the rate of reaction.

The activation energy of 114 kJ mol^{-1} determined for the lime fluxed coal reduction of antimony sulphide is more than the value of 85 kJ mol^{-1} determined for the lime fluxed hydrogen reduction of antimony sulphide by Torma and Inal [59]. This indicates that the carbon reduction is more dependent on temperature since the relationship

$$\frac{d\ln K}{dT} = \frac{E}{RT^2} \qquad [4.5]$$

E - activation energy
K - rate constant
T - temperature
R - gas constant

implies that the greater the activation energy for a reaction, the greater the corresponding increase of reaction rate with temperature.

The limited contact between CaS and the metallic antimony phase observed in the micrograph of the reacted pellet (Plate 4.2) indicates that the wettability of calcium sulphide by antimony is not very significant. This is probably a contributory factor in the formation of antimony droplets on the pellet surface (Plate 4.3). The droplets are fed by capillaries which connect them to the pools of liquid metal in the pellet. The formation and evolution of CO gas during the reduction reaction probably enhances the development of these capillaries which channel liquid antimony to the pellet surface in the path of the evolving CO gas. At the pellet surface, the liquid metal coalesces forming droplets which sit on the pellet surface. The droplets grow in size as they are continuously fed from liquid metal pools inside the pellet through the interconnecting capillaries. At higher temperatures, the higher vapour pressure of antimony leads to its increased volatilisation from the pellet surface.

4.2 The Carbothermic Reduction of Iron-Arsenic Sulphides

The results of the exchange and reduction reactions of arsenopyrite (FeAsS) are presented in this section.

4.2.1 Exchange reactions between arsenopyrite and lime

The rates of weight loss for the isothermal reaction between arsenopyrite concentrate and lime are shown in Figure 4.10 while Figure 4.11 shows the result obtained for initial reaction at 600^{o}C followed by an increase in temperature to 1000^{o}C at an average heating rate of 10^{o}C/min. Results of X-ray diffraction studies of the reaction products are presented in Table 4.3.

The exchange reactions result in the total oxidation of the arsenic component of the complex sulphide to arsenic trioxide $As_4O_6(g)$ and the partial oxidation of the iron component to iron oxide (FeO) leaving behind unreacted pyrrhotite ($Fe_{1-x}S$).

The large weight loss observed is due to the volatilisation of $As_4O_6(g)$ and the observed weight loss at 1000^{o}C is close to the theoretical value of 25.1% expected for the total loss of arsenic as its oxide - $As_4O_6(g)$.

X-ray diffraction studies of the reaction products also show the formation of the oxysulphide phase (1.33) CaS.FeO at all temperatures. Reactions at higher temperatures produce larger quantities of this phase resulting from greater oxidation of $Fe_{1-x}S$ and the subsequent reaction of the products of reaction; FeO with CaS.

Plates 4.4 and 4.5 illustrate the lime exchange reaction products for arsenopyrite concentrate and synthetic arsenopyrite respectively. The white regions represent the oxysulphide [(1.33) CaS.FeO] phase while calcium sulphide (CaS) appears as grey and pyrrhotite ($Fe_{1-x}S$) is black.

A higher Fe:As ratio in the concentrate leads to an increased content of unreacted pyrrhotite ($Fe_{1-x}S$) in the reaction product as observed in the micrographs.

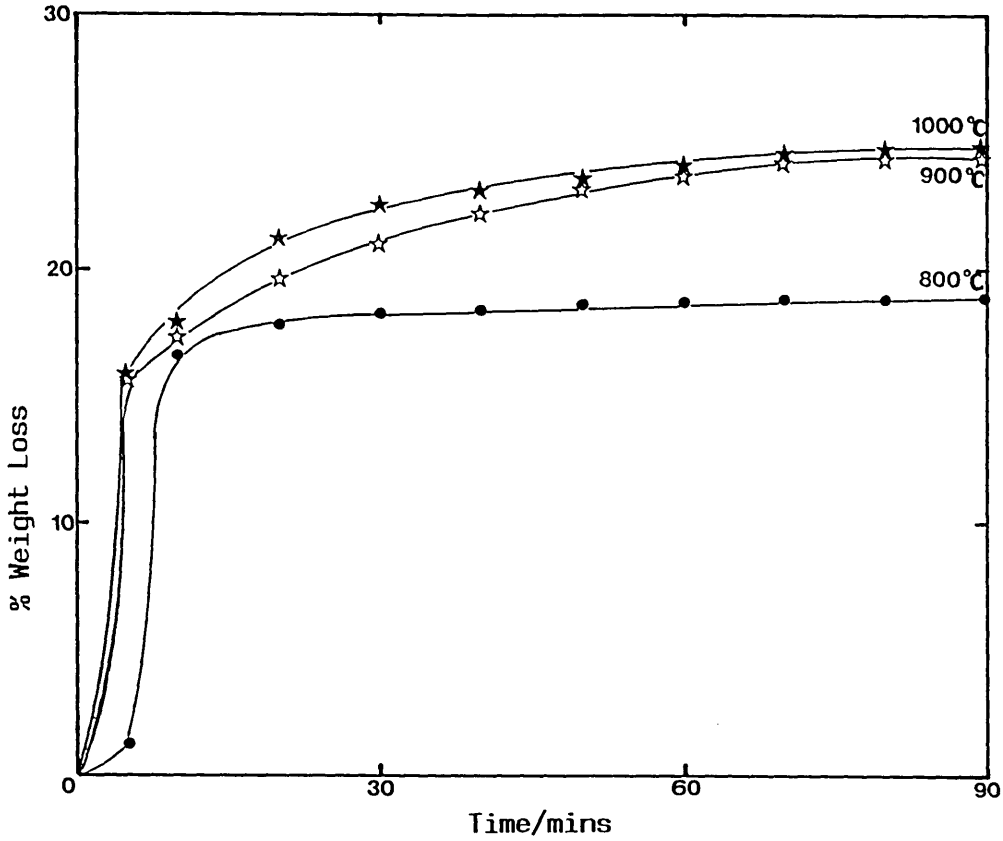

FIGURE 4.10

Rate of Weight Loss for the Exchange Reaction of
Arsenopyrite [FeAsS:CaO (1:1)] at Various Temperatures

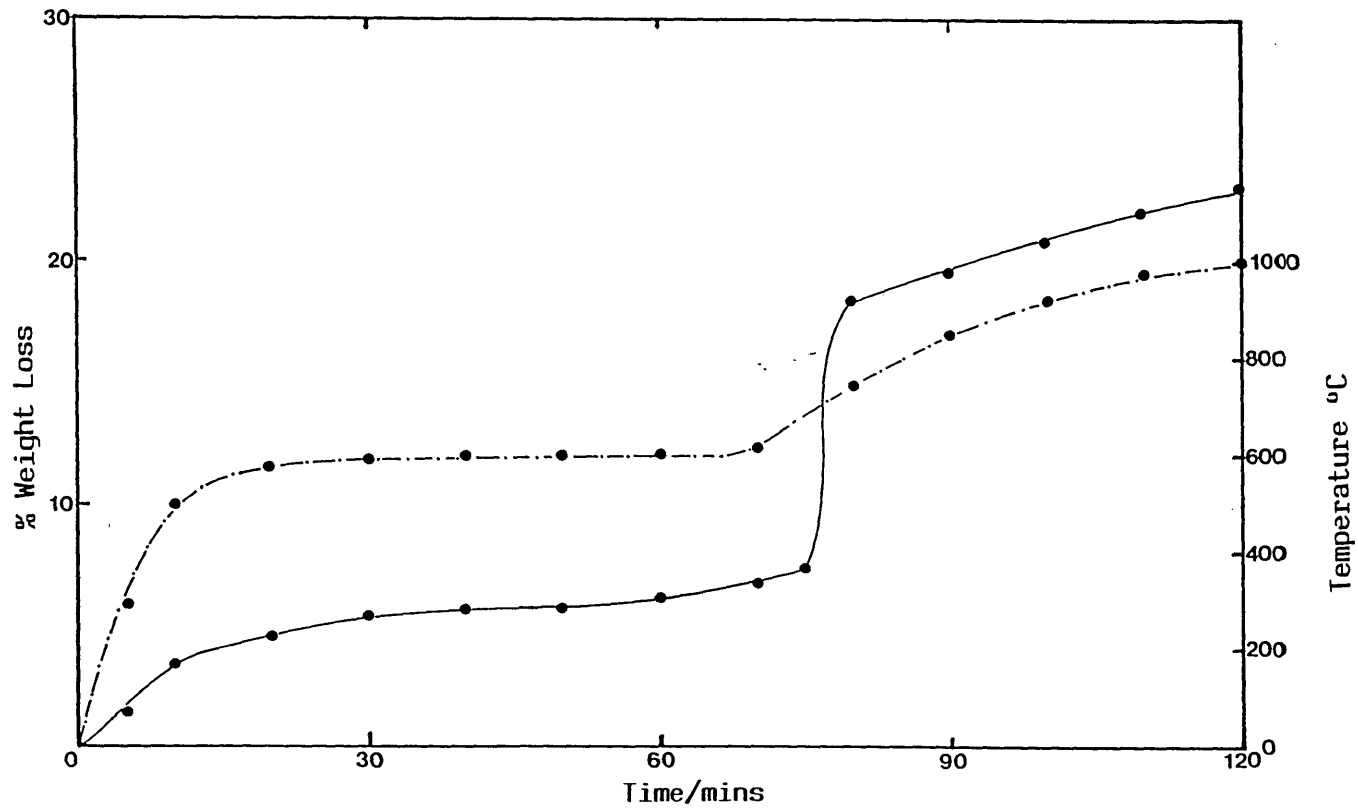

FIGURE 4.11

Rate of Weight Loss for the Exchange Reaction of Arsenopyrite
[FeAsS:CaO (1:1)] with Varying Temperature

Pellet Composition - $FeAsS_{(concentrate)}$:CaO (1:1)

Temp (°C)	Reaction Time (mins)	Mass Balance % wt loss	Phase Analysis, Relative Intensity				
			$Fe_{1-x}S$	1.33CaS.FeO	CaS	CaO	$FeAsO_4$
800	90	18.8	MS	MW	M	M	MW
900	90	24.4	M	S	MW	W	VW
1000	90	24.8	M	S	MW	VVW	-
$600 \rightarrow\uparrow^{1000}$	120	23.2	M	S	MW	VVW	-

Phase Analysis Intensity:

VS - Very Strong
VW - Very Weak
W - Weak
MS - Medium Strong
S - Strong
VVW - Very Very Weak
MW - Medium Weak
M - Medium

TABLE 4.3

Mass Balance and Phase Analysis of the Products of Arsenopyrite-Lime Exchange Reaction

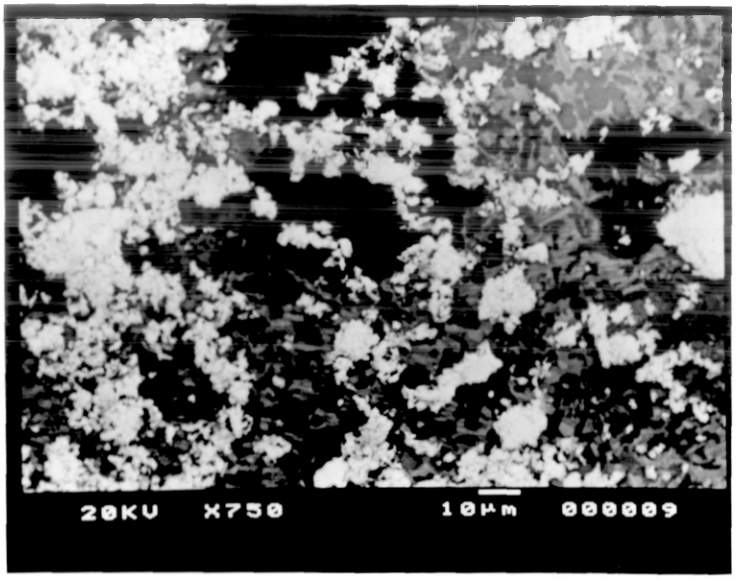

PLATE 4.4

Electron micrograph of arsenopyrite concentrate - lime exchange reaction [1000°C] product

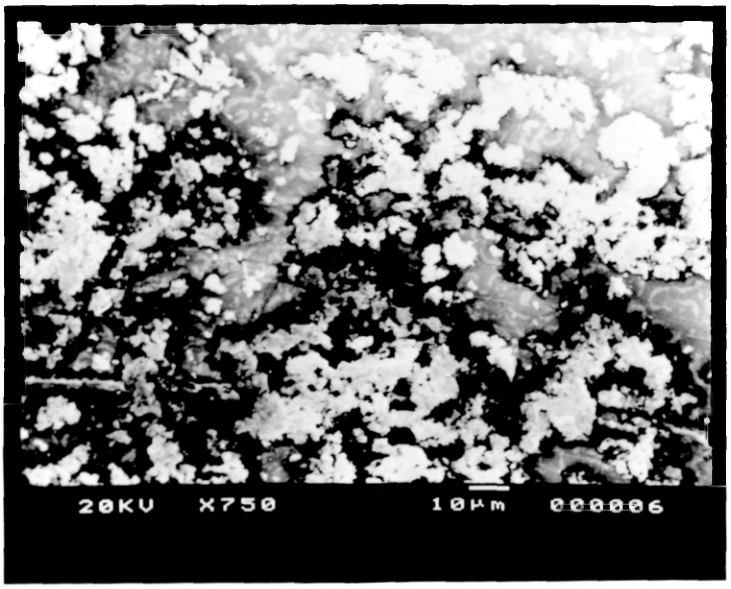

PLATE 4.5

Electron micrograph of synthetic arsenopyrite-lime exchange reaction [1000°C] product

4.2.2 Reduction of Arsenopyrite

The results of kinetic studies of the carbothermic reduction reactions of arsenopyrite (concentrate and synthetic sulphide) using graphite and coal are shown in Figures 4.12 to 4.16. Results of reactions carried out with excess quantities of reducing agents are also shown. Results of X-ray diffraction studies of the reaction products are presented in Table 4.4.

These curves show the temperature dependence of the reduction of arsenopyrite with graphite and collie coal. A comparison of the gradients of the rate curves at different temperatures shows that the rate of reaction (d%R/dt) increases with temperature. Enhanced rates of reduction were observed when coal replaced graphite as the reducing agent.

A significant feature of the graphite rate curves was the presence of periods in which reduction virtually ceased (plateaux in the reduction curves). Any weight loss occurring at these points is due to the volatilisation of arsenous species. At 1000^{o}C, the reduction resumes with an almost identical rate after the termination of the plateau (after 45 mins). At lower temperatures, further significant reduction was not observed beyond the plateau (a small weight loss occurs after 70 mins at 900^{o}C) and reduction is incomplete after 120 minute reaction at 800^{o}C and 900^{o}C. X-ray diffraction analysis of partially reduced pellets indicates the strong presence of the oxysulphide phase - (1.33) CaS.FeO and $Fe_{1-x}S$ at the conditions existing at the plateaux. Beyond the plateaux, these phases are present in reduced quantities while the intensities of Fe and CaS increase indicating that the reduction of FeO and further reaction of $Fe_{1-x}S$ are the main reactions that occur in the later stages.

Figure 4.13 illustrates the rate curves obtained with 100% and 200% excess graphite. A progressive reduction in the length of the plateaux is observed as the amount of graphite increases indicating a gradual breakdown of the kinetic barrier.

When a stoichiometric quantity of coal is used as the reductant, reduction proceeds uninterrupted and was complete in approximately 30

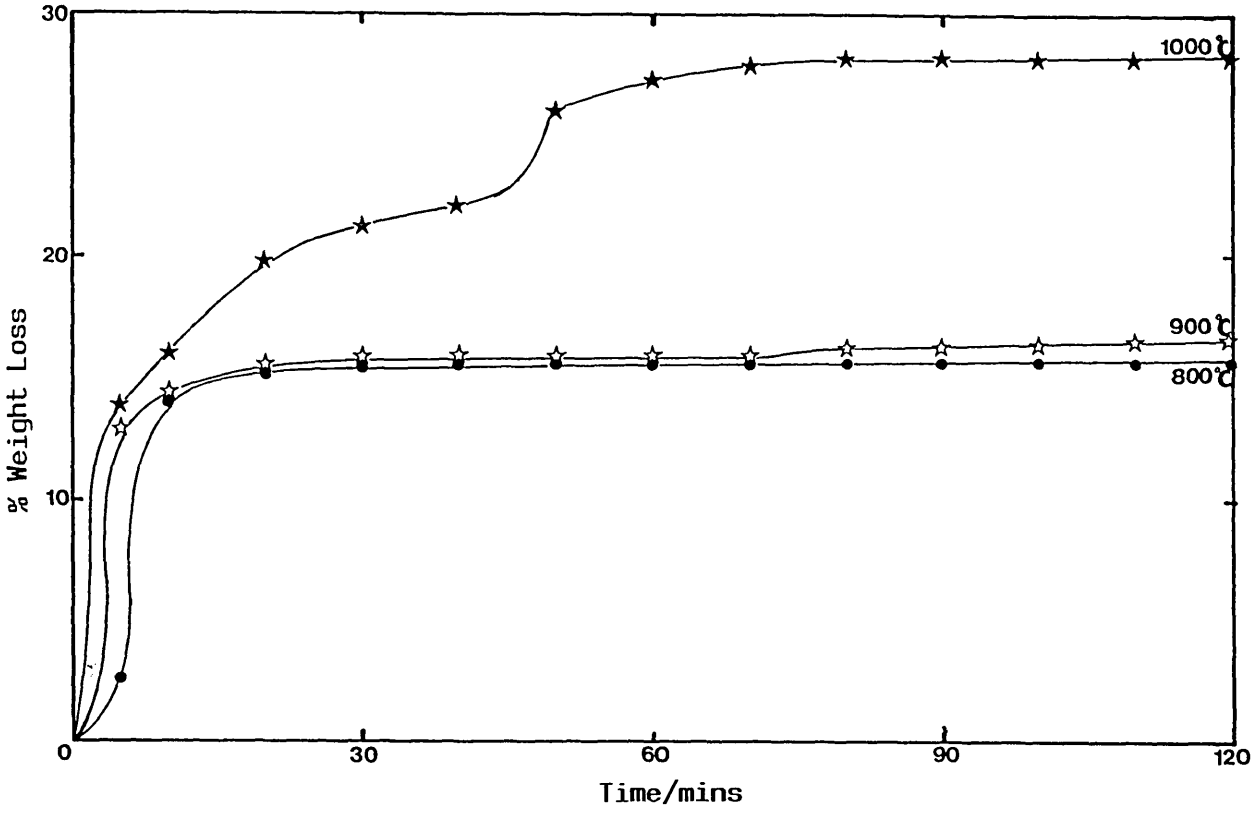

FIGURE 4.12

Rate Plot for the Carbothermic Reduction of Arsenopyrite (Concentrate) with Graphite at Various Temperatures

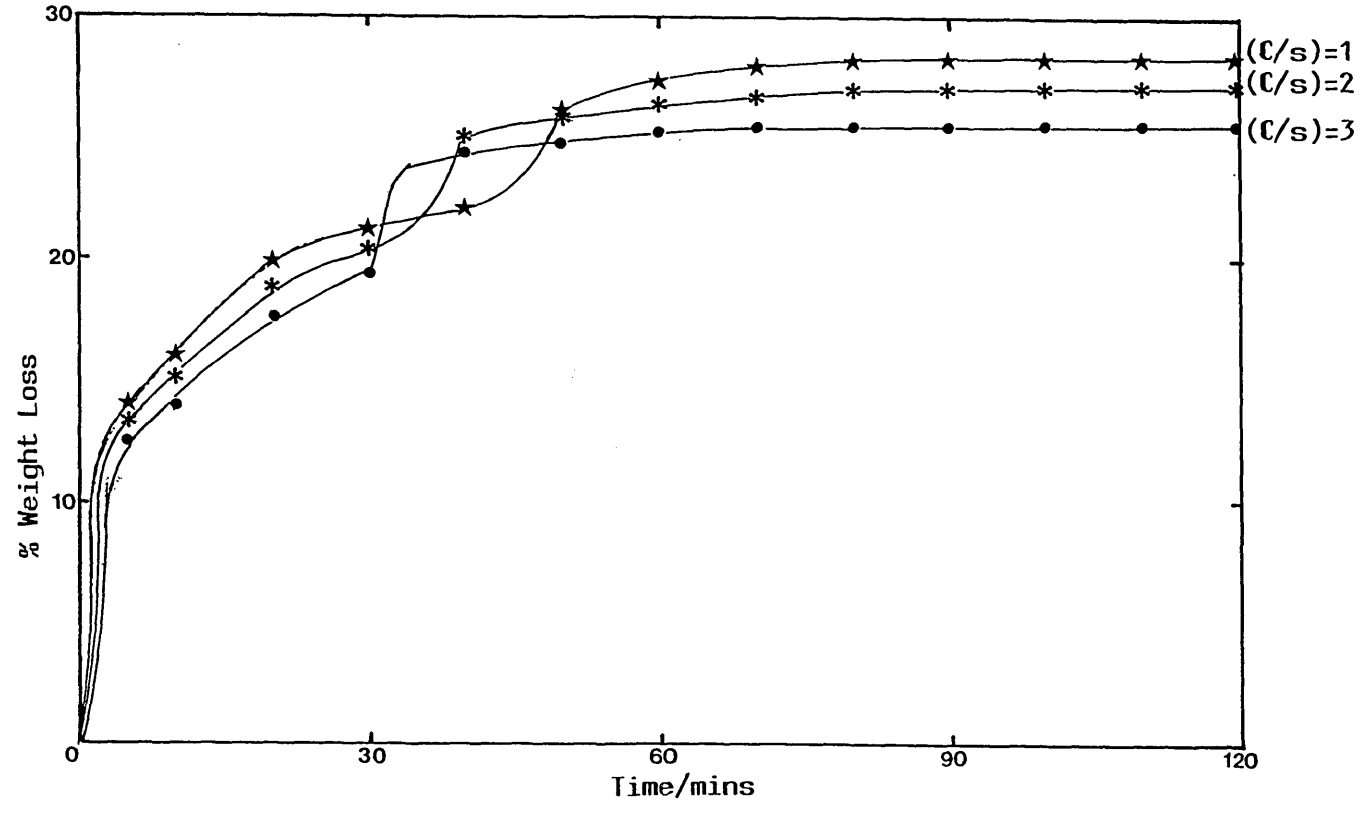

FIGURE 4.13

Rate Plot for the Carbothermic Reduction of Arsenopyrite (Concentrate) at 1000°C at Varying Graphite/Sulphide Ratios

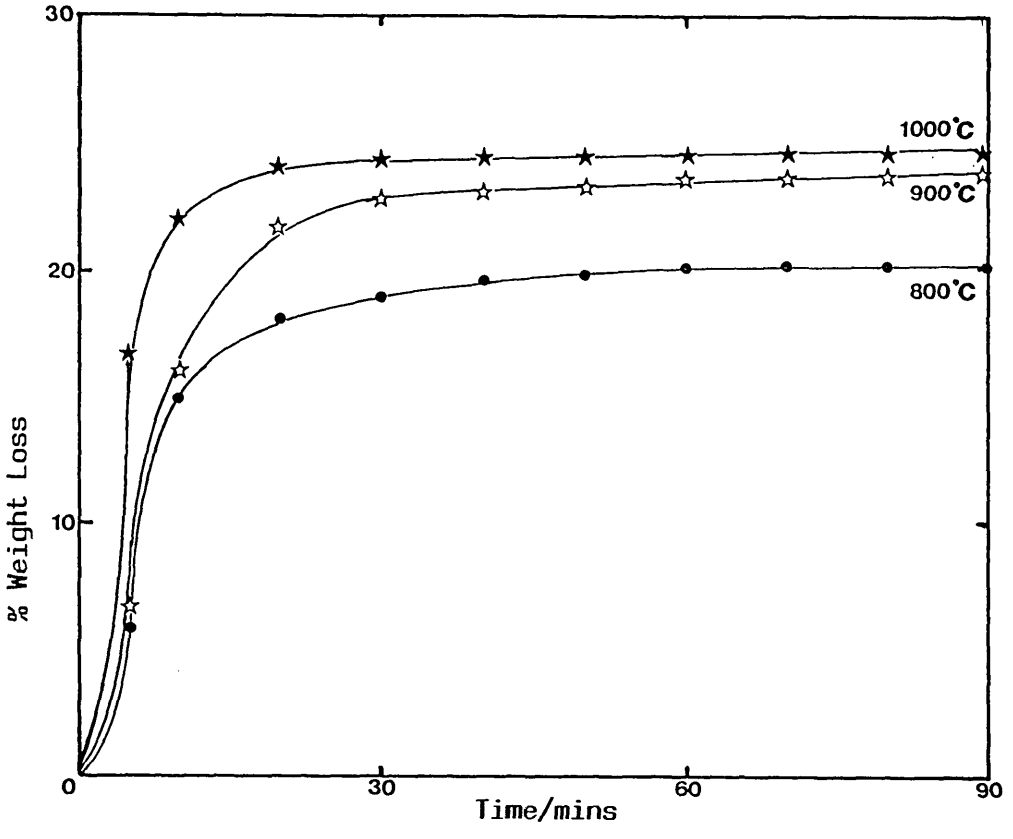

FIGURE 4.14

Rate Plot for the Carbothermic Reduction of Arsenopyrite (Concentrate) with Collie Coal at Various Temperatures

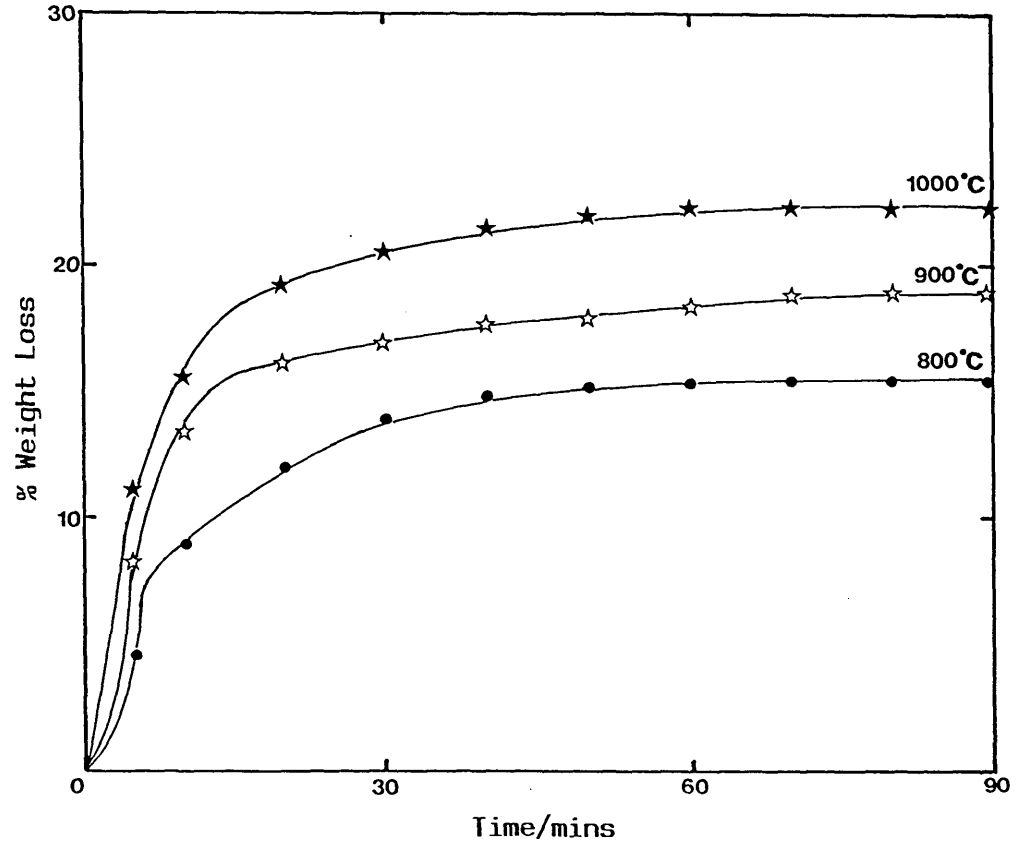

FIGURE 4.15

Rate Plot for the Carbothermic Reduction of Arsenopyrite (synthetic) with Collie Coal at Various Temperatures

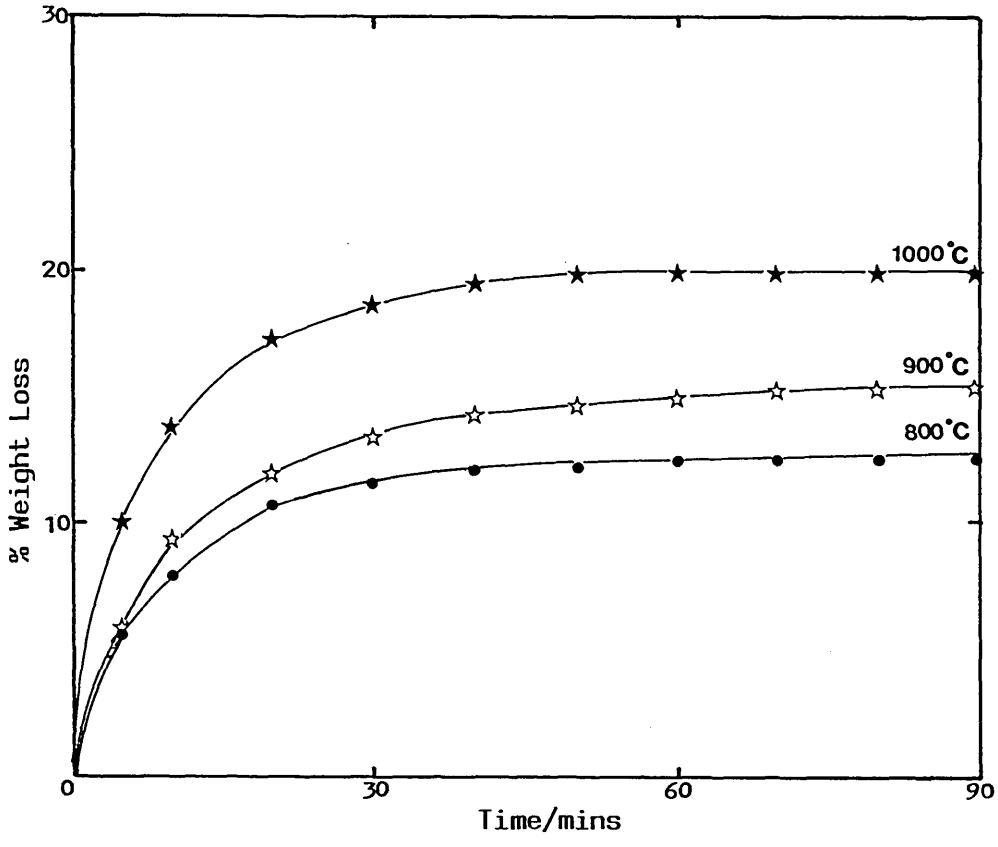

FIGURE 4.16

Rate Plot for the Carbothermic Reduction of Arsenopyrite (Synthetic) with Enhanced Lime/Sulphide and Coal/Sulphide Ratios [FeAsS:CaO:Coal (1:2:2)] at Various Temperatures

Pellet Composition - $FeAsS_{(synthetic)}:CaO:C_{coal}$ (1:2:2)

Temp (°C)	Mass Balance wt. loss	Reaction Time (mins)	Phase Analysis, Relative Intensity							
			FeAsS	$Fe_{1-x}S$	CaO	CaS	(1.33) CaS.FeO	FeAs	$FeAs_2$	Fe
800	12.7	90	VW	VVW	S	VS	-	VS	VW	-
900	15.4	90	VVW	-	S	VS	-	S	M	-
1000	20.0	90	-	-	MS	VS	-	MW	S	-

Phase Analysis Intensity:

VS - Very Strong MS - Medium Strong MW - Medium Weak VW - Very Weak
S - Strong M - Medium W - Weak VVW - Very Very Weak

TABLE 4.4

Mass Balance and Phase Analysis of the Products of the Carbothermic Reduction of Arsenopyrite

Pellet Composition - $FeAsS_{(concentrate)}:CaO:C_{graphite}$ Temp. = 1000°C

Mixture [FeAsS:CaO:Cgr]	Mass Balance % wt loss	Reaction Time (mins)	Phase Analysis, Relative Intensity				
			$Fe_{1-x}S$	CaS	Fe_2As	Fe	CaO
1:1:1	28.2	120	VVW	VS	W	VS	-
1:1:2	27.0	120	VVW	VS	W	VS	-
1:1:3	25.4	120	VVW	VS	MW	VS	-

Pellet Composition - $FeAsS_{(synthetic)}:CaO:C_{coal}$ (1:1:1)

Temp (°C)	Mass Balance % wt loss	Reaction Time (mins)	Phase Analysis, Relative Intensity							
			FeAsS	$Fe_{1-x}S$	CaO	CaS	(1.33) CaS.FeO	FeAs	Fe_2As	$FeAs_2$
800	15.4	90	W	VW	MW	S	W	S	VW	-
900	19.2	90	VW	-	W	VS	VW	S	M	-
1000	22.4	90	-	-	W	VS	-	MW	S	-
1000	21.8	45	VW	VW	VW	VS	-	W	S	-
1000	15.7	10	W	M	W	S	VW	S	MS	-
1000	7.2	5	W	M	M	MS	M	VS	-	M

TABLE 4.4

Mass Balance and Phase Analysis of the Products of the Carbothermic Reduction of Arsenopyrite

(continued ...)

Pellet Composition - $FeAsS_{(concentrate)}$:CaO:$C_{graphite}$ (1:1:1)

Temp (°C)	Mass Balance % wt Loss	Reaction Time (mins)	Phase Analysis, Relative Intensity FeAsS	$Fe_{1-x}S$	CaO	CaS	(1.33) CaS.FeO	FeAs	$FeAs_2$	Fe	FeS.CaO
800	15.6	120	W	MS	M	S	W	MW	W	-	-
900	16.4	120	-	MW	VVW	S	MW	W	MW	-	-
1000	28.2	120	-	VVW	-	VS	-	-	MW	VS	-
1000	27.3	60	VVW	MW	VVW	VS	VVW	-	VW	S	VVW
1000	22.6	45	VW	MS	VVW	S	MW	-	W	MW	W
1000	21.3	30	VW	MS	VVW	MS	MS	-	MW	-	VW

Pellet Composition -$FeAsS_{(concentrate)}$:CaO:C_{coal} (1:1:1)

Temp (°C)	Mass Balance % wt loss	Reaction Time (mins)	Phase Analysis, Relative Intensity FeAsS	$Fe_{1-x}S$	CaO	CaS	(1.33) CaS.FeO	FeAs	$FeAs_2$	Fe
800	20.2	90	VW	M	MW	S	W	VW	S	-
900	23.9	90	-	W	VVW	VS	-	-	S	MW
1000	24.8	90	-	-	VVW	VS	-	-	S	S
1000	24.5	30	-	VVW	VW	VS	-	-	S	S

TABLE 4.4

Mass Balance and Phase Analysis of the Products of the Carbothermic Reduction of Arsenopyrite

(continued....)

minutes at 1000°C. The rates of reduction with coal was faster at all temperatures and complete reduction is attained at 900°C. Volatilisation of arsenic occurs at the early stages of reaction and this contributes to the greater weight losses observed at higher temperatures as the arsenic is more volatile.

The reduction of synthetic arsenopyrite (Figure 4.15) follows an identical reaction path though the reaction rates are slower. The formation of the iron arsenides - Fe_2As and FeAs richer in arsenic is due to the higher arsenic concentration of the synthetic sulphide. The use of excess reducing and exchange reagents (Figure 4.16) does not lead to any marked increase in the rate of reduction.

Scanning electron micrographs of synthetic arsenopyrite pellets reduced at 900 and 1000°C are shown in plates 4.6 and 4.7. The dark areas are calcium sulphide while the grey and bright areas are FeAs and Fe_2As respectively. Plate 4.9 shows the arsenide portion of the pellet reduced at 1000°C. The grey areas are iron while the bright and dark phases are Fe_2As and CaS respectively. The voids result from the volume reduction that follows the reduction of sulphide to metal.

The products of the reduction of both synthetic arsenopyrite and the concentrate are quite similar with the liquid phases distributed throughout the sample. In some portions, Fe_2As is in contact with calcium sulphide. A comparison of Plates 4.6 and 4.8 indicates a lower contrast between calcium sulphide and the arsenide phase in the micrograph of the reduced concentrate. This is due to the greater difference in the molecular/atomic weights of the product phases in the reduced synthetic sulphide - Plate 4.6 [Fe_2As, FeAs, CaS] compared with the reduced ore pellet Plate 4.8 [Fe_2As, Fe, CaS]. The appearance of phases in micrographs obtained from the back-scattered electron detector of the scanning electron microscope is very muchdependent on their relative molecular/atomic weights.

4.2.3 Discussion of the Carbothermic Reduction of Arsenopyrite

The exchange reaction between arsenopyrite and lime results in the oxidation of the arsenic to volatile $As_4O_6(g)$ (b.p. = 459°C). The partial oxidation of the iron sulphide generates FeO which combines with calcium sulphide forming an oxysulphide compound (1.33) CaS.FeO. Some FeO also reacts with arsenic oxide to produce an iron arsenate compound $FeAsO_4$. Iron sulphide oxidation is incomplete in all cases studied. The amount of iron-calcium oxysuphide formed is greater at higher temperatures due to the increased reaction and availability of FeO and CaS. Increasing the reaction temperature also leads to the decomposition of any $FeAsO_4$ formed and the volatilisation of arsenic trioxide.

The compositions of the condensed phases formed by the thermal decomposition of arsenopyrite in a sealed tube were studied by Clark [39], who found that decomposition occurs above 702°C according to

$$FeAsS_{(s)} \rightarrow FeS_{(s)} + FeAs_{2(s)} + \text{As-rich liquid} \qquad [4.6]$$

Volatilisation of arsenic and its compounds occur easily due to their high vapour pressures as is illustrated by Figure 4.17.

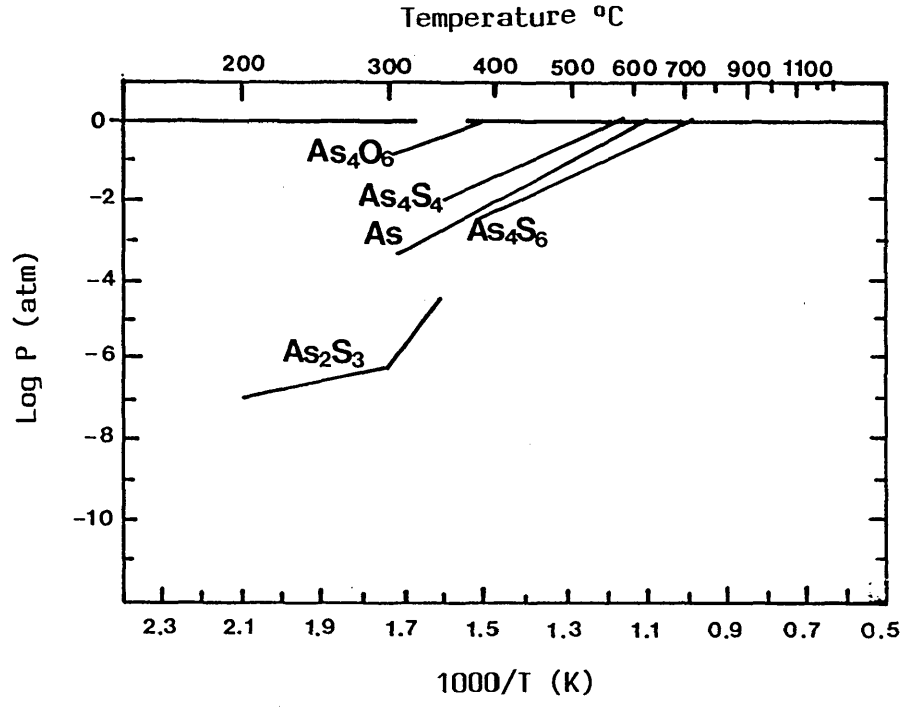

FIGURE 4.17

Various Pressures of Arsenic and Arsenic Compounds Versus Temperature

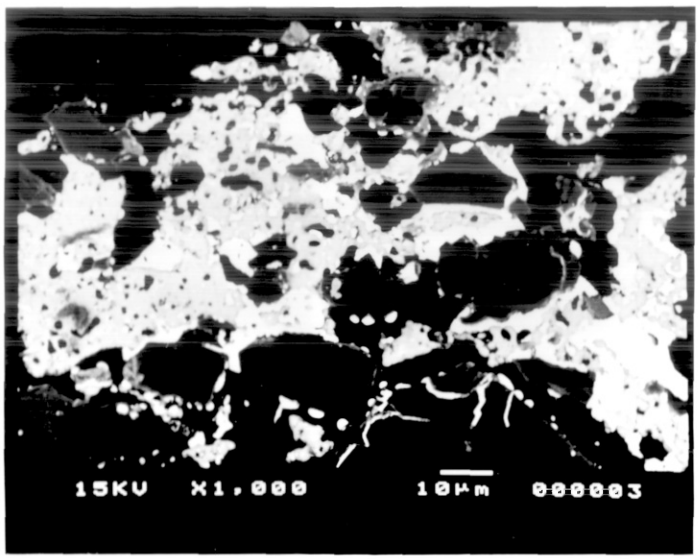

PLATE 4.6

Electron micrograph of synthetic arsenopyrite reduced with collie coal at 900°C for 90 mins [BSE image]

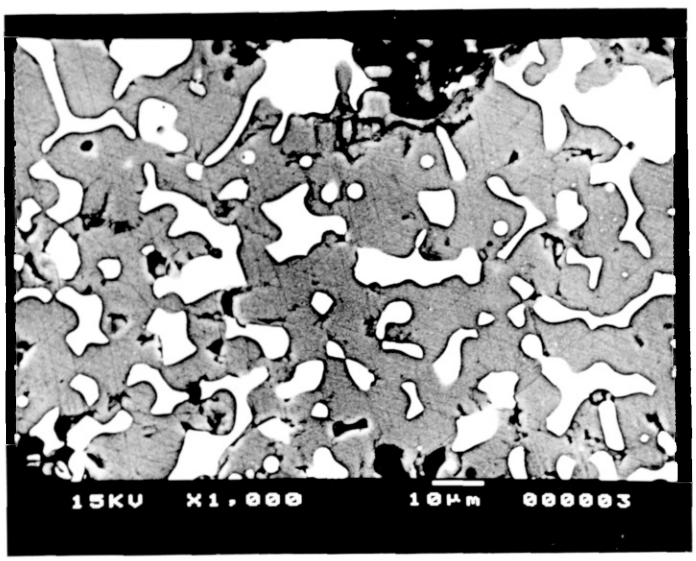

PLATE 4.7

Electron micrograph of synthetic arsenopyrite reduced with collie at 1000°C for 90 mins - illustrating the iron arsenide phases [BSE image]

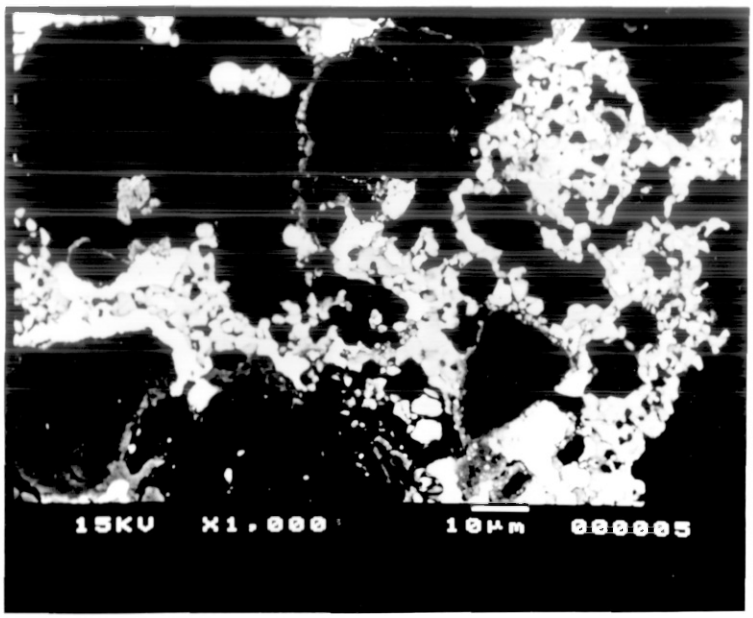

PLATE 4.8

Electron micrograph of arsenopyrite concentrate reduced with collie coal at 1000°C for 90 mins [BSE image]

PLATE 4.9

Electron micrograph of arsenopyrite concentrate reduced with collie coal at 1000°C for 90 mins- illustrating the metallic iron and iron arsenide phases [BSE image]

Chakraborti and Luynch [43] and Rtskhiladze [64] have studied the composition of the gaseous and condensed phases produced by the thermal decomposition of arsenopyrite in inert atmospheres. Arsenic was found to volatilise as $As_{4(g)}$ while the condensed phase consisted mainly of pyrrhotite ($Fe_{1-x}S$). The thermal decomposition of arsenopyrite in a flow of inert gas can therefore be represented as

$$4FeAsS_{(s)} \rightarrow 4FeS_{(s)} + As_{4(g)} \qquad [4.7]$$

According to Rtskhiladze, the volatilisation of $As_{4(g)}$ starts at about 550°C. From an experimental study of the arsenate-oxide equilibria in the Fe-As-O system, Skaeff [42] has determined that the presence of a very small amount of oxygen will cause the formation of significant quantities of arsenic trioxide $As_4O_{6(g)}$ in the gas phase.

Thus, in the presence of CaO, the arsenic component of the decomposition products readily oxidises to form the extremely volatile $As_4O_{6(g)}$.

Under the reaction conditions represented in Figure 4.11, the weight loss observed at 600°C is due to the loss of arsenic as $As_{4(g)}$. Increasing the temperature leads to the rapid oxidation and evolution of the remaining arsenic component of the sulphide, as $As_4O_{6(g)}$. The partial loss of arsenic as $As_{4(g)}$ accounts for the reduced weight loss observed, compared with the isothermal exchange reaction at 1000°C.

Predominance area diagrams constructed for the Fe-As-O system by Skaeff suggest that during the roasting of a concentrate containing arsenopyrite at an oxygen partial pressure of about 10^{-1} atm, the formation of ferric arsenate will occur if the partial pressure of $As_4O_{6(g)}$ in the system is greater than 10^{-15} atm. On the other hand, the roasting of the same concentrate in the presence of even relatively low concentrations of $As_{4(g)}$, for example $P_{AS_4} = 10^{-15}$ atm will cause the formation of ferric arsenate even when the oxygen partial pressure is as low as 10^{-10} atm. However, the formation of the iron arsenate ($FeAsO_4$) requires the prior formation of haematite which is difficult under the prevailing

experimental conditions, thus restricting the production of iron arsenate. The reaction between arsenic trioxide and haematite takes place according to

$$As_4O_{6(s)} + 2Fe_2O_{3(s)} + 2O_{2(g)} \rightarrow 4FeAsO_{4(s)} \qquad [4.8]$$

The decomposition of the iron-arsenate at higher temperatures (> 900^{o}C) leads to the evolution of oxygen as well as arsenic which contributes to the weight losses observed.

The formation of iron by reaction between FeO and $Fe_{1-x}S$ during these exchange reactions is unfavoured due to a large positive free energy for the reaction

$$FeS_{(s)} + 2FeO_{(s)} \rightarrow 3Fe_{(s)} + SO_{2(g)} \qquad [4.9]$$

$$\Delta G_T^{o} = 76650 - 26.98T \text{ cal/mol}$$

$$T_{eq.} = 2841 \text{ K}$$

However, the combination of FeO and CaS results in the formation of the oxy-sulphide compound (1.33) CaS.FeO. Jha [52] has investigated the phase combinations in the Fe-Ca-S-O quartenary system by heat treating mixtures of the reciprocal systems FeS-CaO and FeO-CaS in inert (argon) atmospheres. The heat treated samples were analysed by X-ray diffraction techniques. This investigation found the existence of two phases with compositions (1.33) CaS.FeO and FeS.CaO in the Fe-Ca-S-O quartenary system. The crystallographic data observed for those compounds are shown in the appendix.

The results of the investigation of the carbothermic reduction of arsenopyrite indicate that three reactions occur consecutively - the volatilisation of the arsenous species occurs in addition to the exchange and reduction of iron sulphides. The overall carbothermic reduction reaction is very fast and complete reduction is achieved with coal after

30 minutes at 1000^{o}C compared with the 50 minutes required for the complete reduction of the single pyrrhotite phase [52]. The formation of liquid iron-arsenides at the early stages of the reaction [quenched incompletely reacted pellets showed the presence of iron arsenide alloys], enhances the rate of reaction by creating a medium for the effective transfer of S^{2-} and O^{2-} ions within the reacting system.

The formation of the oxysulphide liquid (1.33) CaS.FeO during the carbothermic reduction of iron sulphide enhances the reaction rate by increasing the surface area available for reaction. The plateaux observed during reduction with graphite indicates the establishment of steady state conditions for oxide ion transport. Temporary cessation of reduction occurs due to the difficulty of transporting the oxide anions to the carbon surface for the nucleation of CO. This kinetic barrier can be overcome either by increasing the reaction temperature or by the use of more reactive reducing agents such as coal. The use of coal as reductant completely eliminates the plateau leading to an uninterrupted reduction reaction which is complete after 30 minutes at 1000^{o}C. Increasing the amount of graphite reductant also lowers the kinetic barrier leading to a reduction in the length of the plateau, although even the use of 200% excess graphite did not completely eliminate the plateau during reaction at 1000^{o}C.

The partial loss of arsenic occurs as $As_{4(g)}$ and $As_4O_{6(g)}$ as discussed in the previous section. Rapid reduction rates quickly generate iron which combine with arsenic to form stable iron-arsenides. Thus conditions that enhance the rate of reduction will lead to a reduced loss of arsenic by volatilisation. Increasing the reaction temperature as a means of increasing the reaction rate is not advisable since it will lead to an increased loss of arsenic by volatilisation due to the increased vapour pressure. Thus the use of very reactive reducing agents like coal will result in the complete reduction of arsenopyrite, forming stable iron arsenides and a calcium sulphide residue with a minimum loss of toxic arsenous species to the atmosphere. The complete conversion of arsenopyrite can be represented as

$$FeAsS_{(s)} + CaO_{(s)} + C_{(gr)} \rightarrow FeAs_{(s)} + CaS_{(s)} + CO_{(g)} \qquad [4.10]$$

The presence of a higher concentration of iron (as pyrrhotite) in the complex sulphide, a common occurence in most arsenopyrite ores leads to the formation of Fe in addition to the arsenide.

$$2Fe_{1-x}S_{(s)} + FeAsS_{(s)} + 3CaO_{(s)} + 3C_{(gr)}$$

$$\rightarrow Fe_{(s)} + Fe_2As_{(s)} + 3CaS_{(s)} + 3CO_{(g)} \qquad [4.11]$$

4.3 The Carbothermic Reduction of Copper-Arsenic Sulphides

In this section, the results of exchange and reduction reactions of synthesised enargite (Cu_3AsS_4) and tennantite ($Cu_{12}As_4S_{13}$) are presented.

4.3.1 Exchange reactions between copper-arsenic sulphides and lime

The weight losses resulting from the isothermal reactions of synthetic tennantite ($Cu_{12}As_4S_{13}$) and enargite (Cu_3AsS_4) with lime (CaO) are shown in Figures 4.18 and 4.19. In Figure 4.20, the weight loss curves shown are those obtained when the exchange reactions were initially carried out at 600^{o}C after which the temperature was increased to 1000^{o}C at an average heating rate of 10^{o}C/min. Results of X-ray diffraction studies of the reaction products are shown in Table 4.5.

The exchange reactions result in the formation of calcium arsenite (Ca-As-O) as well as a copper arsenic oxysulphide phase. The proper identification of the oxysulphide phase has been limited by the dearth of data available for the Cu-As-S-O system. The existence of this oxysulphide phase in the reaction products of the exchange reactions was confirmed by comparing the X-ray diffraction data with those obtained in a series of studies involving reactions between arsenic oxide (As_2O_3), calcium oxide (CaO), copper oxide (Cu_2O) and copper sulphide (Cu_2S).

From the X-ray diffraction results (Table 4.5), it is observed that arsenic in the complex sulphides completely oxidises at all reaction temperatures and the arsenic oxide formed combines with calcium oxide to form calcium arsenite, and with copper sulphide to form a copper-arsenic

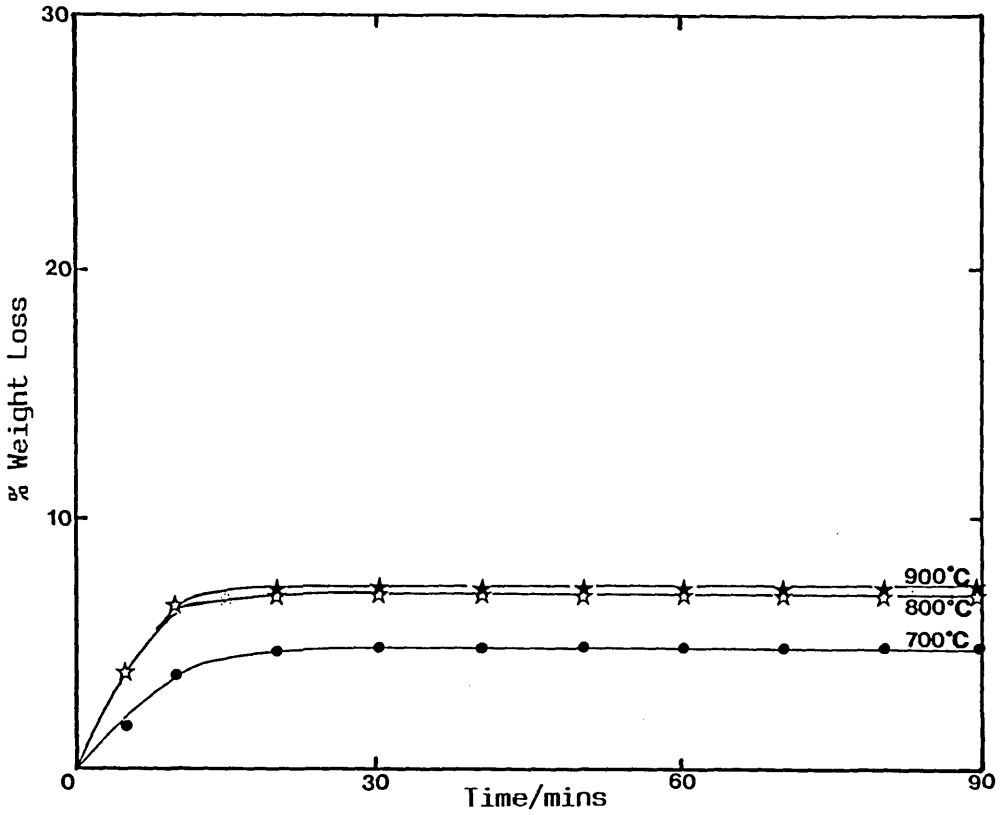

FIGURE 4.18

Rate of Weight Loss for the Exchange Reaction of Tennantite [$Cu_{12}As_4S_{13}$:CaO (1:1)] at Various Temperatures

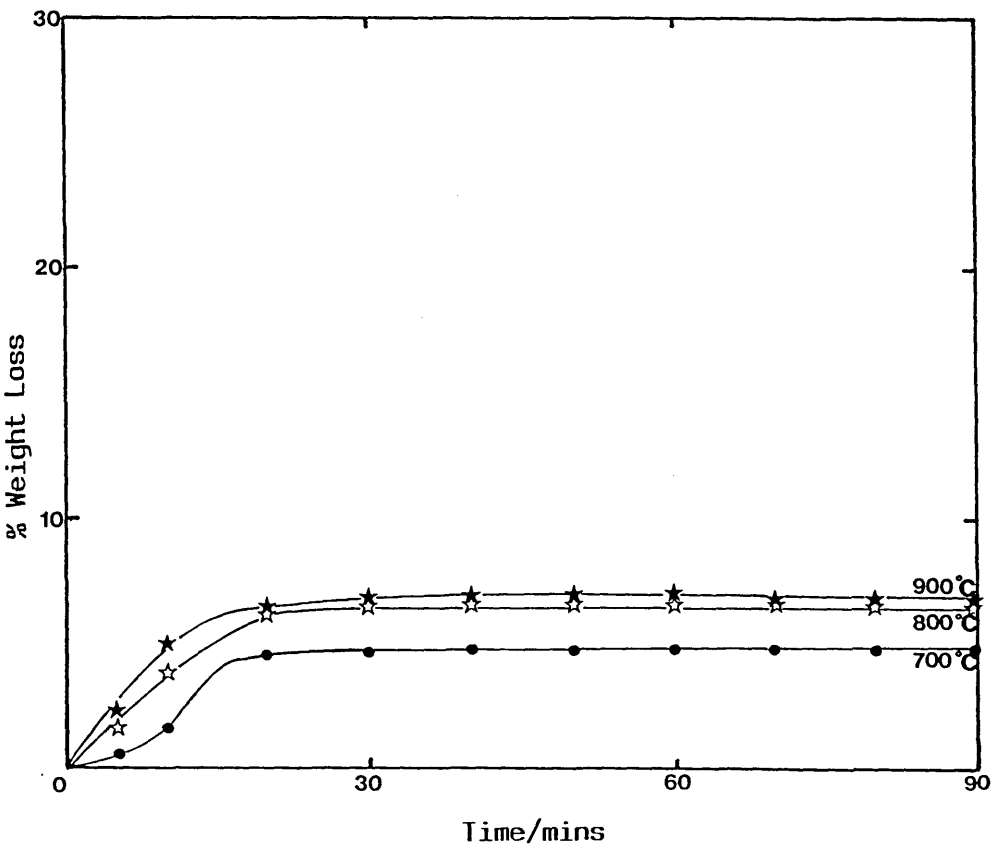

FIGURE 4.19

Rate of Weight Loss for the Exchange of Enargite [Cu_3AsS_4:CaO (1:1)] at Various Temperatures

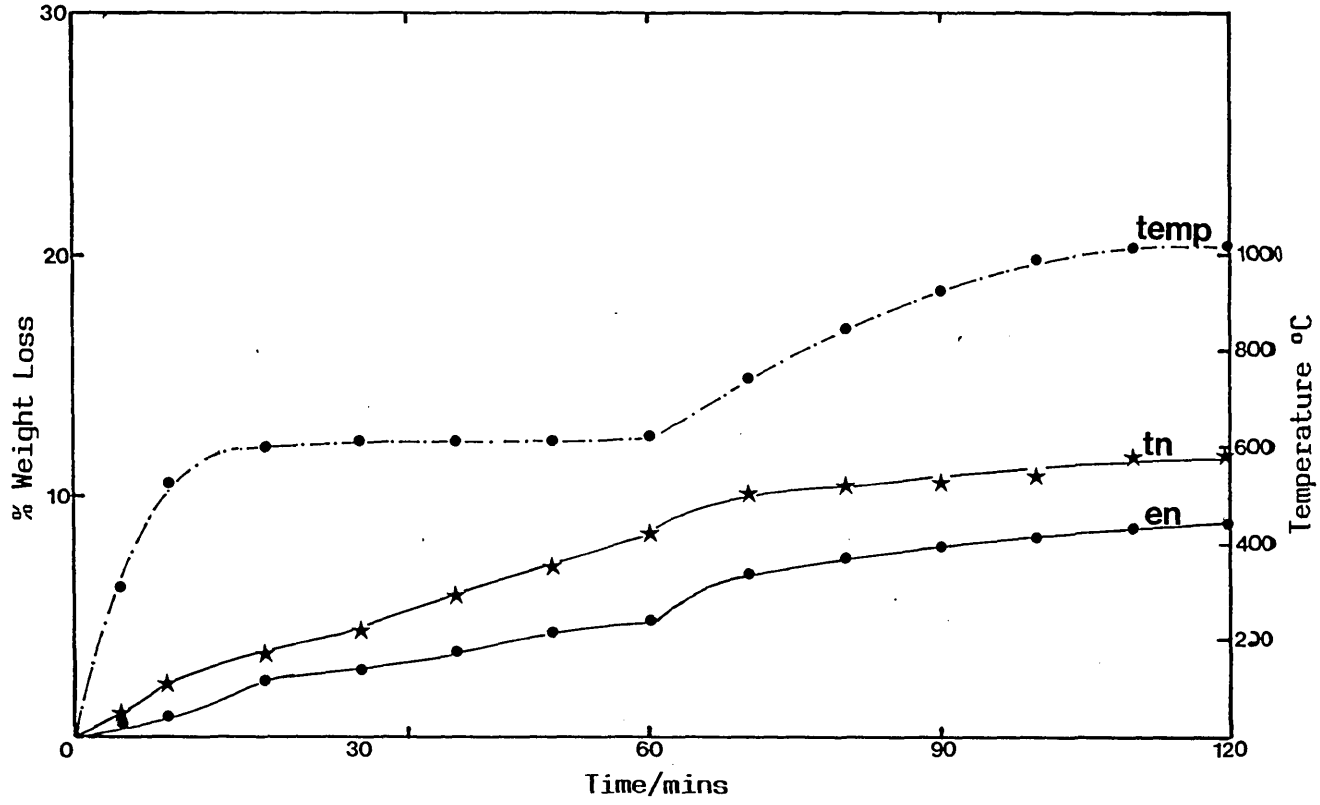

FIGURE 4.20

Rate of Weight Loss for the Exchange Reaction of Tennantite and Enargite with Varying Temperature

TABLE 4.5

Mass Balance and Phase Analysis of the Products of the Exchange Reactions of Tennantite and Enargite with Lime

Mixture Composition - $Cu_{12}As_4S_{13}$:CaO (1:1)

Temp (°C)	Reaction time (mins)	Weight loss %	Phases Present, Relative Intensity					
			CaO	CaS	Cu_2S	$Cu_{1.96}S$	Ca-As-O	Cu-As-S-O
700	90	4.8	MW	S	MW	MW	-	VW
800	90	7.0	W	MS	MW	W	VW	W
900	90	7.2	W	MS	W	W	W	W
600→↑ 1000	120	11.7	M	S	MW	VW	VVW	VW

Mixture Composition - Cu_3AsS_4:CaO (1:1)

Temp (°C)	Reaction time (mins)	Weight loss %	Phases Present, Relative Intensity					
			CaO	CaS	Cu_2S	$Cu_{1.96}S$	Ca-As-O	Cu-As-S-O
700	90	4.7	MW	S	MW	MW	-	W
800	90	6.5	W	MS	W	W	VVW	MW
900	90	6.7	W	MS	W	W	VVW	MW
600 →↑ 1000	120	8.9	MW	MS	MW	VW	VVW	MW

Phase Analysis Intensity:

VS - Very Strong
S - Strong
MS - Medium Strong
MW - Medium Weak
W - Weak
VW - Very Weak
VVW - Very Very Weak

oxysulphide. Higher reaction temperatures lead to an increase in the concentration of calcium arsenite and copper-arsenic oxysulphide in the reaction product.

The weight loss observed is due to the volatilisation of arsenic oxide which occurs before reaction with calcium oxide and copper sulphide. Thus the bulk of the weight loss occurs during the initial stages of the reactions. The increased weight loss at higher temperatures is due to the corresponding increase in the vapour pressure of arsenic oxide. Chalcocite (Cu_2S, $Cu_{1.96}S$) is present in all the reaction products while copper oxide is absent . The weight loss profile obtained for both complex sulphides (enargite and tennantite)are similar. The higher weight loss observed during reaction with tennantite [$Cu_{12}As_4S_{13}$-$5Cu_2S.2CuS.2As_2S_3$] is due to the decomposition of covellite (CuS) to chalcocite (Cu_2S). This decomposition reaction does not occur during reactions with enargite [Cu_3AsS_4-3/2 $Cu_2S.\frac{1}{2}As_2S_5$].

4.3.2 Reduction of tennantite [$Cu_{12}As_4S_{13}$] and enargite [Cu_3AsS_4]

The results of the study of the reduction kinetics of synthesised tennantite ($Cu_{12}As_4S_{13}$) and enargite (Cu_3AsS_4) using carbon (coal and graphite) are shown in Figures 4.21 to 4.25. In Table 4.6, the results of the X-ray diffraction studies of the reaction products are presented.

The plots (Figure 4.21-4.25) show the rate of carbothermic reduction of synthetic tennantite ($Cu_{12}As_4S_{13}$) and enargite (Cu_3AsS_4) with coal and graphite as reducing agent. Reduction with coal is complete only at 1000^oC and the reaction product contains minute traces of unreacted copper-sulphide. The reduction of tennantite ($Cu_{12}As_4S_{13}$) and enargite (Cu_3AsS_4) are complete after about 40 minutes at 1000^oC. Between 700^oC and 900^oC, the reaction products contain varying quantities of copper sulphide (Cu_2S, $Cu_{1.96}S$) indicating incomplete reduction. A comparison of the weight loss profiles for tennantite ($Cu_{12}As_4S_{13}$) and enargite (Cu_3AsS_4) shows that they are similar indicating an identical reduction reaction mechanism for both complex sulphides.

The rate plots show an initial period of rapid weight loss [the rate of which depends on the reaction temperature], followed by a second stage in

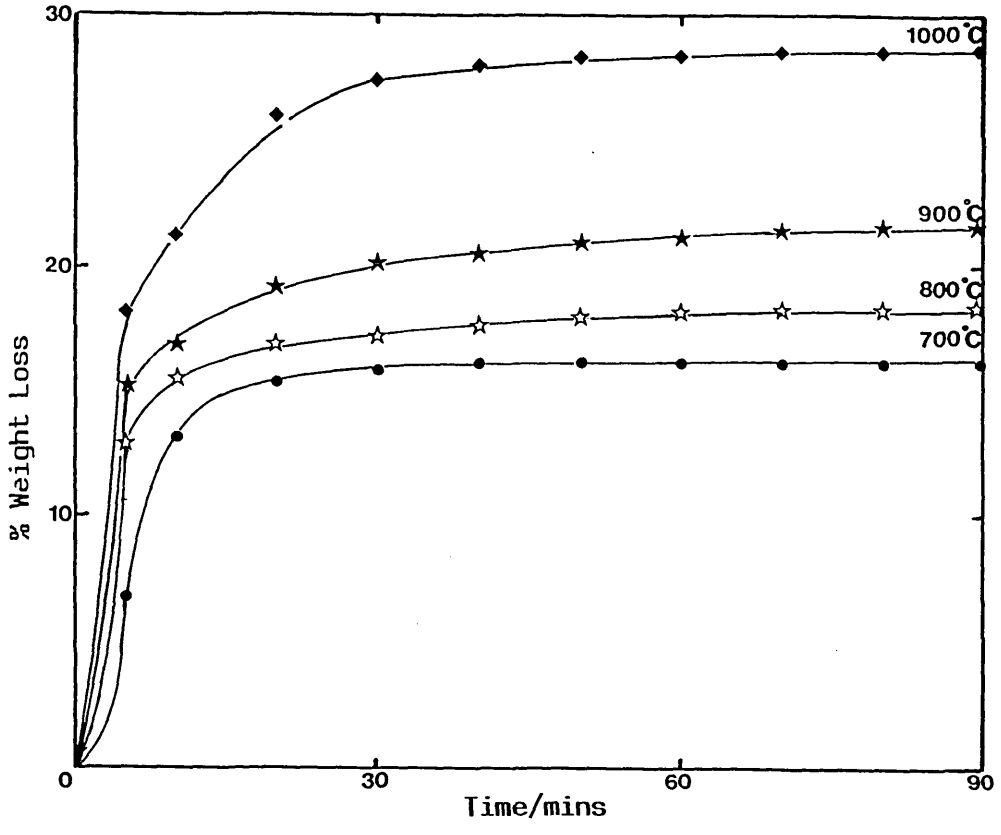

FIGURE 4.21

Rate Plot for the Carbothermic Reduction of Tennantite with Collie Coal at Various Temperatures

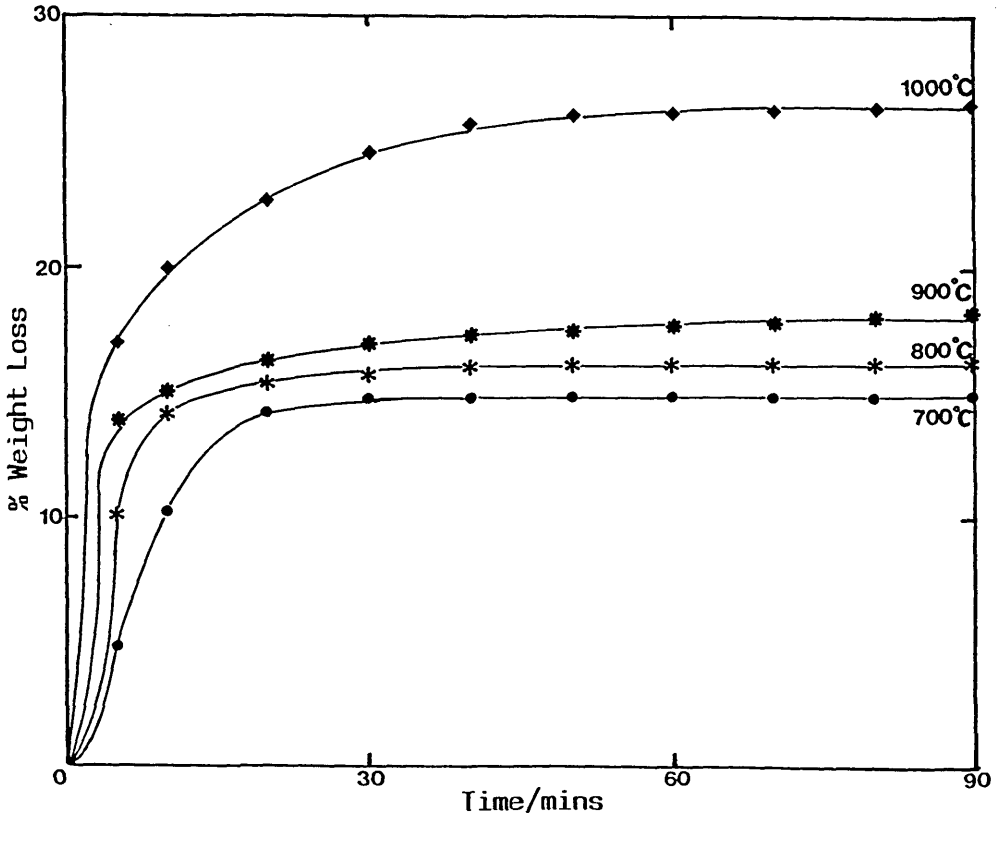

FIGURE 4.22

Rate Plot for the Carbothermic Reduction of Enargite with Collie Coal at Various Temperatures

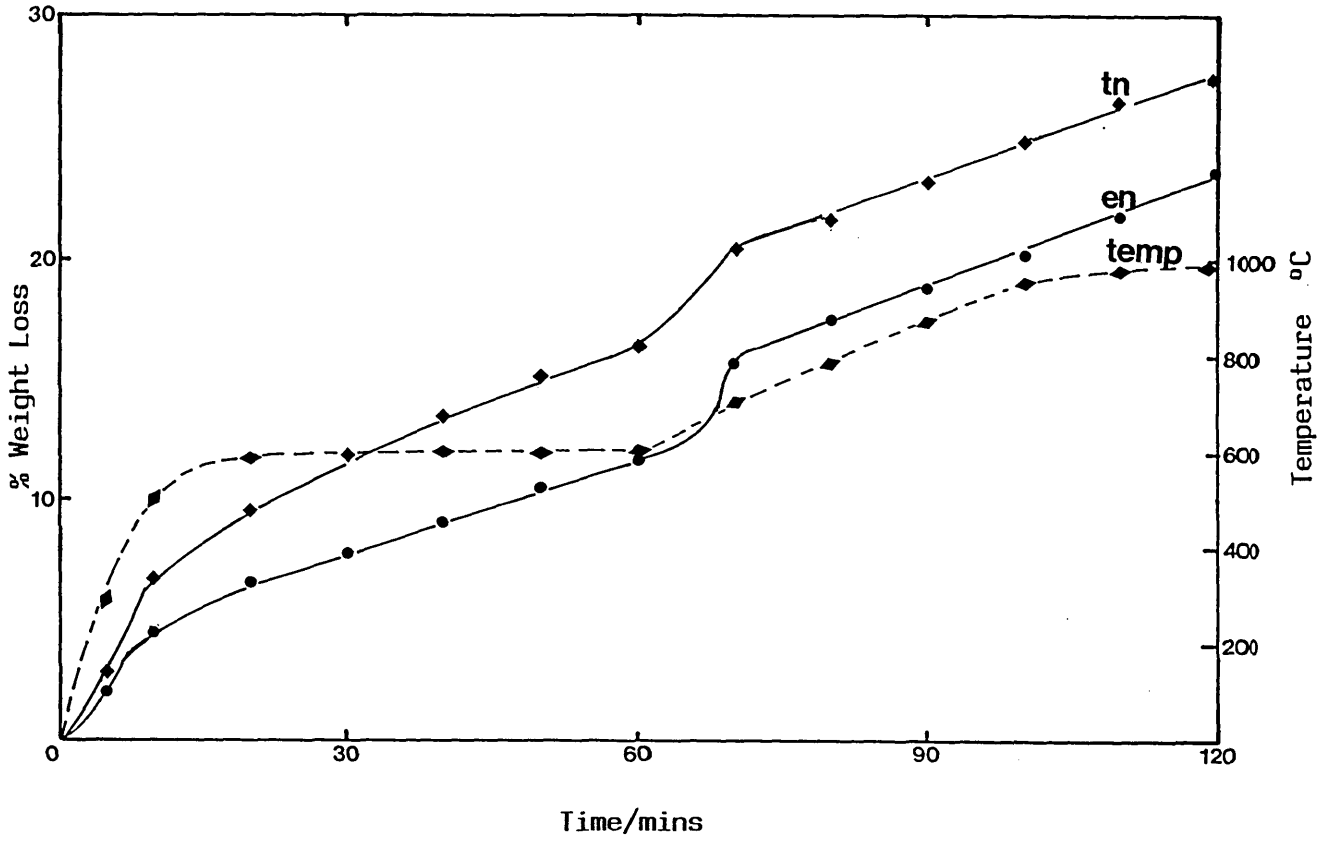

FIGURE 4.23

Rate Plot for the Carbothermic Reduction of Tennantite and Enargite with Collie Coal and Varying Temperature

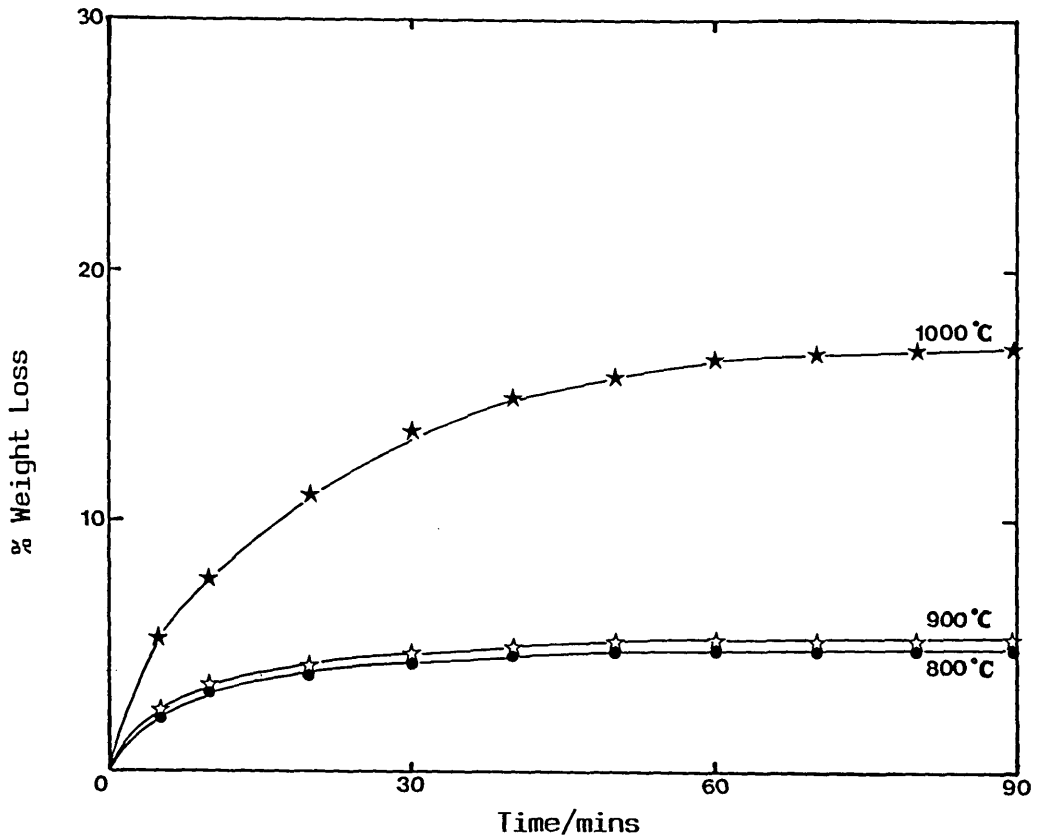

FIGURE 4.24

Rate Plot for the Carbothermic Reduction of Tennantite with Graphite at Various Temperatures

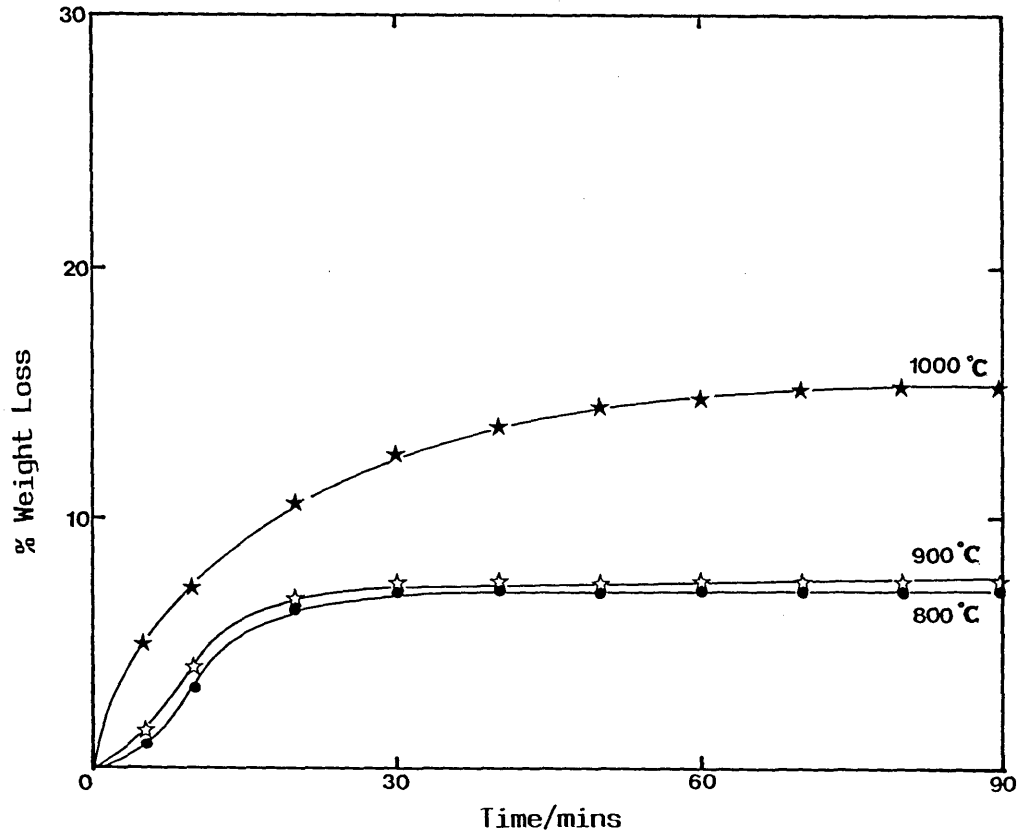

FIGURE 4.25

Rate Plot for the Carbothermic Reduction of Enargite with Graphite at Various Temperatures

Mixture Composition - $Cu_{12}As_4S_{13}$:CaO:C_{coal} (1:1:1)

Temp (°C)	Reaction Time (mins)	Weight loss %	Phase Analysis, Relative Intensity						
			CaO	Cu_2S	$Cu_{1.96}S$	CaS	Cu_3As	Cu	Ca-As-O
700	90	16.1	MS	MS	MW	MS	-	-	-
800	90	18.3	MS	M	W	S	W	VVW	W
900	90	21.6	M	MW	-	VS	M	VW	VW
900	15	18.2	M	M	VW	S	W	-	MW
1000	90	28.5	MW	VVW	-	VS	MS	MS	-
600→↑1000	120	27.5	M	VVW	-	VS	MW	MS	-

Mixture Composition - Cu_3AsS_4:CaO:C_{coal} (1:1:1)

Temp (°C)	Reaction Time	Weight	Phase Analysis, Relative Intensity						
			CaO	Cu_2S	$Cu_{1.96}$	CaS	Cu_3As	Cu	Ca-As-O
700	90	14.7	M	MS	MW	S	-	-	-
800	90	16.1	MW	M	W	S	VW	-	W
900	90	18.2	W	MW	-	VS	MW	VVW	VW
900	15	15.8	MW	MS	VW	S	VW	-	M
1000	90	26.5	W	VVW	-	VS	MS	MW	VVW
600 →↑1000	120	23.8	M	VVW	-	VS	MW	MW	-

TABLE 4.6

Mass Balance and Phase Analysis of the Products of the Carbothermic Reduction of Tennantite ($Cu_{12}As_4S_{13}$) and Enargite (Cu_3AsS_4)

(continued ...)

Mixture Composition - $Cu_{12}As_4S_{13}$:CaO:$C_{graphite}$ (1:1:1)

Temp (°C)	Reaction Time (mins)	Weight loss %	Phase Analysis, Relative Intensity							
			CaO	CaS	Cu_2S	$Cu_{1.96}S$	Cu_3As	Cu	Ca-As-O	Cu-As-O
700	90	4.1	MW	MS	M	MW	-	-	-	MW
800	90	4.7	W	S	MW	MW	-	-	W	M
900	90	5.2	W	S	MW	W	-	-	MW	M
1000	90	17.0	VW	VS	VW	-	S	-	W	-

Mixture Composition - Cu_3AsS_4:CaO:$C_{graphite}$ (1:1:1)

Temp (°C)	Reaction Time (mins)	Weight loss %	Phase Analysis, Relative Intensity							
			CaO	CaS	Cu_2S	$Cu_{1.96}$	Cu_3As	Cu	Ca-As-O	Cu-As-S-O
700	90	5.0	MW	MS	M	MW	-	-	-	MW
800	90	7.0	W	S	MW	W	-	-	VVW	M
900	90	7.4	W	S	MW	VW	-	-	VW	M
1000	90	15.2	VW	VS	VW	-	S	-	W	-

Phase analysis intensity:

VS - Very Strong
S - Strong
MS - Medium Strong
MW - Medium Weak
W - Weak
VW - Very Weak
VVW - Very Very Weak
M - Medium

TABLE 4.6

Mass Balance and Phase Analysis of the Products of the Carbothermic Reduction of Tennantite ($Cu_{12}As_4S_{13}$) and Enargite (Cu_3AsS_4)

which the rate is almost linear. Beyond this stage, there is negligible weight loss since reduction reactions have ceased. The decomposition of CuS to Cu_2S contributes to the observed weight losses for tennantite and the volatilisation of the arsenous species influences the observed weight loss at all temperatures. The weight losses for the coal reduction of tennantite ($Cu_{12}As_4S_{13}$) and enargite (Cu_3AsS_4) at 700°C are close to the values expected for the complete loss of arsenic as $As_4O_6(g)$ [15.6% for $Cu_{12}As_4S_{13}$ and 13.8% for Cu_3AsS_4]. The phase analysis of these reaction products indicate the absence of any arsenic compound and no reduction of copper sulphide occurs suggesting that the arsenic component is lost as the volatile oxide $As_4O_{6(g)}$.

At higher temperatures, reduction of copper sulphide occurs and the copper produced combines with arsenic to form the arsenide Cu_3As. The higher metal/Sulphur ratio in tennantite ($Cu_{12}As_4S_{13}$) compared with enargite (Cu_3AsS_4) accounts for the higher concentration of copper and copper-arsenide in the tennantite reaction products.

The results of the graphite reduction reactions indicate a much slower rate of reduction. Reduction is incomplete at 1000°C after 90 minutes of reaction and below this temperature, there is no appreciable reaction. The presence of the copper-arsenic oxysulphide phase in the reaction products indicates that a kinetic barrier exists, hindering the progress of reaction. The activities of oxide and sulphide are altered by the formation of liquid oxysulphide making the reduction reaction thermodynamically more favourable. The kinetic barrier is lowered by increased temperature, and significant levels of reaction are observed at 1000°C.

A comparison of these results with those obtained for the carbothermic reduction of copper sulphides [52] indicates that the reduction of complex copper-arsenic sulphides is much faster than the reduction of copper sulphides (CuS, Cu_2S). In the present investigation, complete reduction of tennantite ($Cu_{12}As_4S_{13}$) and enargite (Cu_3AsS_4) was attained after about 40 minutes (using stoichiometric quantities of lime and coal) whereas the complete reduction of Cu_2S takes about one hour at the same temperature

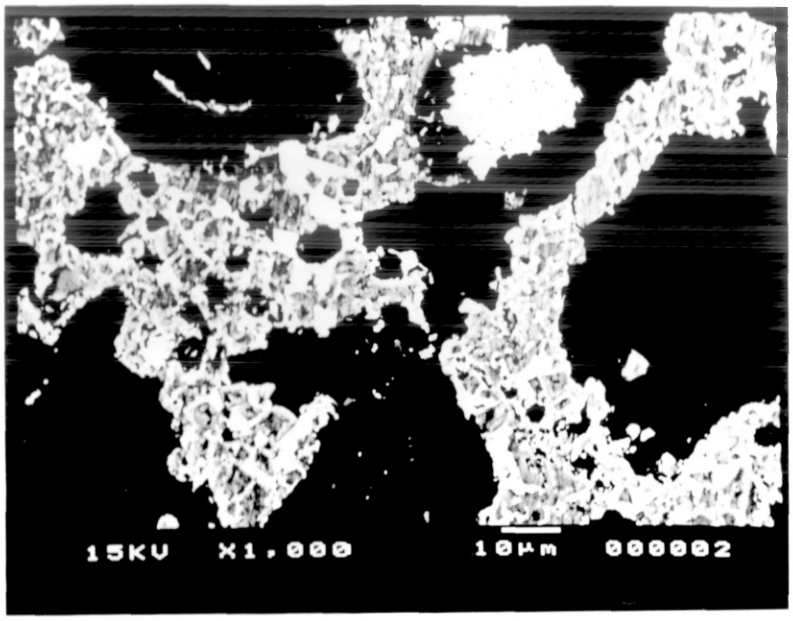

PLATE 4.10

Electron micrograph of synthetic tennantite
reduced with collie coal at 1000°C for 90 mins [BSE image]

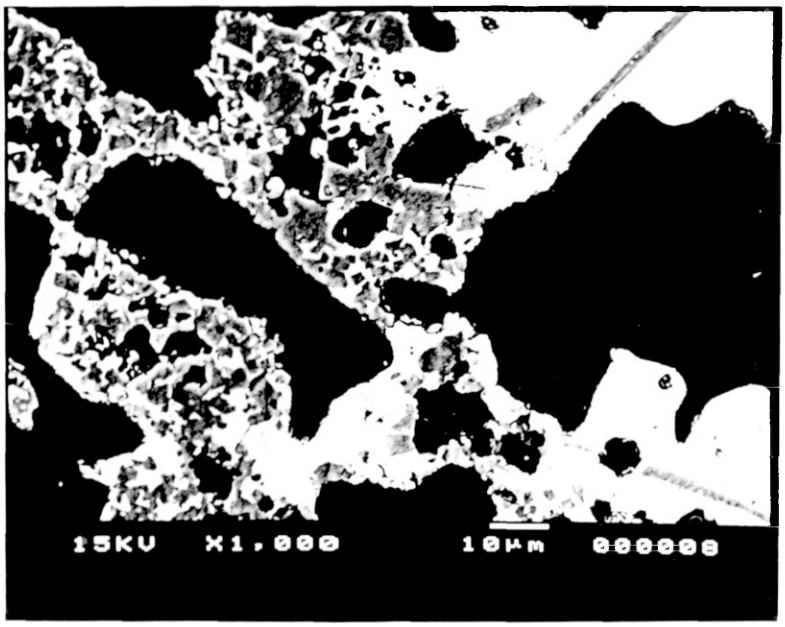

PLATE 4.11

Electron micrograph of synthetic enargite
reduced with collie coal at 1000°C
for 90 mins [BSE image]

using a stoichiometric excess (100%) of coal.

Plates 4.10 and 4.11 are scanning electron micrographs of tennantite ($Cu_{12}As_4S_{13}$) and enargite (Cu_3AsS_4) pellets reduced with coal at 1000°C (90 minutes reaction time). Copper arsenide (Cu_3As) appear as the white regions while the dark areas are the metallic copper phase. The low contrast between copper and calcium sulphide makes it difficult to show the calcium sulphide regions although their outlines are visible. It is observed that in both reduction reaction products, the metallic copper phase is dispersed within the copper arsenide matrix and the copper concentration in the tennantite reduction product is higher than that of enargite as indicated by the phase analysis.

4.3.3 Discussion of the carbothermic reduction of copper-arsenic sulphides

On reaction between calcium oxide and complex copper arsenic sulphides, arsenic is oxidised to $As_4O_6(g)$ while copper sulphide remains largely unreacted. Various investigators have reported that the decomposition of tennantite [$Cu_{12}As_4S_{13}$] enargite [Cu_3AsS_4] begin at about 630°C; the decomposition reaction products are copper sulphides and volatile arsenic sulphides. Smith et al [65] suggested that the decomposition of enargite occurs as:

$$2Cu_3AsS_{4(s)} = Cu_2S_{(s)} + 4CuS_{(s)} + As_2S_{3(g)} \qquad [4.12]$$

while Yoshimura [66] suggested that the reaction is represented by

$$2Cu_3AsS_{4(s)} = 3Cu_2S_{(s)} + As_2S_{3(g)} + S_{2(g)} \qquad [4.13]$$

A similar decomposition reaction has been suggested in another investigation by Smith [67]

$$4Cu_3AsS_{4(s)} = 6Cu_2S_{(s)} + As_4S_{6(g)} + 2S_{2(g)} \qquad [4.14]$$

Thermodynamic data suggest that the stable gaseous compound of orpiment (As_2S_3) is $As_2S_{3(g)}$ and not $As_4S_{6(g)}$ indicating that the

decomposition reactions represented by equations 4.12 and 4.13 are more probable. In contact with CaO, $As_2S_{3(g)}$ rapidly oxidises to volatile $As_4O_{6(g)}$:

$$As_2S_{3(l)} + 3CaO(s) = \tfrac{1}{2}As_4O_{6(g)} + 3CaS_{(s)} \qquad [4.15]$$

$$\Delta G_T^o = -640 - 3.89T \text{ cal/mol}$$

$As_4O_{6(g)}$ reacts with CaO to form calcium arsenite while it's reaction with Cu_2S leads to the formation of copper-arsenic oxysulphide (Cu-As-S-O). The calcium arsenite phase formed probably has the formula $Ca_3(AsO_3)_2$ [no formula is given in the JCPDS diffraction data files]. Shigematsu [68] has determined the equilibrium data for the formation of various metal arsenates and arsenites. Calcium arsenite is formed in the absence of free oxygen by the reaction:

$$3CaO_{(s)} + \tfrac{1}{2}As_4O_{6(g)} = Ca_3(AsO_3)_{2(s)} \qquad [4.16]$$

$$\Delta G_T^o = -26,620 + 18.43T \text{ cal/mol}$$

For the above reaction $K_{1073} = 25$, and $P_{As_4O_6} = 1.6 \times 10^{-3}$ atm. Thus when the pressure of $As_4O_{6(g)}$ is 1.6×10^{-3} atm, there is a considerable driving force for the formation of calcium arsenite [$Ca_3(AsO_3)_2$] during reaction at 1073K.

Chalcocite (Cu_2S) is formed as a result of the decomposition of tennantite ($Cu_{12}As_4S_{13}$) and enargite (Cu_3AsS_4) according to equations 4.12 and 4.13. The difficulty of oxidation of chalcocite is reflected by the large positive value of the Gibb's free energy for the oxidation reaction:

$$Cu_2S_{(s)} + CaO_{(s)} = Cu_2O_{(s)} + CaS_{(s)} \qquad [4.17]$$

$$\Delta G_T^o = 13,250 + 8.54T \text{ cal/mol}$$

In addition, a kinetic barrier also exists to the diffusion of oxygen atoms through the non-porous chalcocite. Investigations by Holmstrom [2] on

the removal of arsenic from Gold-rich copper-arsenic and iron-arsenic concentrates by roasting show that the transport of reaction products through the decomposed layer is the rate controlling step. A comparison of the removal rate of arsenic from concentrates containing arsenopyrite (FeAsS) with those containing enargite (Cu_3AsS_4) and tennantite ($Cu_{12}As_4S_{13}$) shows that the removal rate of arsenic from arsenopyrite was much faster. The observed difference in arsenic removal rate is attributed to the higher transport rate for the gaseous diffusion of arsenic through the porous pyrrhotite ($Fe_{1-x}S$) layer formed during the roasting of arsenopyrite compared with the solid state diffusion of arsenic and sulphur through the non-porous layer of chalcocite (Cu_2S) surrounding the enargite and tennantite.

The overall carbothermic reduction reaction of enargite (Cu_3AsS_4) and tennantite ($Cu_{12}As_4S_{13}$) can be represented as

$$Cu_3AsS_{4(s)} + 4CaO_{(s)} + 4C_{(gr)} = Cu_3As_{(s)} + 4CaS_{(s)} + 4CO_{(g)} \quad [4.18]$$

$$Cu_{12}As_4S_{13(s)} + 13CaO_{(s)} + 13C_{(gr)} = 4Cu_3As_{(s)} + 13CaS_{(s)} + 13CO_{(g)} \quad \ldots [4.19]$$

The experimental results show that the formation of Cu_3As begin at about 800^oC. The weight loss observed at lower reaction temperatures is due to the vaporisation of arsenic ($As_{4(g)}$). The rate of reduction increases with temperature and the reaction is practically complete after about 40 minutes at 1000^oC with copper arsenide (Cu_3As) and copper as the reaction products. The rapid volatilisation of arsenic at the early stages of the reaction (before any appreciable reduction of chalcocite takes place) leads to a depletion in the arsenic content of the samples. Thus, at the completion of reaction, the sample is copper-rich and the reaction products are Cu_3As + Cu with a higher copper/arsenic ratio than in the unreacted sample.

Figure 4.26 shows a section of the copper-arsenic phase diagram. The Cu-Cu_3As eutectic occurs at 685^oC (21.0 wt% Cu) and Cu_3As melts at 827^oC. Hence copper and arsenic will form liquid Cu_3As at relatively low temperatures, lowering the activities of copper and arsenic thus making

the reduction reactions thermodynamically more favourable. The higher metal/sulphur ratio in tennantite ($Cu_{12}As_4S_{13}$) accounts for the higher

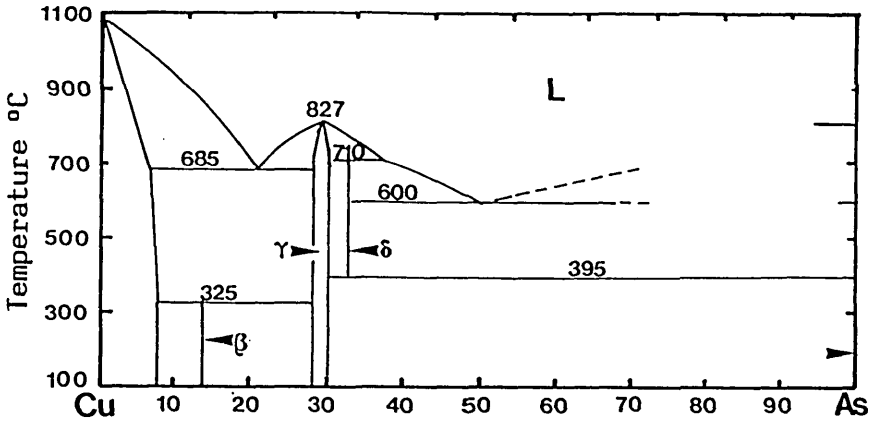

Phase	Formula
β	$Cu_{8.9}As$
γ	Cu_3As
δ	Cu_5As_2

FIGURE 4.26

The Copper-Arsenic Phase Diagram

concentration of Cu_3As and Cu in it's reaction product. The results indicate that the ß copper arsenide phase ($Cu_{8.9}As$) is not stable at room temperatures.

Mertz and Mathewson [69] have determined the variation in the lattice parameter of copper alloys with concentration and this is represented in Figure 4.27.

The lattice parameter of the metallic copper phase obtained in this study is 3.641 A indicating a dissolution of 7.8 wt% As in the metallic product. This represents the maximum level of solubility of arsenic in copper at room temperature (Figure 4.27).

Hino and Azakami [70] have calculated the total pressure of arsenic and the vapour pressure of copper over the copper-arsenic alloy system at 1150°C (Figure 4.28).

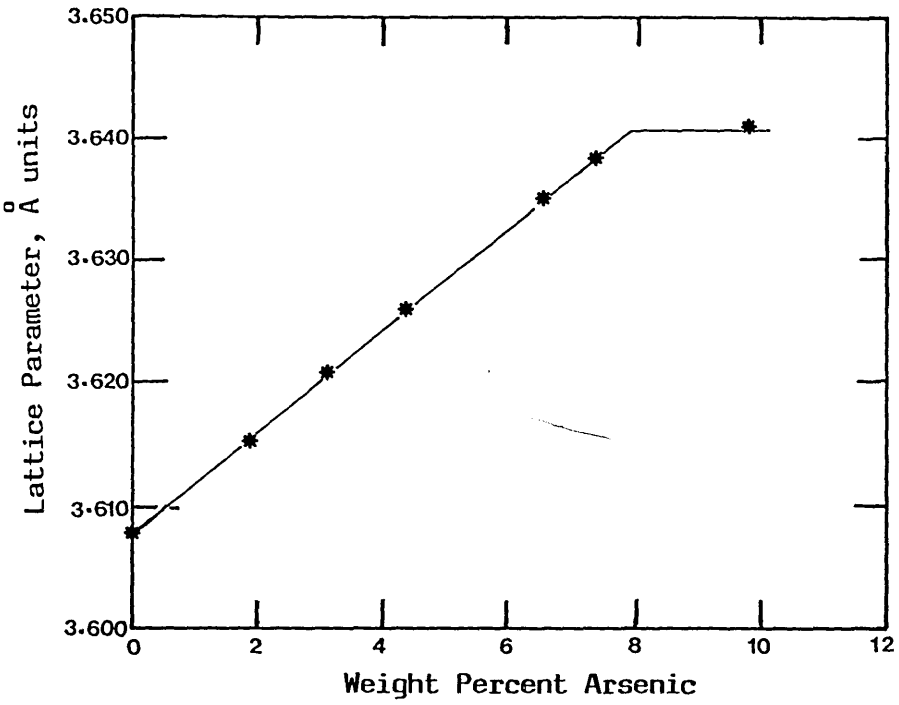

FIGURE 4.27

Variation in the Lattice Parameter of Copper-Arsenic Alloys with Concentration [69]

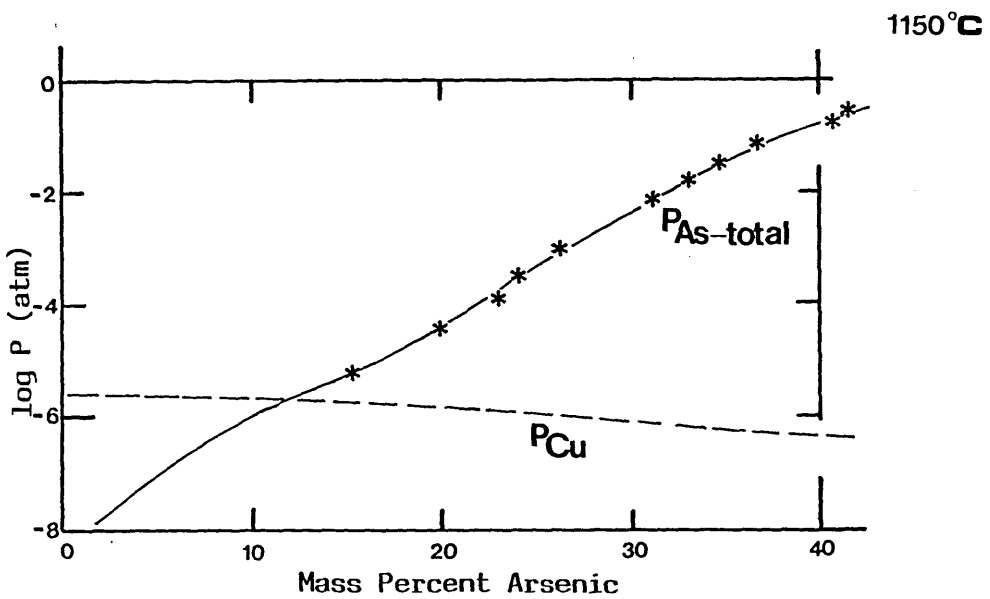

FIGURE 4.28

The Total Pressure of Arsenic and the Vapour Pressure of Copper in the Cu-As System [70]

From Kellogg [71], vaporisation metallurgy can only be applied when the vapour pressure of a component is more than about 1×10^{-4} atmosphere. This corresponds to about 22.0 wt% arsenic in the Cu-As binary system at 1150°C. The arsenic vapour pressure is less than that of copper in the composition range below 11.0 wt% arsenic. Thus the removal of arsenic from molten copper by evaporation techniques will be extremely difficult.

Thermodynamic data indicate a relatively high chemical stability of the copper-arsenide Cu_3As

$$As_{(s)} + 3Cu_{(s)} = Cu_3As_{(s)} \qquad [4.20]$$

$$\Delta G_T^o = -25{,}920 + 0.33T \text{ cal/mol}$$

This underlines the relative difficulty encountered during the elimination of arsenic from copper-arsenides.

4.4 The carbothermic reduction of copper-antimony sulphides

The results and discussion of the exchange and reduction reactions of synthesised famatinite (Cu_3SbS_4) and tetrahedrite ($Cu_{12}Sb_4S_{13}$) are presented in this section.

4.4.1 Exchange reactions between copper-antimony sulphides and lime

Figures 4.29 and 4.30 show the weight losses obtained during the reaction of synthetic famatinite (Cu_3SbS_4) and tetrahedrite ($Cu_{12}Sb_4S_{13}$) with lime at various temperatures. X-ray diffraction studies of the phases resulting from the exchange reactions are presented in Table 4.7.

The exchange reactions result in the oxidation of the antimony component of the complex sulphide. Only partial oxidation of copper sulphide occurs and unreacted chalcocite (Cu_2S, $Cu_{1.96}S$) is present in the reaction product.

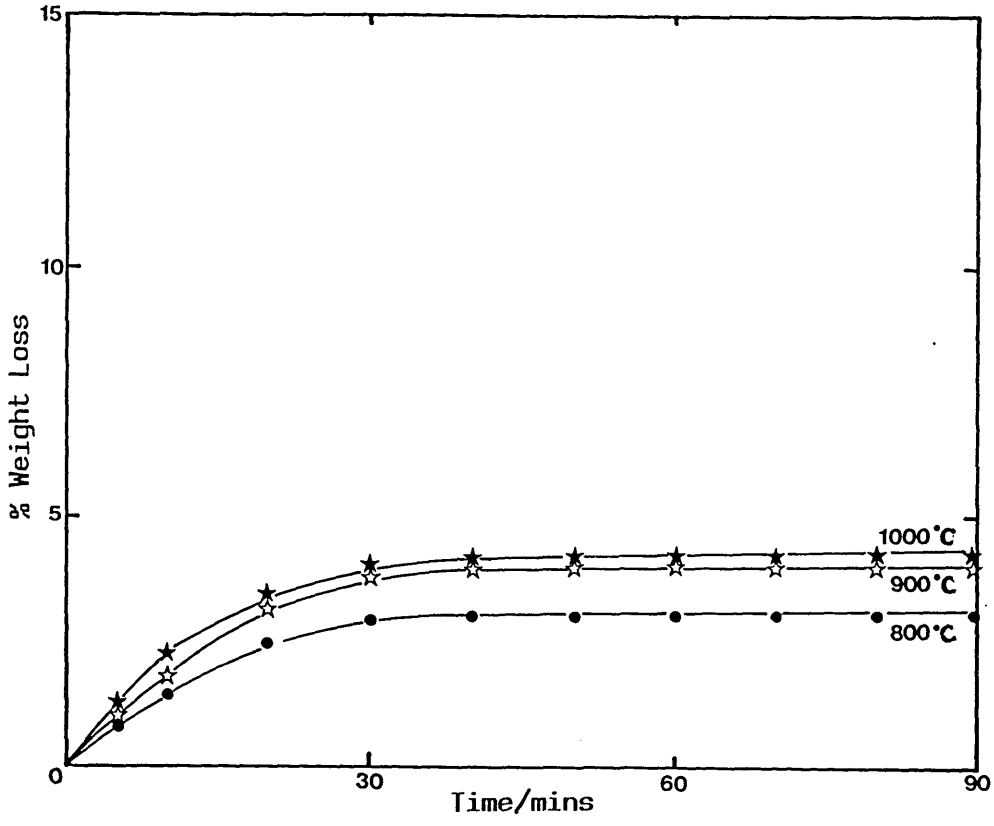

FIGURE 4.29

Rate of Weight Loss for the Exchange Reaction of Famatinite [Cu_3SbS_4:CaO (1:1)] at Various Temperatures

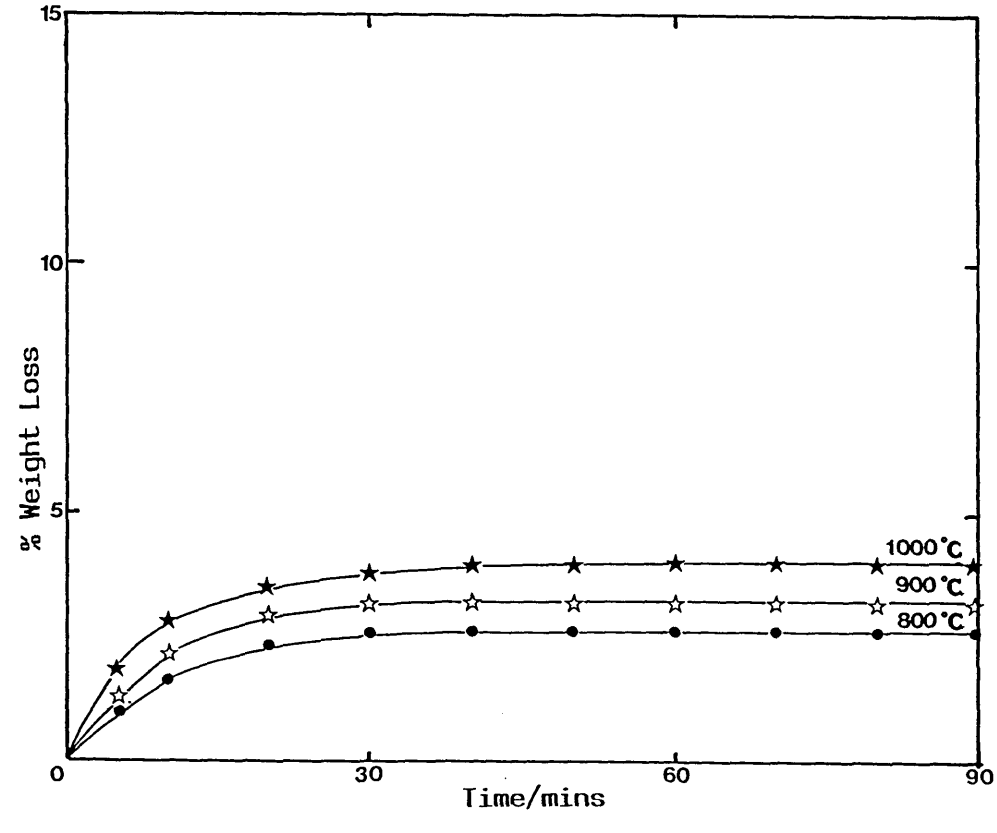

FIGURE 4.30

Rate of Weight Loss for the Exchange Reaction of Tetrahedrite [$Cu_{12}Sb_4S_{13}$:CaO (1:1)] at Various Temperatures

Mixture Composition - Cu_3SbS_4:CaO (1:1)

Temp (°C)	Reaction Time (mins)	Wt Loss (%)	Phase Analysis, Relative Intensity					
			Cu_2S	$Cu_{1.96}S$	CaO	CaS	$Ca_2Sb_2O_5$	Cu-O-Sb
800	90	3.0	MW	W	W	MS	M	VW
900	90	4.0	M	VW	MW	VS	VW	MW
1000	90	4.2	M	VW	MW	VS	VVW	MW
700→↑1000	120	4.1	M	VW	MW	VS	VW	MW

Mixture Composition - $Cu_{12}Sb_4S_{13}$:CaO (1:1)

Temp (°C)	Reaction Time	Wt Loss (%)	Phase Analysis, Relative Intensity					
			Cu_2S	$Cu_{1.96}S$	CaO	CaS	$Ca_2Sb_2O_5$	Cu-O-Sb
800	90	2.6	MW	W	MW	S	MW	W
900	90	3.1	M	W	M	VS	W	MW
1000	90	4.0	M	W	M	VS	W	MW
700→↑1000	120	4.0	M	W	M	VS	VW	MW

Phase Analysis Intensity:

VS - Very Strong
S - Strong
MS - Medium Strong
M - Medium
MW - Medium Weak
W - Weak
VW - Very Weak
VVW- Very Very Weak

TABLE 4.7

Mass Balance and Phase Analysis of the Products of the Lime Exchange Reactions Of Famatinite (Cu_3SbS_4) and Tetrahedrite ($Cu_{12}Sb_4S_{13}$)

4.4.2 Reduction of famatinite (Cu_3SbS_4) and tetrahdedrite ($Cu_{12}Sb_4S_{13}$)

The results of the study of the reduction of famatinite (Cu_3SbS_4) and tetrahedrite ($Cu_{12}Sb_4S_{13}$) with carbon (coal and graphite) are shown in Figures 4.31 to 4.34 while the phase analysis of the reaction products are shown in Table 4.8.

The curves illustrated in Figures4.31-4.34 represent the rate of the carbothermic reduction of famatinite (Cu_3SbS_4) and tetrahedrite ($Cu_{12}Sb_4S_{13}$) at various temperatures. Reduction is only complete when coal is used as the reductant at 1000^oC and only traces of unreacted copper sulphide remain in the reaction product (the coal reduction of famatinite (Cu_3SbS_4) and tetrahedrite ($Cu_{12}Sb_4S_{13}$) is complete after about 45 minutes of reaction at 1000^oC). At lower temperatures (700-900^oC), the reaction products contain varying quantities of copper sulphide - Cu_2S, $Cu_{1.96}S$ and calcium antimonate - $Ca_2Sb_2O_5$ indicating incomplete reduction. The identical rate loss profiles for the reduction of famatinite and tetrahedrite indicate that their reduction mechanism is similar.

The isothermal reduction curves show an initial period of weight losses during which the main reaction is the reduction of the antimony sulphide component of the sample. This is followed by a second reaction stage during which the rate of weight loss is less rapid and reduction of copper sulphide is the dominant reaction. These two reaction steps are more obvious at lower reaction temperatures (700^oC, 800^oC) when the reduction of copper sulphide is not appreciable in which case a greater proportion of the weight loss is due to the reduction of antimony sulphide. This is reflected in the presence of the antimony-rich copper antimonide (Cu_2Sb) in the reaction products.

The weight loss for the reduction of both famatinite (Cu_3SbS_4) and tetrahedrite ($Cu_{12}Sb_4S_{13}$) with coal at 1000^oC are slightly higher than the theoretical values expected for complete reduction of the complex sulphides - 14.6% for Cu_3SbS_4 and 13.4% for $Cu_{12}Sb_4S_{13}$. The higher experimental weight losses observed are due to the vaporisation of antimony.

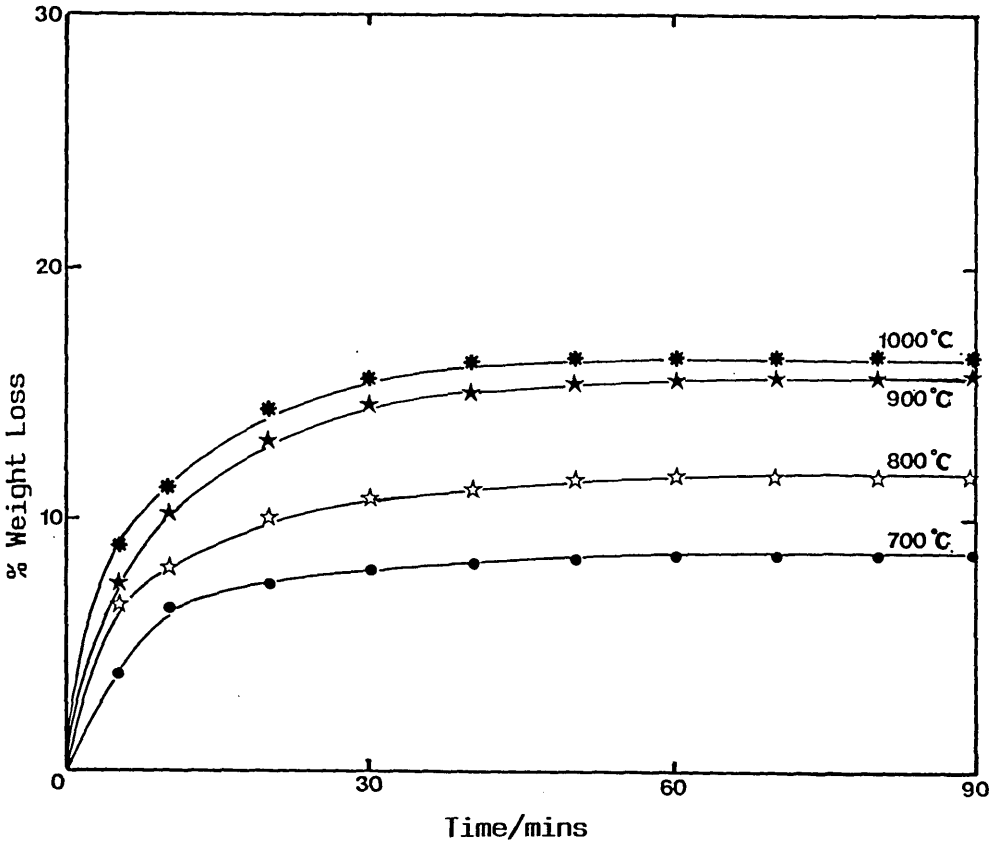

FIGURE 4.31

Rate Plot for the Carbothermic Reduction of Famatinite with Collie Coal at Various Temperatures

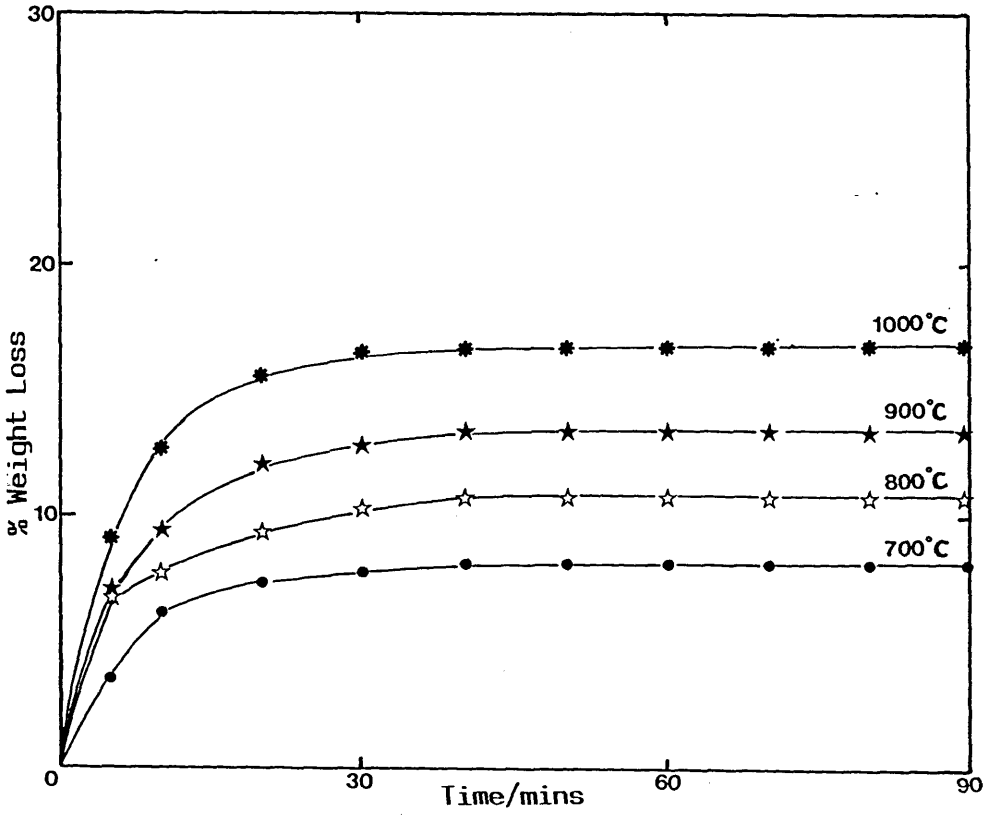

FIGURE 4.32

Rate Plot for the Carbothermic Reduction of Tetrahedrite with Collie Coal at Various Temperatures

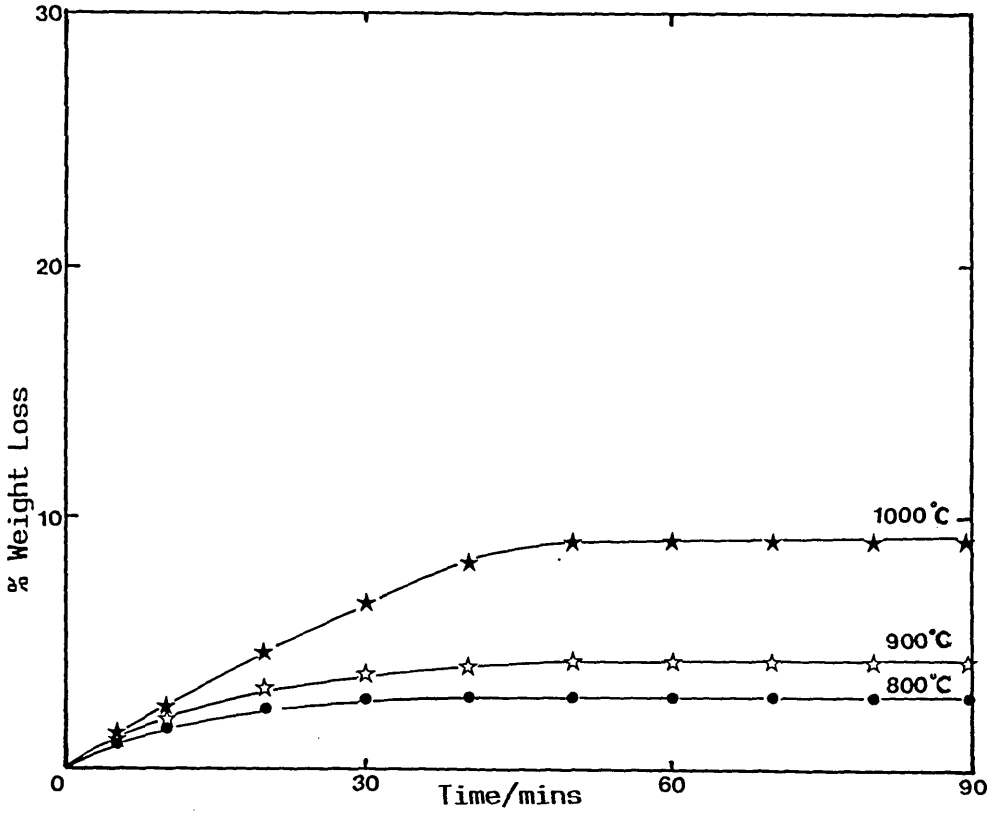

FIGURE 4.33

Rate Plot for the Carbothermic Reduction of Famatinite with Graphite at Various Temperatures

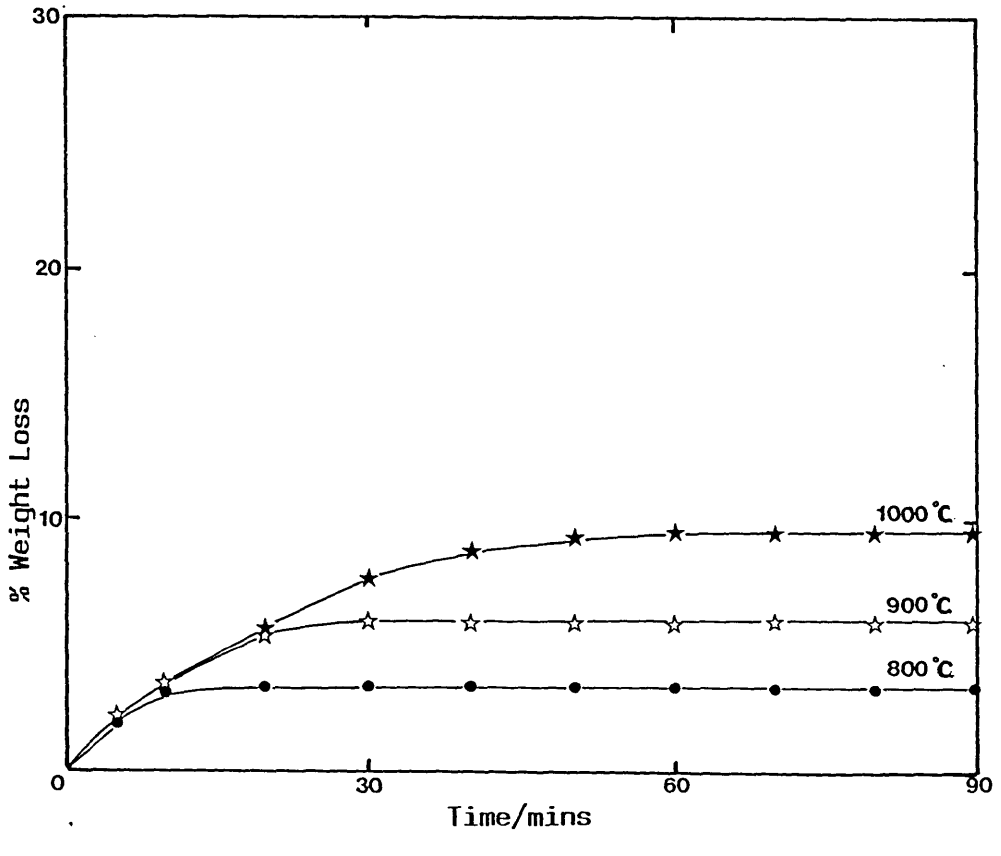

FIGURE 4.34

Rate Plot for the Carbothermic Reduction of Tetrahedrite with Graphite at Various Temperatures

Mixture Composition - Cu_3SbS_4:CaO:C_{Coal} (1:1:1)

Temp (°C)	Reaction Time (mins)	Wt Loss (%)	Phase Analysis, Relative Intensity						
			Cu_2S	$Cu_{1.96}S$	CaO	CaS	Cu_2Sb	$Cu_{4.5}Sb$	$Ca_2Sb_2O_5$
700	90	8.5	M	W	M	MS	W	-	MS
800	90	11.7	M	VW	M	S	MS	-	-
900	90	15.8	W	-	MW	VS	MS	MS	-
1000	90	16.4	VVW	-	W	VS	W	S	-
1000	15	13.0	MW	VVW	MW	S	S	-	VW
1000	45	16.3	VW	-	W	VS	VW	S	-

Mixture Composition - $Cu_{12}Sb_4S_{13}$:CaO:C_{Coal} (1:1:1)

Temp (°C)	Reaction Time	Wt Loss (%)	Phase Analysis, Relative Intensity						
			Cu_2S	$Cu_{1.96}S$	CaO	CaS	Cu_2Sb	$Cu_{4.5}Sb$	$Ca_2Sb_2O_5$
700	90	8.1	M	W	M	MS	MW	-	MS
800	90	10.8	M	W	M	S	S	-	-
900	90	13.4	MW	VW	MW	VS	W	S	-
1000	90	16.7	VVW	-	W	VS	MW	S	-
1000	15	14.4	MW	VVW	MW	S	MW	MS	VVW
1000	45	16.7	VW	-	W	VS	W	S	-

(continued...)

TABLE 4.8

Mass Balance and Analysis of the Products of the Carbothermic Reduction of Famatinite (Cu_3SbS_4) and Tetrahedrite ($Cu_{12}Sb_4S_{13}$)

Mixture Composition - Cu_3SbS_4:CaO:$C_{graphite}$ (1:1:1)

Temp (°C)	Reaction Time (mins)	Wt Loss (%)	Phase Analysis, Relative Intensity							
			Cu_2S	$Cu_{1.96}$	CaO	CaS	Cu_2Sb	$Cu_{4.5}Sb$	$Ca_2Sb_2O_5$	Cu-Sb-O
800	90	2.8	M	W	M	S	-	-	MS	VW
900	90	4.3	MS	VW	M	VS	MW	-	W	W
1000	90	9.1	MW	VVW	MW	VS	S	W	-	-

Mixture Composition - $Cu_{12}Sb_4S_{13}$:CaO:$C_{graphite}$ (1:1:1)

Temp (°C)	Reaction Time	Wt Los (%)	Phase Analysis, Relative Intensity							
			Cu_2S	$Cu_{1.96}$	CaO	CaS	Cu_2Sb	$Cu_{4.5}Sb$	$Ca_2Sb_2O_5$	Cu-Sb-O
800	90	3.3	MS	W	MS	S	VVW	-	M	VW
900	90	5.9	MS	W	M	VS	M	-	VW	W
1000	90	9.5	MW	VW	M	VS	MS	MS	-	-

Phase Analysis Intensity:

VS - Very Strong
S - Strong
MS - Medium Strong
M - Medium
MW - Medium Weak
W - Weak
VW - Very Weak
VVW- Very Very Weak

TABLE 4.8

Mass Balance and Analysis of the Products of the Carbothermic Reduction of Famatinite (Cu_3SbS_4) and Tetrahedrite ($Cu_{12}Sb_4S_{13}$)

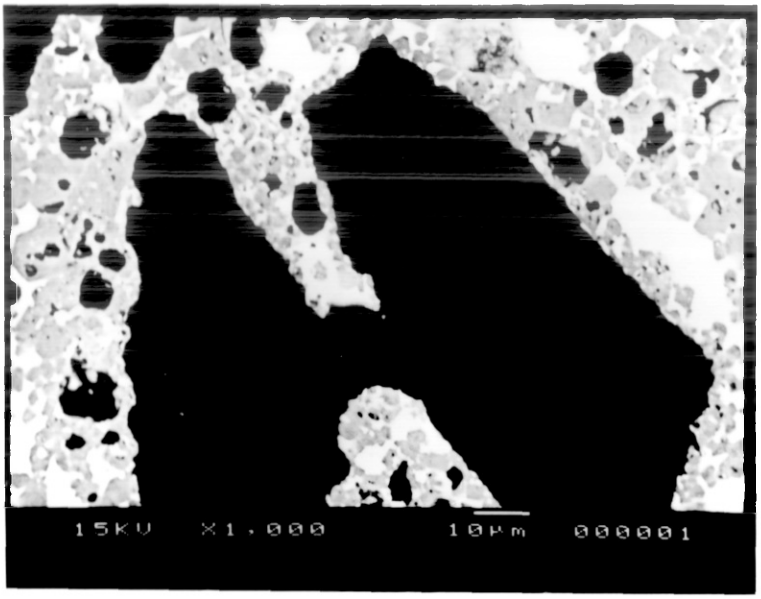

PLATE 4.12

Electron micrograph of synthetic famatinite reduced with collie coal at 1000°C for 90 mins [BSE image]

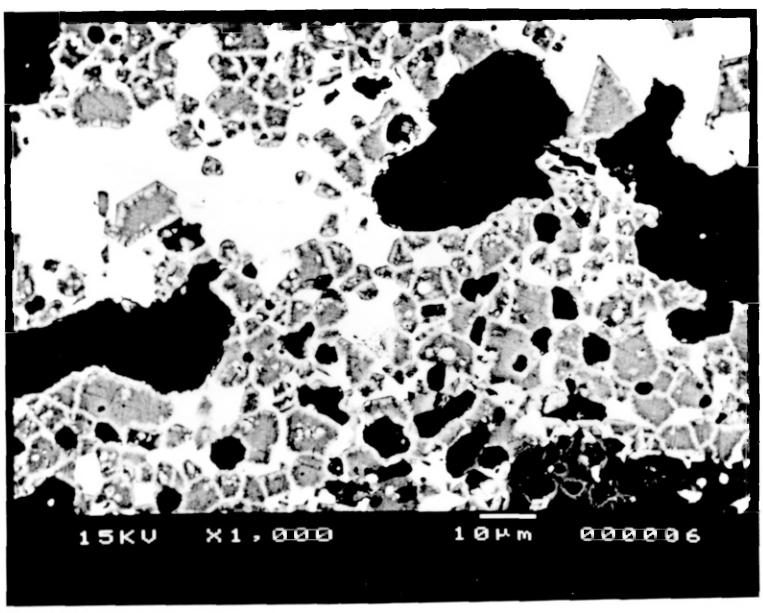

PLATE 4.13

Electron micrograph of synthetic tetrahedrite reduced with collie coal at 1000°C for 90 mins [BSE image]

The results of the graphite reduction reactions indicate a much slower reduction rate. Reduction is incomplete at 1000^{o}C after 90 mins of reaction and below this temperature, there is no significant level of reaction. In addition to unreacted chalcocite (Cu_2S, $Cu_{1.96}S$), the reaction products contain large quantities of calcium antimonate - $Ca_2Sb_2O_5$ and copper-antimony oxide indicating that the overall carbothermic reduction reaction is limited by the reduction of the intermediate oxide products of the exchange reaction.

A comparison of these results with those obtained by Jha et al [72] for the carbothermic reduction of copper sulphides indicates that the reduction of copper-antimony sulphides is more rapid than the reduction of copper sulphides. Whereas complete reduction of famatinite (Cu_3SbS_4) and tetrahedrite ($Cu_{12}Sb_4S_{13}$) is attained after 45 minutes reaction at 1000^{o}C, the complete reduction of Cu_2S requires about 60 minutes reaction at the same temperature using excess (100%) coal.

Plates 4.12 and 4.13 are scanning electron micrographs of famatinite (Cu_3SbS_4) and tetrahedrite ($Cu_{12}Sb_4S_{13}$) pellets reduced with coal at 1000^{o}C (90 minutes reaction time). The bright region is $Cu_{4.5}Sb$, while the grey area is the Cu_2Sb phase. The outline of the CaS phase field is discernible in the dark regions. The large difference between the molecular weights of the copper antimonide phases compared with calcium sulphide makes it difficult to properly highlight all three phases simultaneously. In both reduction products Cu_2Sb is dispersed in the $Cu_{4.5}Sb$ matrix and the CaS phase regions are completely separated from the liquid copper antimonide phases. The morphology of Cu_2Sb in the famatinite reduction reaction product is different from that of tetrahedrite.

4.4.3 Discussion of the carbothermic reduction of copper-antimony sulphides

The reaction between copper-antimony sulphides and calcium oxide leads to the oxidation of the antimony component of the complex sulphide to Sb_2O_3 while only partial oxidation of copper sulphide occurs. Cambi and

Elli [73] have determined a melting temperature of 610°C for tetrahedrite ($Cu_{12}Sb_4S_{13}$). However, in subsequent studies of the phases and phase relations in the Cu-Sb-S system, Skinner, Luce and Makovicky [29] have observed that tetrahedrite breaks down by reaction, not melting at 543°C. They also reported that famatinite (Cu_3SbS_4) melts at 627°C. These reactions are schematically represented by:

$$Cu_{12}Sb_4S_{13(s)} \xrightarrow{543°C} Cu_2S_{(s)} + Cu_3SbS_{4(s)} + Cu_3SbS_{3(s)} \quad [4.21]$$

$$Cu_3SbS_{3(s)} \xrightarrow{607.5°C} \text{liquid} \quad [4.22]$$

$$Cu_3SbS_{4(s)} \xrightarrow{627°C} \text{liquid} \quad [4.23]$$

Thus the reaction between tetrahedrite ($Cu_{12}Sb_4S_{13}$) and lime above 700°C involves reactions between Cu_3SbS_4 and CaO, Cu_3SbS_3 and CaO as well as Cu_2S and CaO. The lime exchange reaction results in the oxidation of the antimony component of the liquid complex sulphides (Cu_3SbS_4, Cu_3SbS_3)

$$Cu_3SbS_{3(l)} + 3CaO_{(s)} \rightarrow \tfrac{1}{2}Sb_2O_{3(l)} + 3/2Cu_2O_{(s)} + 3CaS_{(s)} \quad [4.24]$$

The antimony oxide (Sb_2O_3) product combines with CaO to form calcium antimonate ($Ca_2Sb_2O_5$) and with Cu_2O to form copper antimony oxide.

$$Sb_2O_{3(l)} + 2CaO_{(s)} \rightarrow Ca_2Sb_2O_{5(s)} \quad [4.25]$$

The reaction with Cu_2O probably occurs according to

$$Sb_2O_{3(l)} + Cu_2O_{(s)} \rightarrow Cu_2Sb_2O_{4(s)} \quad [4.26]$$

The limited data available on the copper-antimony-oxygen system has made it difficult to properly assess the conditions under which this reaction occurs and confirm the stoichiometry of the complex oxides.

As discussed in section 4.3.3 [reactions of copper-arsenic sulphides] the lime-exchange reaction of chalcocite (Cu_2S) is thermodynamically unfeasible at all temperatures, thus Cu_2S remains largely unreacted in the exchange reaction products.

The carbothermic reduction of famatinite (Cu_3SbS_4) and tetrahedrite ($Cu_{12}Sb_4S_{13}$) can be represented as

$$Cu_3SbS_{4(s)} + 4CaO_{(s)} + 4C_{(gr)} \rightarrow Cu_3Sb_{(s)} + 4CaS_{(s)} + 4CO_{(g)} \quad [4.27]$$

$$Cu_{12}Sb_4S_{13(s)} + 13CaO_{(s)} + 13C_{(gr)} \rightarrow 4Cu_3Sb_{(s)} + 13CaS_{(s)} + 13CO_{(g)} \quad \ldots [4.28]$$

On cooling the copper antimonide phases $Cu_{4.5}Sb$ and Cu_2Sb, corresponding to the room temperature stable ε and γ copper-antimony alloys, are observed. The β-Cu_3Sb phase is stable from temperatures of about 950°C down to 720°C. Below this temperature, the β-phase decomposes into the $\varepsilon(Cu_{4.5}Sb)$ and γ (Cu_2Sb) phases. The thermodynamic stability of the copper antimony alloys is reflected by the negative free energy for the formation of Cu_2Sb [74].

$$2Cu_{(s)} + Sb_{(s)} = Cu_2Sb_{(s)} \quad [4.29]$$

$$\Delta G_T^{\circ} = -2410 - 4.39T$$

The formation of stable copper-antimonides and the antimonate intermediate product prevents the loss of antimony by volatilisation and the rapid rate of reduction leads to the rapid formation of stable antimony products. The lack of thermodynamic data for most antimony compounds make the quantitative evaluation of their relative stabilities difficult.

4.5 Carbothermic reduction of a complex tetrahedrite concentrate

In this section, the applicability of carbothermic reduction reactions to the extraction of metallic species from a complex sulphide

concentrate is considered. This concentrate contains relatively high levels of impurity phases.

The tetrahedrite concentrate originates from Peru and was obtained from Gregory, Bottley and Lloyd Limited, London. A chemical analysis of the sample is presented in Table 3.2. X-ray diffraction analysis indicates the presence of tennantite [$(Cu,Fe)_{12}As_4S_{13}$], famatinite (Cu_3SbS_4) as the main constituents of the concentrate while spharelite (β-ZnS and silica (SiO_2) appear as minor phases. Trace quantities of galena (PbS) are also present. The tetrahedrite-tennantite and famatinite-enargite series are common minerals in many ore deposits. Arsenic and antimony partioning between a tetrahedrite -tennantite phase and a stably co-existing enargite or famatinite is a unique function of temperature and sulphur activity, a feature which enables their frequent use of a geothermer[75].

The selective removal of the various metallic species in such a complex concentrate presents numerous problems and the investigation of the application of carbothermic reduction techniques for the efficient extraction and separation of the metallic species contained in the complex sulphide concentrate could provide a viable alternative extraction technique.

Significant results of the exchange and reduction reactions conducted are presented in Figures 4.35, 4.36 and Table 4.9.

Initially, exchange reactions were conducted with only the quantity of lime (CaO) needed to exchange the arsenic component (10% CaO), converting it to volatile As_4O_6 gas. From the phase analysis of the reaction products (Table 4.9), it is observed that this does not occur, instead, the available CaO reacts with famatinite (Cu_3SbS_4), leaving tennantite [$(Cu,Fe)_2As_4S_{13}$] completely unreacted. The weight losses observed are less than that necessary for the complete loss of arsenic as As_4O_6 gas which is calculated to be 10.8%. The weight loss observed is due to the volatilisation of sulphur, and deposits of sulphur were observed in the upper (cooler) regions of the quartz reaction tube at the end of the experiment.

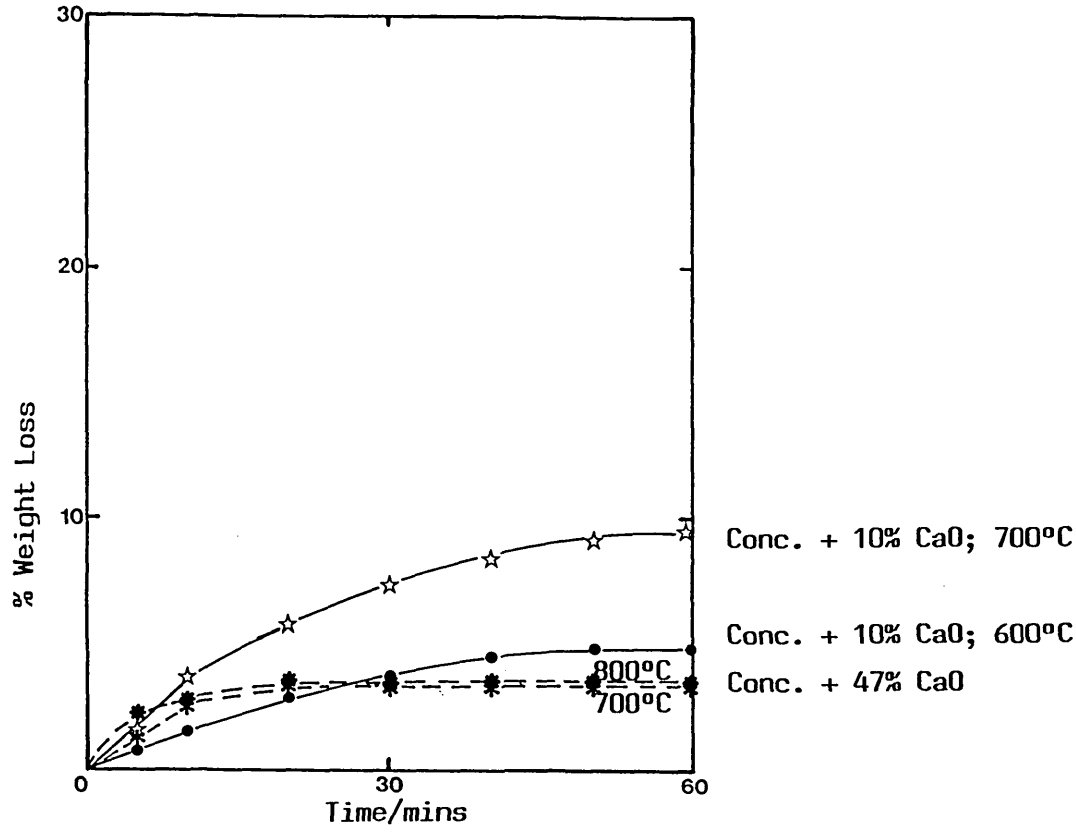

FIGURE 4.35

Rate of Weight Loss for the Exchange Reaction of Tetrahedrite Concentrate with Varying Lime/Sulphide Ratios at Various Temperatures

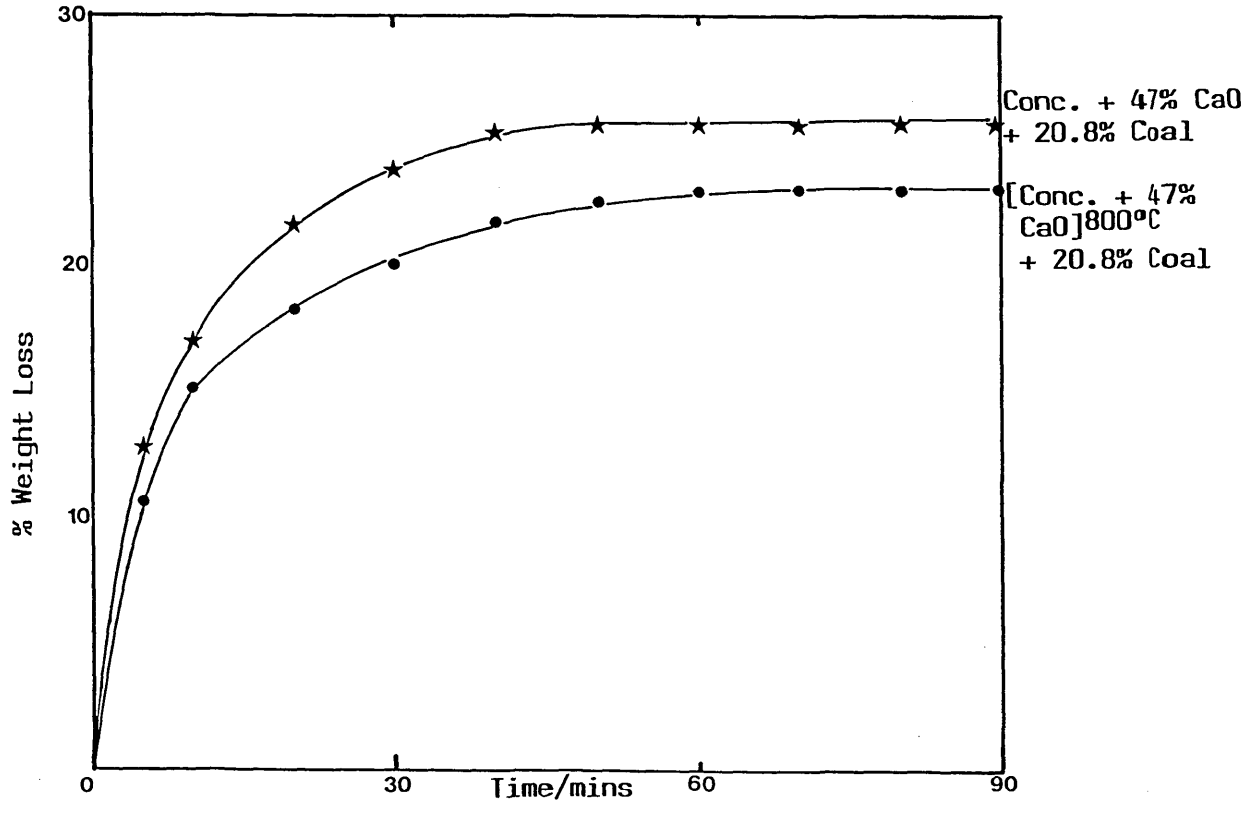

FIGURE 4.36

Rate Plot for the Carbothermic Reduction of Tetrahedrite Concentrate with Collie Coal at 1000°C

Pellet Composition	Temp (°C)	Reaction Time (mins)	Weight loss (%)	Phase Analysis, Relative Intensity									
				CaS	CaO	$Ca_2Sb_2O_5$	Cu_2S	$Cu_{1.96}S$	$(Cu,Fe)_{12}As_4S_{13}$	Cu-Fe-S-Ca-O	Ca-As-O	ZnS	PbS
I concentrate + 10% CaO	600	60	4.8	MW	M	M	VW	W	VS	-	VVW	M	VW
II concentrate + 10% CaO	700	60	9.5	M	M	M	VW	W	VS	-	VW	M	VW
III concentrate + 47% CaO	700	60	3.3	MS	M	M	W	VW	-	VW	VW	M	VW
IV concentrate + 47% CaO	800	60	3.5	S	W	M	VW	VW	-	W	VW	M	VW

(continued ....)

TABLE 4.9

Mass Balance and Phase Analysis of the Products of the Carbothermic Reduction of the Tetrahedrite Concentrate

Pellet Composition	Temp (°C)	Reaction Time (mins)	Weight Loss (%)	Phase Analysis, Relative Intensity					
				CaO	CaS	$(Fe,Cu_2)As$	$Cu_{4.5}Sb$	Cu	Pb
V (IV) + 20.8% Coal	1000	90	23.1	VVW	VS	MS	MS	MS	VVW
VI concentrate + 47% CaO + 20.8% Coal	1000	90	25.8	VVW	VS	MS	MS	M	VVW

Phase Analysis Intensity:

VS - Very Strong	S - Strong	MS - Medium Strong
M - Medium	MW - Medium Weak	W - Weak
VW - Very Weak	VVW- Very Very Weak	

TABLE 4.9

Mass Balance and Phase Analysis of the Products of the Carbothermic Reduction of the Tetrahedrite Concentrate

With the addition of the stoichometric quantity of lime (CaO) required to completely exchange the sulphide samples, reaction of tennantite [$(Cu,Fe)_{12}As_4S_{13}$] occurs but the observed weight loss [3.3% (700^oC); 3.5 (800^oC)] is much less that the expected value if the complete loss of arsenic as $As_4O_{6(g)}$ were to occur (8.0%). This weight loss is probably due to the partial loss of arsenic as $As_4O_{6(g)}$ which occurs before the formation of stable arsenate compounds.

The formation of a quinary compound belonging to the Cu-Fe-S-Ca-O system is also observed. This is similar to the complex oxysulphide compound obtained by Jha [52] during his study of the carbothermic reduction of complex copper-iron sulphides. The presence of calcium arsenate compounds in all the exchange reaction products was also observed. It is possible that there is some dissolution of arsenic in the complex calcium oxysulphide liquid. The antimony component of the concentrate is oxidised and reacts with CaO to form stable calcium antimonate ($Ca_2Sb_2O_5$). Chalcocite (Cu_2S, $Cu_{1.96}S$) is present in all the reaction products while spharelite (ß-ZnS) and trace levels of galena (PbS) remains unreacted in all the exchange reaction products.

On reaction with coal, complete reduction occurs accompanied by a large weight loss. Apart from the evolution of CO product gas, weight losses occur due to the vaporisation of zinc as well as the loss of volatiles contained in the coal. The expected weight loss due to the loss of CO gas resulting from complete reduction is 13.9%; a complete loss of zinc vapour from the reacted sample will lead to a 3.8% weight loss while the volatiles in the coal account for a loss of approximately 6.4%. These losses add up to 24.1% a figure which is comparable to that observed experimentally. When the previously reacted exchange reaction product is reduced with coal a reduced weight loss is observed due to the lower concentration of arsenic in the sample (partial loss of arsenic as $As_4O_{6(g)}$ occurs during the exchange reaction). If it is assumed that the 3.8% weight loss resulting from the exchange reduction reaction is due to the loss of arsenic as $As_4O_{6(g)}$, this would be expected to lead to a decrease of 1.4% in the amount of CO gas evolved.

Phase analysis indicates the formation of copper (Cu), copper antimonide ($Cu_{4.5}Sb$) and a complex arsenide [$(Cu,Fe)_2As$]. The observation that antimony tends to associate with copper while arsenic associates with iron in the reaction product is very remarkable with regard to the separation of the various metallic species present in the reaction product. Traces of metallic lead was detected in the reaction product while zinc is completely absent.

Plate 4.14 shows a scanning electron micrograph of a tetrahedrite concentrate pellet reduced with coal at 1000^{o}C. Copper antimonide ($Cu_{4.5}Sb$) appears as the bright regions while the grey area is copper-iron arsenide [$(Cu,Fe)_2As$]. Calcium sulphide (CaS) shows up as the dark phase regions. In Plate 4.15 a higher magnification micrograph of the metallic region of the specimen is shown. The copper antimonide ($Cu_{4.5}Sb$) and copper-iron arsenide [$(Cu,Fe)_2As$] are observed as clearly separate regions. Furthermore, the appearance of a darker phase field within the arsenide phase region is clearly apparent. This probably represents the copper phase field. An EDS (energy dispersive spectrum) elemental analysis indicates an average of composition of 71.24 at % Cu, 19.25 at % Sb, for the bright phase. For the dark grey phase, the EDS analysis yields an average concentration of 24.73 at % Cu, 44.88 at % Fe, 28.27 at % As.

As discussed in Section 4.4.3 and 4.3.3 which detail the mechanisms of the carbothermic reduction of copper-antimony sulphides and copper-arsenic sulphides respectively, famatinite (Cu_3SbS_4) melts at about 627^{o}C while the decomposition of tennantite ($Cu_{12}As_4S_{13}$) starts at about 630^{o}C. In the complex tetrahedrite concentrate, the lime-exchange reaction of the antimony component of the liquid famatinite (Cu_3SbS_4) phase is more favourable. The antimony oxide (Sb_2O_3) formed readily combines with lime to form the stable calcium antimonate ($Ca_2Sb_2O_5$). The retention of the arsenic component of the concentrate as $(Cu,Fe)As_4S_{13}$ at 700^{o}C is probably due to the incorporation of iron in the tennantite structure. The absence of thermodynamic data makes it impossible to assess the effect of iron addition on the stability of tennantite. The relative stability shown by tennantite [$(Cu,Fe)_{12}As_4S_{13}$] relative to famatinite (Cu_3SbS_4) makes it difficult to remove arsenic [as volatile $As_4O_{6(g)}$] by lime oxidations.

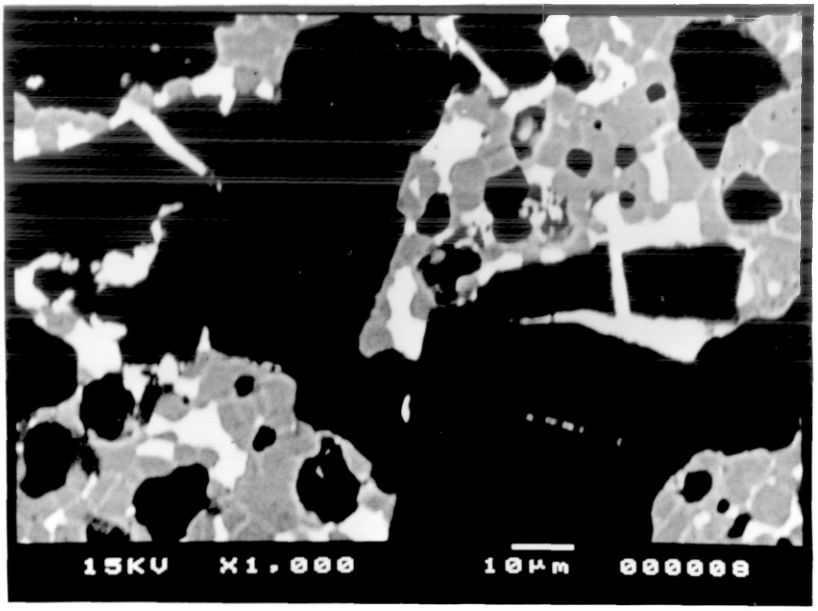

PLATE 4.14

Electron micrograph of tetrahedrite concentrate reduced with collie coal at 1000°C for 90 mins [BSE image]

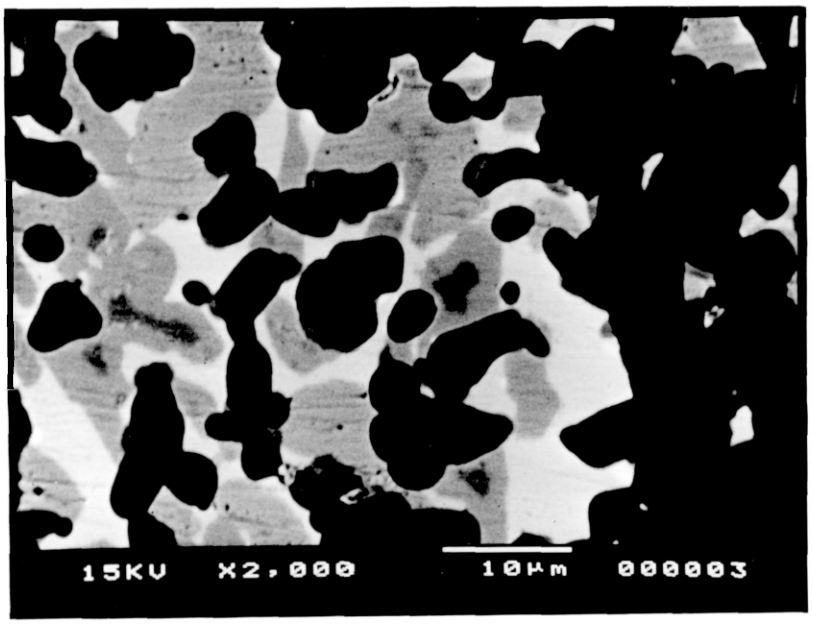

PLATE 4.15

Electron micrograph of tetrahedrite concentrate reduced with collie coal at 1000°C for 90 mins - illustrating the antimonide and arsenide alloy phases [BSE image]

In the carbothermic reduction reaction product, it is observed that arsenic tends to associate with copper and iron while antimony combines with copper. This separation of arsenic and antimony is very important in relation to the ease of separation of the reaction products. The morphological observation presented in the scanning electron micrograph (Plate 4.15) indicate that the arsenide and antimonide phases are formed separately.

The most effective separation technique that could be applied will depend on the relative physical and chemical properties of the arsenide and antimonide phases. The antimonide ($Cu_{4.5}Sb$) decomposes to Cu + Cu_3Sb at 735^{o}C and a eutectic exists between Cu and Cu_3Sb at 912^{o}C. Available data on the complex arsenide $(Cu,Fe)_2As$ is rather limited. This phase is probably a solid solution of the Cu_3As and Fe_2As phases; the complex arsenide $(Cu,Fe)_2As$ probably exists with copper in a reaction represented by

$$Cu_3As_{(s)} + Fe_2As_{(s)} \rightleftarrows (Cu,Fe)_2As_{(s)} + Cu_{(s)} \qquad [4.30]$$

Cu_3As melts at 827^{o}C and the eutectic Cu-Cu_3As occurs at 17.5 wt% Cu; 685^{o}C while Fe_2As has a melting point of about 919^{o}C. Thus the antimonide phase has a higher melting temperature than that at which the $(Cu,Fe)_2As$ + Cu liquid mixture exists. Relevant data on the relative magnetic susceptibilities of the Fe_2As, Cu_3As and $Cu_{4.5}Sb$ phases will enable the proper assessment of the viability of a magnetic separation procedure. This could be used in conjunction with other separation techniques.

The zinc sulphide present in the concentrate is easily reduced below 1000^{o}C forming zinc vapour (boiling point 907^{o}C) which can be collected in retorts. The formation of zinc vapour in the CO product gas stream offers the possibility of the use of the reducing CO gas for the prevention of zinc re-oxidation.

4.6 General Discussion of the Mechanism of Carbothermic Reduction Reactions

The single stage carbothermic reduction of metal sulphides, with lime as the exchange medium can be represented as:

$$MS_{(s)} + CaO_{(s)} + C_{(gr)} = M_{(s)} + CaS_{(s)} + CO_{(g)} \qquad [4.31]$$

The overall reaction consists of two steps represented by the **Exchange Reaction:**

$$MS_{(s)} + CaO_{(s)} = MO_{(s)} + CaS_{(s)} \qquad [4.32]$$

and the **Reduction Reaction:**

$$MO_{(s)} + C_{(gr)} = M_{(s)} + CO_{(g)} \qquad [4.33]$$

The exchange reaction is extremely important since the rate of the reduction reaction will depend on the nature and rate of formation of the exchange reaction (intermediate) product. From observations made during this investigation, the lime-exchange reaction of simple and complex sulphides results in the formation of one or more of the following types of phases.

1) pure metal oxide (MO)
2) metal-calcium oxysulphide (MCaOS)
3) lime-metal oxide compound (MO.nCaO)
4) lime-metal sulphide solid solution (MS-CaO)
5) metal oxysulphide (MOS)

Factors that influence the kinetics of the exchange reaction include the reaction temperature, the nature of reactants and reaction products as well as the rate at which the reduction reaction consumes the exchange reaction (intermediate) product. To this extent, the reactivity of the reducing agent and the use of stoichiometric excess quantities of exchange and reducing agents have been found to greatly enhance the rate of carbothermic reduction reaction. The reduction reaction is controlled by

the relationship:

$$C + \{\underline{O}\} = [CO] \qquad [4.34]$$

for which $K_{4.34} = p_{CO}/a_O$

Thus the rate of the reduction reaction depends on the oxygen potential $[a_O \alpha p^{\frac{1}{2}}O_2]$ that exists in the exchange reaction (intermediate) product and the rate of transfer of CO gas from the reacting pellet to the bulk phase. Hence the rate limiting step during carbothermic reduction with graphite is expected to be the rate at which CO_2 is absorbed on the carbon surface (Boudouard reaction).

$$CO_{2(g)} + C_{(gr)} = 2CO_{(g)} \qquad [4.35]$$

Such reasoning is supported by several investigations where it has been demonstrated that slow surface reaction kinetics occur for this reaction.

During the carbothermic reduction of antimony sulphide (Sb_2S_3) with collie coal, the oxide intermediate is never observed in partially reacted samples. The absence of the antimony oxide intermediate compound strongly suggests that the reduction of oxide proceeds at a significantly faster rate than that at which the lime-sulphide exchange reaction can produce the oxide intermediate phase (when reactive coal is used as reductant).

In contrast, during the reduction of antimony sulphide (Sb_2S_3) with graphite, the antimony oxide intermediate compound ($Ca_2Sb_2O_5$) was found to be present in the partially reacted samples. This observation indicates that the overall rate of reaction is controlled by the graphite reduction of the intermediate oxide compound.

From temperature dependence relationships, Turkdogan and Vinters [76, 77] have determined that charcoal is more reactive than graphite by a factor of about 10^2. Further investigations by Coley [78] established that the reactivity of collie coal is similar to that of charcoal. Thus

the rate of collie coal reduction of antimony sulphide is expected to be considerably greater than the rate of graphite reduction by a similar margin ($\sim 10^2$); whereas in this investigation, the use of collie coal as reductant only results in a 4-fold increase in reaction. Thus during carbothermic reduction with coal, the reduction reaction and thus the adsorption of CO_2 on the carbon surface is not the rate controlling step and the absence of the intermediate oxide compound in partially reduced samples strongly indicates that reaction rate is now dependent on the exchange reaction. The fact that the rate enhancement observed with the use of coal as reductant is less than the value expected from comparison of coal and graphite reactivities, is evidence of the physical limitations on the ability of the exchange reaction to generate the oxide intermediate product at a rate commensurate with the reduction reaction in conditions of high carbon reactivity.

The reduction mechanism does not seem to be dependent on the solubility of neither calcium oxide (CaO) or calcium sulphide (CaS) in the exchange reaction product even though calcium sulphide is thought to be soluble in some oxysulphide liquids to significant levels. However, it is unlikely that a solid layer of calcium sulphide exists during the reaction. If this was the case, it would be extremely difficult to obtain the rapid reaction rates that have been observed during carbothermic reduction, due to the difficulty that will arise from the need for the oxide ion (O^{2-}) to diffuse through the solid calcium sulphide layer. The diffusivity of O^{2-} through CaS is comparable to that of O^{2-} through CaO which has been measured to be of the order of 10^{-12} mm^2/sec [79]. This would be equivalent to an extremely slow rate of reduction.

An alternative mechansism for the carbothermic reduction of sulphides based on the production of COS gas has been elaborately discussed by several workers [53, 55, 81, 82], none of whom have presented any experimental evidence. In gas chromatographic analysis of reaction product gases conducted by El-Rahaiby and Rao [53], no detectable level of COS gas was reported.

Consider the reactions

$$Cu_2S_{(s)} + CO_{(g)} = 2Cu_{(s)} + COS_{(g)} \qquad [4.36]$$

$$\Delta G_T^o = 10{,}370 + 10.76T \text{ cal mol}^{-1}$$

$$K_{4.36} = \frac{P_{COS}}{P_{CO}}; \quad P_{COS} = K_{4.36} \cdot P_{CO}$$

$$C_{(gr)} + CO_{2(g)} = 2CO_{(g)} \qquad [4.37]$$

$$\Delta G_T^o = 39{,}810 - 40.8T \text{ cal mol}^{-1}$$

$$K_{4.37} = \frac{p^2_{CO}}{P_{CO_2}} ; \quad P_{CO_2} = \frac{p^2_{CO}}{K_{4.37}}$$

$$COS_{(g)} + CaO_{(s)} = CaS_{(s)} + CO_{2(g)} \qquad [4.38]$$

$$\Delta G_T^o = -24{,}020 + 1.12T \text{ cal mol}^{-1}$$

$$K_{4.38} = \frac{P_{CO_2}}{P_{COS}} = \frac{p^2_{CO}}{K_{4.37} \cdot P_{COS}}$$

$$\therefore \quad P_{CO} = [K_{4.38} \cdot K_{4.37} \cdot P_{COS}]^{\frac{1}{2}}$$

Hence, $P_{COS} = K_{4.36}^2 \cdot K_{4.37} \cdot K_{4.38}$ [4.39]

at 1273K, $P_{COS} = 5.2 \times 10^{-3}$ atm

whereas for the reaction,

$$Cu_2S_{(s)} + CaO_{(s)} + C_{(gr)} = 2Cu_{(s)} + CaS_{(s)} + CO_{(g)} \qquad [4.40]$$

$$\Delta G_T^o = 26{,}160 - 28.99T \text{ cal mol}^{-1}$$

at 1273K, $K_{4.40} = P_{CO} = 7.0 \times 10^{1}$ atm

The large positive free energy change associated with the formation of COS gas in these reducing conditions indicates that this gas is unstable under the thermodynamic conditions existing during carbothermic reduction. In contrast, the formation of CO gas in an exchange-reduction reaction scheme is accompanied by a large negative free energy change.

With regard to kinetic considerations, the rate equations for the production of COS and CO gases during carbothermic reduction reactions will be given by:

$$\eta_{COS} = \frac{Q_1}{RT} (p^i_{COS} - p^b_{COS}) \qquad [4.41]$$

and

$$\eta_{CO} = \frac{Q_2}{RT} (p^i_{CO} - p^b_{CO}) \qquad [4.42]$$

p^b and p^i designate the bulk and equilibrium partial pressures respectively. R is the gas constant while T is absolute temperature. Q_1 and Q_2 represent the proportionality constant which depends on the binary interdiffusivity coefficients of COS and CO gases [D_{COS-Ar}, D_{CO-Ar}] in argon respectively.

The values of D_{COS-Ar} and D_{CO-Ar} have to be estimated from the Chapman-Enskog [83] relationship given by

$$D_{AB} = 0.0018583 \sqrt{\frac{T^3 (1/m_A + 1/M_B)}{P \sigma^2_{AB} \Omega_{D,AB}}} \qquad [4.43]$$

in which, D_{AB} - binary diffusivity for system A-B ($cm^2\ sec^{-1}$)

T - temperature (K)

P - pressure (atm)

σ_{AB} - collision diameter ($\mathring{A}$)

$\Omega_{D,AB}$ - collision integral (dimensionless)

Computation yields values of $D_{COS-Ar} = 1.50\ cm^2\ sec^{-1}$ and $D_{CO-Ar} = 2.31\ cm^2\ sec^{-1}$ for the diffusivities of COS and CO in argon at 1273K for a total pressure of one atmosphere. These relatively large diffusivity values indicate that the binary diffusivity of the product gases in argon will not be rate determining.

Assuming that, the gas partial pressures in the bulk phase is negligible, the rate of COS and CO gas production will be mainly dependent on the COS and CO gas equilibrium partial pressures. From thermodynamic considerations, it has been shown that the CO partial pressure will be much higher than that of COS under the reducing conditions prevailing during carbothermic reduction. Thus the rate of CO gas production will be very much higher than the rate of COS generation. Hence, it seems unlikely that COS production plays a significant role in those reactions, many of which proceed very rapidly indeed. Furthermore, studies of the carbothermic reduction mechanism of lead sulphide carried out as part of this project (see Appendix) have revealed that metallic lead can be formed directly by the lime-exchange reaction (without carbon). This obviously indicates that reduction is not dependent on the formation of COS gas since the formation of COS gas cannot occur in the absence of carbon.

During the carbothermic reduction of complex sulphides; in addition to the various reactions that have been considered, the interaction of the respective metal sulphides with their compounds and the resulting effect on the thermodynamics and kinetics of the reacting systems must be considered. The formation of liquid oxysulphide phases between the sulphide and oxide compounds present during the lime-exchange reaction of complex sulphides enhance the overall carbothermic reduction reaction. The common occurence of complex sulphides that incorporate the low melting compounds of the group V^A elements (As, Sb) with transition metal sulphides result in the formation of complex oxysulphide compounds (during carbothermic reduction) which are liquid at relatively low temperatures.

The formation of liquid intermediate phases enhance the rate of the reduction reaction by increasing the surface area available for reaction. In addition, the formation of stable intermetallic compounds from the

reaction products reduces the activity of the metallic products in the reacting system, thus enhancing the rate of reaction. For example, the formation of the stable iron arsenide (FeAs) phase during the carbothermic reduction of arsenopyrite (FeAsS) reduces the activity of iron and arsenic in the reaction product, thus enhancing the rate of the reduction reaction. The reduction of arsenopyrite can be represented as

$$FeAsS_{(s)} + CaO_{(s)} + C_{(gr)} = Fe_{(s)} + As_{(s)} + CaS_{(s)} + CO_{(g)}$$

$$K_{4.44} = \frac{a_{Fe} \cdot a_{As} \cdot P_{CO}}{a_{FeAsS}} \qquad [4.44]$$

The formation of iron arsenide (FeAs) phase from the reaction products alters the equilibrium, enhancing the reduction reaction. FeAs formation proceeds according to

$$Fe_{(s)} + As_{(s)} = FeAs_{(s)} \qquad [4.45]$$

$$\Delta G_T^{o} = -4175 - 8.35T \text{ cal/mol}$$

The negative free energy change associated with arsenide formation underlines the relatively high stability of these intermetallic phases.

CHAPTER 5

CONCLUSIONS

CHAPTER 5

CONCLUSIONS

The following conclusions have been reached from the observations made during this investigation.

1) the complete reduction of antimony sulphide (Sb_2S_3) with collie coal is attained after only 30 minutes reaction at 700°C, with liquid antimony (Sb) and calcium sulphide (CaS) as the reaction products. The rate of reduction increases with temperature and the loss of antimony by volatilisation of the metallic product, the oxide and sulphide compounds becomes significant at higher reaction temperatures.

2) Exchange reactions between antimony sulphide (Sb_2S_3) and calcium oxide (CaO) in the temperature range 700-900°C lead to the formation of calcium antimonate ($Ca_2Sb_2O_5$) and calcium sulphide (CaS). The antimony oxysulphide phase (Sb_2OS_2) is also present in the product of reaction at 700°C. The use of stoichiometric excess (100%) calcium oxide (CaO) leads to the formation of the antimonate phase - $Ca_3Sb_2O_6$ richer in CaO in addition to $Ca_2Sb_2O_5$.

3) Carbothermic reduction of antimony sulphide (Sb_2S_3) with graphite is significantly slower than reduction with collie coal and complete reduction is not attained with graphite even after 90 minutes reaction at 900°C.

4) The presence of the antimonate ($Ca_2Sb_2O_5$) intermediate compound during the graphite reduction of antimony sulphide (Sb_2S_3) indicates that the rate of graphite carbothermic reduction reaction is controlled by the carbon reduction of the intermediate oxide phase. In contrast, the absence of the intermediate oxide phase during the collie coal reduction of antimony sulphide (Sb_2S_3) strongly suggests that the reduction of the oxide proceeds at a rate faster than the lime-sulphide exchange reaction can generate the oxide intermediate.

5) The activation energy for the reduction of antimony sulphide (Sb_2S_3) and antimony oxide (Sb_2O_3) with collie coal were determined to be 114 kJ mol^{-1} and 94 kJ mol^{-1} respectively.

6) The rate of carbothermic reduction of Stibnite (Sb_2S_3) is dependent on the Sb:S ratio in the concentrate. Reduction of the Canadian (Sb_2S_3) concentrate is faster than the rate of reduction of the synthetic (Sb_2S_3) sulphide which reacts faster than the Bolivian (Sb_2S_3) and South African (Sb_2S_3) concentrates which have lower antimony concentrations.

7) Agglomeration of the liquid antimony product which leads to the formation of 'globules' on the pellet surface occurs during the carbothermic reduction of antimony sulphide at 700°C. Droplet formation does not occur at higher reaction temperatures (800°C, 900°C) and longer periods of heat treatment lead to globule enlargement during reaction at 700°C. This unique phenomena will enhance the effective separation and recovery of antimony from the reaction product.

8) The exchange reactions between arsenopyrite (FeAsS) and calcium oxide (CaO) in the temperature range 800-1000°C results in the oxidation of the arsenic component to arsenic trioxide (As_4O_6) gas and the partial oxidation of pyrrhotite ($Fe_{1-x}S$) to iron oxide (FeO). FeO combines with the calcium sulphide (CaS) reaction product to form iron-calcium oxysulphide (1.33CaS.FeO) and with the arsenic trioxide to form the stable iron arsenate $FeAsO_4$. The extent of pyrrhotite ($Fe_{1-x}S$) oxidation increases with reaction temperature.

9) Carbothermic reduction arsenopyrite (FeAsS) with collie coal occurs rapidly in the temperature range 800-1000°C resulting in the formation of stable iron arsenides and calcium sulphide. The reaction is incomplete at 800°C and unreacted arsenopyrite remains in the reaction product. Complete reduction of synthetic arsenopyrite is attained after 45 minutes using stoichiometric quantities of exchange (CaO) and reducing (collie coal) agents.

10) Increased reaction time and temperature progressively lead to an increased production of metallic iron resulting in the formation of iron arsenides with a higher Fe:As ratio. The reduction of synthetic arsenopyrite [at% Fe/at% As = 1.0] with collie coal at 1000°C (90 minutes reaction time) results in the formation of FeAs and Fe_2As along with CaS, while the corresponding reduction of the arsenopyrite concentrate [at% Fe/at% As = 1.5] produces Fe_2As, Fe and CaS.

11) Iron-calcium oxysulphide (1.33 CaS.FeO) is present in the reaction product in all cases when reduction is incomplete indicating that the overall reaction is controlled by the coal reduction of the oxysulphide [1.33CaS.FeO] intermediate phase.

12) Carbothermic reduction of arsenopyrite (FeAsS) is more rapid than the corresponding reduction of pyrrhotite ($Fe_{1-x}S$). The coal reduction of the arsenopyrite concentrate is complete after 30 minutes reaction at 1000°C while the complete reduction of synthetic arsenopyrite requires 45 minutes whereas the reduction of the single phase pyrrhotite ($Fe_{1-x}S$) is only complete after reaction for 50 minutes at 1000°C. The formation of iron arsenides during the reduction of complex iron-arsenic sulphides is thought to enhance their rate of carbothermic reduction.

13) Reduction of arsenopyrite with graphite is comparatively slower than the reduction with collie coal and the reaction is incomplete at 800°C and 900°C after reduction for 120 minutes. A significant feature of the graphite rate curves is the existence of 'plateaux' in the rate curves, corresponding to conditions in which reduction virtually ceases. These 'plateaux' are similar to those that have been reported during the carbothermic reduction of iron sulphide. A high concentration of the iron-calcium oxysulphide (1.33 CaS.FeO) was observed at the conditions existing at the plateaux. This temporary cessation of reaction occurs due to the difficulty of transporting the oxide ions (O^{2-}) to the carbon surface to nucleate CO gas under the prevailing reaction conditions.

14) 'Plateau' length is redcued by the use of stoichiometric excess graphite reductant. However, even the use of 200% excess graphite at 1000°C, does not completely eliminate the plateau. The 'kinetic barrier' to reduction represented by the temporary cessation of reaction can be overcome by the use of excess reducing agent or more reactive reducing agents such as collie coal or indeed by increasing the reaction temperature.

15) Increasing the reaction temperature as a means of increasing the yield rate is not advisable since this leads to an increased loss of arsenic by volatilisation. The use of reactive reductants like collie coal result in the rapid reduction of arsenopyrite, forming stable iron arsenides and calcium sulphide with minimisation of the loss of toxic arsenic to the atmosphere. On the other hand, in conditions in which the selective removal of arsenic is desired, this is best achieved by the lime-exchange reaction (in the absence of carbon) which copmletely eliminates arsenic by volatilisation of As_4O_6 gas.

16) The lime-exchange reduction of synthetic enargite (Cu_3AsS_4) and tennantite ($Cu_{12}As_4S_{13}$) in the temperature range 700°C-1000°C results in the formtion of calcium asenite and copper-arsenic oxysulphide. Unreacted chalcocite (Cu_2S, $Cu_{1.96}S$) remains in the reaction products. The proper identification of the oxysulphide is hindered by the limited data available on the Cu-As-S-O system.

17) The calcium arsenite phase formed probably has the formula $Ca_3(AsO_3)_2$. Available data on this system mainly relates to the formation of calcium asenates under oxidising conditions.

18) Carbothermic reduction of enargite (Cu_3AsS_4) and tennantite ($Cu_{12}As_4S_{13}$) with coal in the temperature range 700-1000°C generates the copper arsenide (Cu_3As) and metallic copper. Reduction is complete after 40 minutes reaction at 1000°C, and incomplete at lower temperatures (90 minutes reaction time). Covellite (Cu_2S, $Cu_{1.96}S$) is present in the incomplete reaction products.

19) Tennantite ($Cu_{12}As_4S_{13}$) reduction proceeds at a more rapid rate than the reduction of enargite (Cu_3AsS_4) due to a higher metal: sulphur ratio in the former. However, their weight loss profiles are similar indicating an identical reduction mechanism for both complex sulphides.

20) The carbothermic reduction of copper-arsenic sulphides with graphite is significantly slower than the corresponding collie coal reduction reactions. Reduction is incomplete after 90 minutes reaction at 1000°C. Below this temperature, there is no appreciable level of reaction.

21) The presence of copper sulphide in the reaction product in all cases when reaction is incomplete suggests that the overall reaction is controlled by the rate of the copper sulphide reaction. The increase in the rate of copper sulphide reaction with temperature leads to the production of more metallic copper which combines with arsenic to form the stable copper asenide (Cu_3As), thus enhanching the overall carbothermic reaction. Thus, whereas the complete reduction of enargite (Cu_3AsS_4) and tennantite ($Cu_{12}As_4S_{13}$) takes about 40 minutes at 1000°C, the complete reduction of chalcocite (Cu_2S) requires 60 minutes reaction time at the same temperature using a stoichiometric excess (100%) of coal.

22) The lattice parameter of the metallic copper phase obtained by carbothermic reduction of complex copper-arsenic sulphides is 3.641Å

indicating a dissolution of 7.8 wt% As in the metallic product. This represents the maximum level of arsenic solubilty in copper.

23) The exchange reactions between synthetic famatinite ($Cu_{13}SbS_4$) and tetrahedrite ($Cu_{12}Sb_4S_{13}$) with calcium oxide (CaO) in the temperature range 800-1000°C result in the complete oxidation of antimony and partial oxidation of the copper component of the complex sulphides. The antimony oxide (Sb_2O_3) formed combines with calcium oxide (CaO) and copper oxide (Cu_2O) to form calcium antimonate

($Ca_2Sb_2O_5$) and copper-antimony oxide (Cu-O-Sb) respectively. Calcium sulphide (CaS) and unreacted chalcocite (Cu_2S, $Cu_{1.96}S$) are also present in the reaction product.

24) Proper identification of the copper-antimony oxide phase is hindered by the limited data available on the Cu-O-Sb system. Most of the data available on this system relate to those complex oxides formed under oxidising atmospheres. The formation of the stable calcium antimonate and copper-antimony oxide phases prevents the volatilisation of antimony during the exchange reactions.

25) The carbothermic reduction of famatinite (Cu_3SbS_4) and tetrahedrite ($Cu_{12}Sb_4S_{13}$) with coal in the temperature range 700-1000^{o}C results in the formation of the copper antimonides - Cu_2Sb, $Cu_{4.5}Sb$ and calcium sulphide (CaS). Complete reduction is attained after 45 minutes reaction at 1000^{o}C using stoichiometric quantitites of reactants. Below this temperature, reduction is incomplete and calcium antimonate ($Ca_2Sb_2O_5$) is present in the product of reaction at 700^{o}C.

26) Higher reaction temperatures lead to a higher concentration of $Cu_{4.5}Sb$ in the reaction product corresponding with a decrease in the concentration of chalcocite (Cu_2S, $Cu_{1.96}S$) indicating that the carbothermic reduction reaction depends on the rate of copper sulphide reaction.

27) As with the reduction of complex copper-arsenic sulphides, the reduction of tetrahedrite ($Cu_{12}Sb_4S_{13}$) is more rapid than the reduction of famatinite (Cu_3SbS_4) which possess a lower metal:sulphur ratio.

28) The carbothermic reduction of the copper-antimony sulphide with graphite proceeds at a much slower rate compared with the corresponding coal reduction reactions. Reduction is incomplete after 90 minutes reaction at 1000^{o}C, below this temperature there is no appreciable level of reaction.

29) The complete reduction of famatinite (Cu_3SbS_4) and tetrahedrite ($Cu_{12}Sb_4S_{13}$) with coal requires 45 minutes reaction at 1000°C. In comparison, the complete reduction of chalcocite (Cu_2S) needs 60 minutes reaction at the same temperature using a stoichiometric excess (100%) of coal while the complete reduction of antimony sulphide (Sb_2S_3) only requires 30 minutes reaction at 700°C. This illustrates the rate limiting nature of the copper sulphide reduction reaction, and the rate enhancement generated by the formation of stable copper antimonides.

30) The carbothermic reduction of a complex tetrahedrite concentrate (which contains tennantite ($[Cu,Fe]_{12}As_4S_{13}$) and famatinite (Cu_3SbS_4) as the main constituents and spharelite (ZnS), silica (SiO_2) and galena (PbS) as minor constituents) with coal at 1000°C, results in the formation of a complex arsenide ($[Cu,Fe_2]As$), copper antimonide ($Cu_{4.5}Sb$), metallic copper (Cu) and calcium sulphide (CaS). Traces of metallic lead appear in the reaction product while zinc is completely absent. Reduction is complete after 45 minutes reaction at 1000°C.

31) The higher affinity of antimony for copper and of arsenic for iron is evident from the selective formation of copper antimonide and iron arsenide and this is very important with regard to the separation of the reaction product. The removal of zinc will be enhanced by the formation of zinc vapour by the reduction reaction. The presence of CO (reducing) gas in the product gas stream will help prevent the re-oxidation of zinc.

REFERENCES

REFERENCES

1) **Cranstone, D.A.**
Complex sulphides, TMS-AIME, San Diego, Calfornia 1985

2) **Holmstrom, A.**
Scand. J. Metall. 18, 12, (1989)

3) **Jokilaakso, A.T., Souminen, R.O., Taskinen, P.A. and Lilius, K.R.**
Scand. J. Metall. 18, 50 (1989)

4) **Holmstrom, A.**
Scand. J. Metall. 17, 248 (1988)

5) **Holmstrom, A.**
Scand. J. Metall. 17, 259 (1988)

6) **Holmstrom, A.**
Scand. J. Metall. 17, 272 (1988)

7) **Allaire, A., Herbert, M., Harris, R.**
Rheinhadt Schuhmann Int. Symp. TMS-AIME, Frankfurt, West Germany, 1984

8) **Harris, R.**
Met. Trans. B 15B, 251, (1984)

9) **Kametani, J., Yamaguchi, C., Murao, K., Hayashida, M.**
Trans. Jpn. Inst. Met. 14, 218 (1973)

10) **Allaire, A., Harris, R.**
Complex Sulphides, TMS-AIME, San Diego, California 1983

11) **Edwards, C., Melville, R.,**
Conf. Can. Min., Winnipeg, Canada 1984

12) **Holmes, W.C.**
Eng. Min. J. 145, 145(1944)

13) **Plunkert, P.**
Antimony-Min. facts and problems, US Dept. of the interior, Washington 1985

14) **Crowson, P.**
Minerals Handbook (pp29), Stockton, London 1987

15) **Crowson, P.**
Minerals Handbook (pp37), Stockton, London 1987

16) **Hansen, M., Andenko, K.,**
Constitution of binary alloys, McGraw Hill, New York 1958

17) **Henning, H., Kohlmeyer, E.,**
Z. Erzbergbau Metall, 10, 12 (1957)

18) **Elliot, R.P.**
Constitution of Binary alloys, McGraw Hill, New York, 1965

19) **Shunk, F.A.**
Constitution of binary alloys, McGraw Hill, New York, 1969

20) **Charkraborti, D.J., Laughlin, D.E.**
Bull. Alloy Phase Diagrams, 4, 254, (1983)

21) **Morimoto, N., Koto, N.**
Am. Mineral, 55, 106 (1970)

22) **Neumann, J.P., Zhong, T., Chang, Y.A.**
Bull. Alloy Phase Diagrams, 5, 136 (1984)

23) **Roberts, J., Smyth, F.**
J. Am. Chem. Soc., 43, 1061 (1921)

24) **Osawa, A., Shibata, N.**
Sci. repts., Tohoku Imp. Univ., Japan, 28, 1 (1939)

25) **Schubert, K., Ilschner, M.**
Z. Metall. 45, 366 (1954)

26) **Sorensen, J., Semenov, E., Bezsmertnaya, M., Khalezova, E.**
Zap. Vses. Min. Obsch., 98, 716 (1969)

27) **Shimada, S., Mackenzie K.**
Thermocimica acta, 56, 73 (1982)

28) **Shimada, S., Kodaira, K., Matsushita, T.**
J. Solid State Chem., 59, 237 (1985)

29) **Skinner, B., Luce, F., Makovicky, E.**
Econ. Geology, 67, 924 (1972)

30) **Schmedil, J., Repcak, V., Cempa, S.**
Trans. C Inst. Min. Met., 86, c88 (1977)

31) **Kullerud, G.**
Fortschr. Miner., 41, 221 (1964)

32) **Karutz, I., Stranski, I.**
Z. anorg. u. allgem. chem., 292, 332 (1957)

33) **Heyding, R.G., Despault, G.J.**
Can. J. Chem., 38, 2477 (1960)

34) **Maske, S., Skinner, B.**
Econ. Geol., 66, 901 (1971)

35) **Kubacheski, O.**
Iron-binary phase diagrams, Springer-Verlag, New York, 1982

36) **Friedrich, K.**
Metallurgie, 4, 129 (1907)

37) **Hagg, G., Krist, E.**
Nova Acta Regia Soc. Upsaliensis 7, 44 (1929)

38) **Kullerud, G.**
Carnegie Inst. Yearbook, Washington, 56, 198 (1957)

39) **Clark, L.A.**
Econ. Geol., 55,1346 (1960)

40) **Ramdohr, P., Ahlfeld, F., Berndt, F.**
Neus. Jahcb. Min. monatsh, 7, 145 (1959)

41) **Knorring, V.P., Sahama, Th. G., Rehtijarvi, P.**
Lithos, 6, 265 (1973)

42) **Skaeff, J.M.**
Can. Met. Quart., 28, 117 (1989)

43) **Chakraborti, N., Lynch, D.**
Met. Trans. B, 14B, 239 (1983)

44) **Gilchrist, J.D.**
Extraction Metallurgy, pergamon, London, 1980

45) **Coudurier, L., Hopkins, D., Wilkomirsky, I.**
Fundamentals of metallurgical processes, Pergamon, London 1978

46) **Turkdogan, E.T.,**
Physical chemistry of high temperature technology, Academic, New York, 1980

47) **Barin, I., Knacke, O., Kubachewski, O.**
Supplement to thermochemical properties of inorganic substances, Springer-Verlag, New York 1977

48) **Prasad, P.M., Mankhand, T.R.**
Advances in sulphide smelting, Met. Soc. AIME, San Francisco, Cal., 1983

49) **Chen, Y.O., Chang. Y.A.**
Trans. AIME, 9B, 61 (1978)

50 **Kerby, R.**
Candadian mines branch investigative report, IR, 73, 1973

51) **Habashi, F., Dugdale, R.**
Met. Tans., 4, 1865, (1973)

52) **Jha, A.**
Ph.D. Thesis, Imperial College, London 1984

53) **Abramowitz, H., Rao, Y.**
Trans. C. Inst. Min. Met., 87, C180 (1978)

54) **Machingawuta, N., Jha, A., Grieveson P.**
Scand. J. Metall. 18, 81 (1989)

55) **Abramowitz, H.**
D.Sc. Thesis, Columbia University, U.S.A., 1983

56) **Rao Y., El-Rahaiby, S.**
Met. Trans. B, 16B, 465 (1985)

57) **Panfilov, P.F.**
Isvet Met., 4, 22 (1969)

58) **Cech. R.E., Tiemann, T.D.**
Trans. MS-AIME, 245, 1727, (1969)

59) **Torma, E., Inal, O.**
J. Less-Common Met., 64, 107 (1979)

60) **Prasad, P., Mankhand, T.**
Trans. Ind. Inst. Met., 32, 253, (1979)

61) **Wanmaker, W.L., Hoekstra, A.H., Verriet, J.G.**
Recueil, 86, 537, (1967)

62) **Nakai, I., Adachi, H., Matsubara, S., Kato, A., Masutomi, K., Fujiwara, T., Nagashima K.**
Am. Min., 63, 715 (1978)

63) **Querigh, E.,**
Atti. Reale accad. Lincei sez., 21, 418 (1912)

64) **Rtskhilaze, V.G.**
Metallurgiya, 70, 44 (1969)

65) **Smith, E.H. Foster, L.W., Minet, P., Caneve, P.**
'Selective Roasting-El Indio Mine - From Pilot Plant to Commercial Operation', The Inst. Min. Met., London 1987

66) **Yoshimura, Z.**
J. MMIJ, 18 (1962)

67) **Smith, E.H.**
Min. Eng., 38, 971 (1986)

68) **Shigematsu, K.**
Met. Rev. MMIJ, 3, 49 (1986)

69) **Mertz, J.C. Mathewson, C.H.**
Trans. AIME, 124, 59 (1937)

70) **Hino, M., Azakami, T.**
Met. Rev. MMIJ, 3, 61 (1986)

71) **Kellogg, H.H.**
Trans. MS-AIME, 236, 602 (1966)

72) **Jha, A., Grieveson, P., Jeffes, J.**
Scand. J. Met., 18, 31 (1989)

73) **Cambi, L. Elli, M.**
Chimica industria, 47, 2(1965)

74) **Itagaki, K., Nishimura, T.**
Met. Rev. MMIJ, 3, 29 (1986)

75) **Feiss, P.G.**
Econ. Geol., 69, 383 (1974)

76) **Turkdogan, E.T., Vinters J.V.**
Carbon, 7, 101 (1969)

77) **Turkdogan, E.T., Vinters, J.V.**
Carbon, 8, 39 (1970)

78) **Coley, K.S.**
Ph.D. Thesis, Imperial College, London 1986

79) **Kingery, W.D., Bowen, H.K., Uhlmann, D.R.**
Introduction to ceramics, John Wiley, New York, 1976

80) **Turkdogan, E.T., Rice, B.B., Vinters, J.V.**
Met. Trans., 5, 1527 (1974)

81) **Rao, Y.K., El-Rahaiby, S.K.**
AIChE. J., 31, 918 (1985)

82) **Rao, Y.K., Moinpur, M.**
Can. Met. Quart., 24, 69 (1985)

83) **Bird, R.B., Stewart, W.E., Lightfoot, E.N.**
Transport phenomena, Wiley, New York 1960

APPENDIX

APPENDIX 1

In this section, significant results and discussion of reactions relating to the carbothermic reduction of zinc and lead sulphides are presented. This study was made necessary by the common occurence of these base metal sulphides as important constituents of most complex sulphide minerals.

The experimental methods and analytical techniques applied are similar to that described in the main section.

Appendix 1A: Phase Combinations in the Zn-Ca-S-O System

The composition and properties of the oxysulphide compound present in the Zn-Ca-S-O system have been determined by Yarygen et al [a1, a2] from a preliminary study of the behaviour of lime metal sulphide mixtures. This study aimed to determine the variation in the fusibility of those mixtures with lime (CaO) concentration. It was reported that the solidification temperature of a spharelite (ZnS) melt falls sharply when lime is added to it, reaching a minimum value of 1230^{o}C with 10 wt% CaO in the melt. With further increase in the concentration of CaO in the melt, the temperature at which a solid phase first separates rises, reaching 1350^{o}C at a CaO concentration of about 50 wt%.

In this study, further investigations have been conducted on the phase combinations in the Zn-Ca-S-O system by heat treating stoichiometric mixtures of ZnS-CaO and ZnO-CaS in sealed evacuated silica tubes (inert atmosphere) at 1250^{o}C for one hour, after which the samples were slowly cooled to 400^{o}C. The heat treated samples were analysed by X-ray diffraction techniques. Results of significant reactions conducted are presented in Table A1.1. On the basis of this investigation, the diffraction pattern of the zinc calcium oxysulphide (ZnCaOS) compound has been determined and this is listed in Table A1.2. The calculated diffraction data has been included for the purpose of comparison.

Mixture Composition - ZnS:CaO (1:1)

Temp (°C)	Reaction Time (mins)	Weight Loss (%)	Phases Present, Relative Intensity ZnS	CaO	ZnCaOS	ZnO	CaS
900	60	0.6	S	M	M	MW	-
1000	60	1.5	S	M	M	MW	-

Mixture Composition - ZnS:CaO (1:2)

Temp (°C)	Reaction Time (mins)	Weight Loss (%)	Phases Present, Relative Intensity ZnS	CaO	ZnCaOS	ZnO	CaS
900	60	-	MS	S	M	M	-
1000	60	1.3	MS	S	M	M	-

Mixture Composition - ZnO:CaS (1:1)

Temp (°C)	Reaction Time (mins)	Weight Loss (%)	Phases Present, Relative Intensity ZnS	CaO	ZnCaOS	ZnO	CaS
900	60	4.2	MW	W	M	S	W
1000	60	13.2	MW	M	MS	MS	-

Phase Analysis Intensity:

VS - Very Strong
S - Strong
MS - Medium Strong
M - Medium
MW - Medium Weak
W - Weak
VW - Very Weak
VVW- Very Very Weak

TABLE A1.1

X-Ray Diffraction Analysis of Reaction Products of the Zn-Ca-O-S System

Crystallographic structure - simple hexagonal $a = 6.48\text{Å}$, $c = 3.78\text{Å}$

Indices (hkl)	d°A Calculated	Observed	Relative intensity
(100)	5.61	5.67	MS
(110)	3.24	3.24	M
(101)	3.13	3.11	MS
(200)	2.81	2.84	VS
(111)	2.45	2.46	VS
(201)	2.25	2.26	VW
(210)	2.12	2.14	MS
(002)	1.89	1.87	MS
(301)	1.68	1.69	VW
(102)	1.79	1.78	W
(112)	1.63	1.64	VS
(220)	1.62	1.63	W
(202), (310)	1.57	1.57	M
(221)	1.49	1.49	W
(212)	1.41	1.41	W
(103)	1.23	1.23	W
(203)	1.15	1.15	W
(213)	1.13	1.13	VW

Key

VS - Very Strong S - Strong MS - Medium Strong

M - Medium MW- Medium Weak W - Weak

VW - Very Weak VVW - Very Very Week

TABLE A1.2

Crystallographic Data for the Zinc Calcium Oxysulphide [ZnCaOS] Compound

ZINC CALCIUM OXYSULPHIDE (ZnCaOS)

Crystal Structure - Simple Hexagonal

a = 6.48 Å

c = 3.78 Å

c/a = 0.58

CRYSTAL IONIC RADII DATA [a3]

Element	Valency State	Ionic Radii, Å
Ca	+2	0.99
O	-2	1.32
S	-2	1.84
Zn	+2	0.74
Fe	+2	0.74

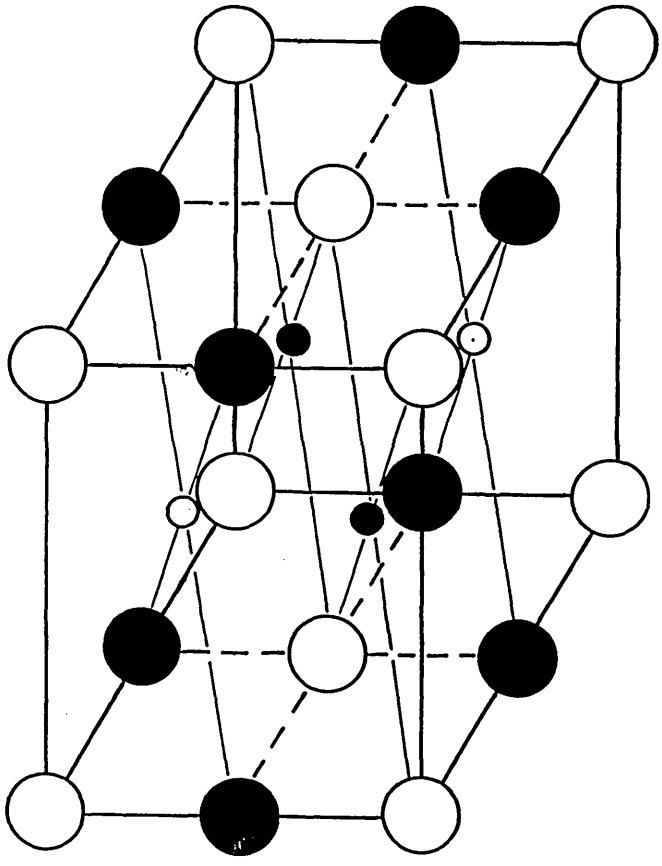

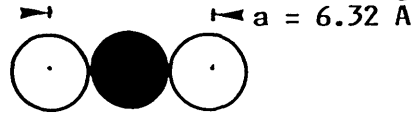

S atoms - ½, 0,0; 0,½,0

O atoms - 0,0,0; ½,½,0

Ca atoms - 1/4,3/4,½; 3/4,1/4,½

Zn atoms - 1/4,1/4,½; 3/4,3/4,½

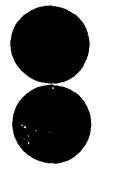

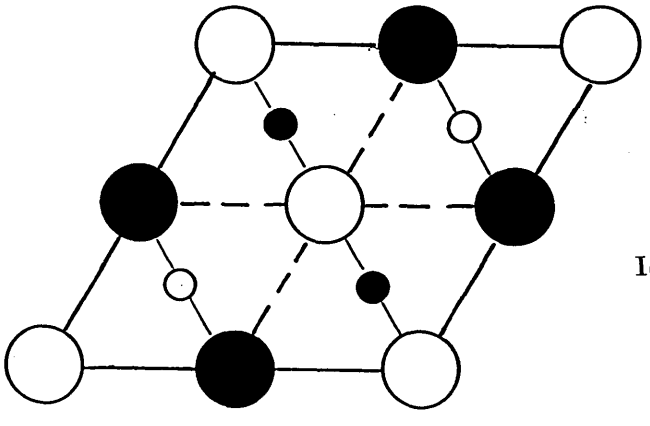

FIGURE A1.1

Ionic Data and Idealised Crystal Structure of Zinc Calcium Oxysulphide (ZnCaOS)

Zinc calcium oxysuphide (ZnCaOS) is present in all the reaction products. The relatively low intensities of calcium sulphide in the reaction products suggests that the oxysulphide is formed by the combination ZnO and CaS. The free energy change of the zinc sulphide-lime exchange reaction (A1.1) only becomes negative at temperatures above 1900K indicating that ZnS and CaO are relatively more stable than ZnO and CaS.

$$ZnS_{(s)} + CaO_{(s)} = ZnO_{(s)} + CaS_{(s)} \qquad [A1.1]$$

$$\Delta G_T^o = 6630-3.49T \text{ cal/mol.}$$

The crystallographic structure of the zinc calcium oxysulphide (ZnCaOS) compound has been interpreted assuming a simple hexagonal lattice [a = 6.48A, c = 3.78 A]. From the illustrations in Figure A1.1, it is clear that the lattice parameters are determined by the ionic dimensions, and ionic radii data conform well with the proposed crystallographic arrangement.

Each Zn^{2+} ion is surrounded by four S^{2-} ions and two O^{2-} ions, but is actually bonded to the four S^{2-} ions while each Ca^{2+} ion sits in a nest of four O^{2-} ions and two S^{2-} ions forming bonds with the O^{2-} ions. This arrangement conforms with established thermodynamic data which indicates that ZnS and CaO are more stable than ZnO and CaS implying that zinc has a higher affinity for sulphur than for oxygen; whereas calcium has a higher affinity for oxygen than for sulphur.

The remarkable similarity of the crystal ionic dimensions of Fe^{2+} and Zn^{2+} ions indicates that the crystallographic structure of the iron calcium oxysulphide [FeCaOS] compound found by Jha [a4] could be determined by applying similar principles as have been used to describe the zinc equivalent. This could be obtained by simply replacing the Zn^{2+} ions in the simple hexagonal structure illustrated in Figure A1.1 with Fe^{2+}, the resulting structure in shown in Figure A1.2.

On the basis of this interpretation of the iron calcium oxysulphide (FeCaOS) structure assuming a simple hexagonal lattice, the diffraction

data for the FeCaOS compound have been computed and these are compared with the experimental data obtained by Jha [a4] in Table A1.3. The remarkably close agreement between the computed and experimental data further indicates that theiron calcium oxysulphide (FeCaOS) structure is best described by a simple hexagonal structure and not the simple tetragonal arrangement suggested by Jha.

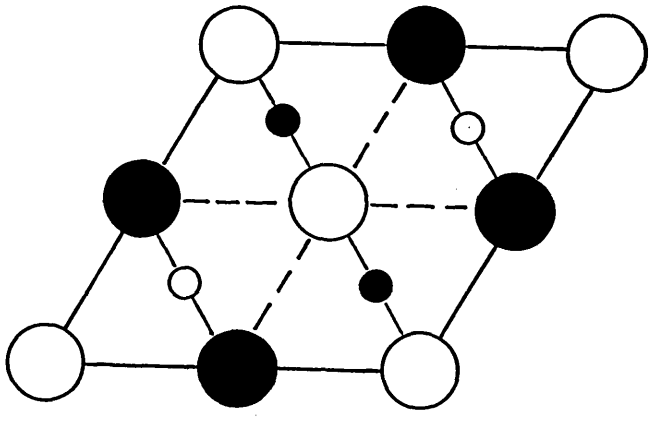

IRON CALCIUM OXYSULPHIDE (FeCaOS)
Crystal Structure - Simple hexagonal

S atoms - $\frac{1}{2},0,0$; $0,\frac{1}{2},0$

O atoms - $0,0,0$; $\frac{1}{2},\frac{1}{2},0$

Ca atoms - $1/4,3/4,\frac{1}{2}$; $3/4,1/4,\frac{1}{2}$

Fe atoms - $1/4,1/4,\frac{1}{2}$; $3/4,3/4,\frac{1}{2}$

FIGURE A1.2

Idealised Crystal Structure of Iron Calcium Oxysulphide (FeCaOS)

Crystallographic structure - simple hexagonal $a = 6.32\text{Å}^{*}$
$c = 3.68\text{Å}$

Indices (hkl)	$d^{o}A$ Calculated	Observed [a4]	Relative Intensity
(100)	5.50	5.70	W
(110)	3.16	3.25	W
(101)	3.06	3.10	S
(200)	2.74	2.82	M
(111)	2.39	2.46	VS
(210)	2.07	2.09	VW
		2.08	VW
(002)	1.84	1.94	MW
(300)	1.82	1.88	S
(211)	1.80	1.82	VW
(301)	1.64	1.74	VW
(112)	1.59	1.635	S
(202)	1.53	1.558	S
(310)	1.52	1.54	VW
		1.49	VW
(221)	1.45	1.48	VW
(212)	1.37	1.465	VW

Intensity

VS - Very Strong S - Strong MS - Medium Strong M - Medium
MW - Medium Weak W - Weak VW - Very Weak VVW - Very Very Weak

*lattice parameters corresponding to exact ionic radii data have been used in the calculation of the 'd'-spacings. The deviation of the observed data from these calculated values indicates an expansion of the unit cell as is observed with ZnCaOS.

TABLE A1.3

Crystallographic Data for the Iron Calcium Oxysulphide (FeCaOS) Compound

Apendix 1B: The Carbothermic Reduction of Lead Sulphide

A brief review and general discussion of significant reactions pertaining to the carbothermic reduction of lead sulphide will be conducted in this section. Rao and El-Rahaiby [a5, a6] have conducted studies on the direct reduction of lead sulphide with carbon in the presence of lime in the temperature range 795-989^{o}C. Samples of lead sulphide mixed with 300% excess CaO and Carbon (PbS:4CaO:4C) were reacted isothermally in nitrogen and nitrogen rich He-N atmospheres. The kinetics of reduction were determined for both the uncatalysed and catalysed reduction processes by thermogravimetric techniques. The effect of catalysts was said to be appreciable and the following ranking was developed for the catalysts studied $LiCO_3$ > Rb_2CO_3 > ternary $(K,Li,Na)CO_3$ eutectic = NaF = K_2CO_3 >N a_2CO_3 >Na_2SO_4. It was also reported that X-ray diffraction analysis of the reduction product revealed the presence of CaS and Pb as well as unreacted lime and carbon, their relative intensities were not indicated. Rao and El-Rahaiby [a7] have also studied the kinetics of the vaporisation of lead sulphide from PbS/4CaO mixtures in which it was claimed that lime behaves as a chemically inert material. The stated aim of the study was to determine the kinetics of lead sulphide vaporisation during the direct reduction of PbS/4CaO/4C mixtures; PbS vaporisation was said to be an important step in the carbothermic reduction sequence.

In this project, preliminary investigations have been carried out on the various reactions of significance in the PbS-CaO-Carbon system with regard to the intermediate phases present during carbothermic reduction, in order to gain a better understanding of the reduction mechanism. Only a brief summary of the results will be presented since it will be necessary to conduct further experiments in order to fully describe the reaction mechanism.

On the reduction of galena (PbS) with stoichiometric quantities of lime and coal at 1000^{o}C, the reaction proceeded rapidly reaching completion after about 60 minutes. X-ray diffraction analysis of the reaction product indicated that the residue contained liquid lead, calcium sulphide and unreacted CaO. The associated weight loss was 19.8% compared

with a theoretical weight loss of 12.8% required for complete reduction. This difference is due to the loss of PbS by volatilisation (hence the presence of unreacted lime in the reduction product). The reactions at 800°C and 900°C were incomplete. On the use of 100% excess reducing and exchange reagents, complete reduction was achieved at 800°C with a 10.4% weight loss. This is close to the value expected for complete reduction (10.2%) and no PbS was detected in the reaction product. Thus it has been possible to rapidly reduce galena (PbS) with carbon (in the presence of lime), without the necessity of catalysts and with a minimum loss of PbS by volatilisation.

Further reactions involving PbS/CaO, PbS/2PbO and 2PbO/CaS mixtures at various temperatures have been studied. The lime exchange reaction at 1000°C results in the partial reaction of PbS and CaO to produce liquid Pb and calcium sulphide accompanied by a large weight loss (31.4% after 90 minutes). This weight loss is attributed to the generation and loss of SO_2 in addition to PbS volatilisation. A weight loss of 7.2% was observed at 900°C and this is quite close to the value expected for the loss of SO_2 (= 7.7%) from a 3PbS/2CaO mixture on the formation of Pb and CaS by the reaction:

$$3PbS_{(s)} + 2CaO_{(s)} = 3Pb_{(l)} + 2CaS_{(s)} + SO_{2(g)} \qquad [A1.2]$$

The volatilisation of PbS would be expected to account for a 3.0% weight loss at this temperature. Reaction of the PbS/2PbO mixture leads to the formation of liquid lead; unreacted PbS and PbO remain in the reaction product and a 10.2% weight loss was recorded after 60 mins reaction at 800°C. The loss of SO_2 from such a mixture should result in net weight loss of 9.3%. The reaction of 2PbO + CaS results in the formation of liquid lead and calcium sulphate and unreacted PbO remains in the reaction product. The weight losses at 800°C and 900°C are 2.6% and 2.8% respectively (60 minutes reaction). Traces of the basic lead sulphate ($PbSO_4.2PbO$) were identified in the reaction product of the PbS/2PbO mixture.

The exchange and carbothermic reduction reactions of lead sulphide can be represented as:

$$PbS_{(s)} + CaO_{(s)} = PbO_{(l)} + CaS_{(s)} \qquad [A1.3]$$

$$\Delta G^{o}_{T} = 17,700 - 5.91T \text{ cal/mol} \quad Teq = 2995 \text{ K}$$

$$PbS_{(s)} + CaO_{(s)} + C_{(gr)} = Pb_{(l)} + CaS_{(s)} + CO_{(g)} \qquad [A1.4]$$

$$\Delta G^{o}_{T} = 33,660 - 42.67T \text{ cal/mol} \quad Teq = 789 \text{ K}$$

Thus, whereas the carbothermic reduction reaction is feasible above 789K, the exchange reaction can only be carried out above 2995K. But the occurrence of the reduction reaction indicates the necessary presence of some oxide intermediate product.

The thermodynamic properties of the Pb-S-O system have been determined by Kellog and Basu [a8]. Figure A1.3 shows the composition diagram for the ternary Pb-S-O system above 733^{o}C (1006K) but below the melting point. Figure A1.4 shows the thermodynamic phase diagram for the Pb-S-O system while Figure A1.5 illustrates the bivariant equilibria in the ternary system at 1100K.

These diagrams illustrate the impossibility of a stable equilibrium between PbO and PbS because their area of stability are spatially separated. The great stability of the lead sulphates is also apparent and extremely low pressures of SO_2 must be achieved in order to decompose the sulphates of lead to PbO.

The equilibrium between Pb, PbS and PbO which can be represented by the reaction

$$PbS_{(s)} + 2PbO_{(l)} = 3Pb_{(l)} + SO_{2(g)} \qquad [A1.5]$$

is clearly metastable at all temperatures. Figure A1.5 indicates that the reaction of a PbS/2PbO mixture should result in a stable equilibrium between PbS, $PbSO_4$.2PbO and Pb. The reaction sequence could be:

$$PbS_{(s)} + 6PbO_{(l)} = PbSO_4.2PbO_{(s)} + 4Pb_{(l)} \qquad [A1.6]$$

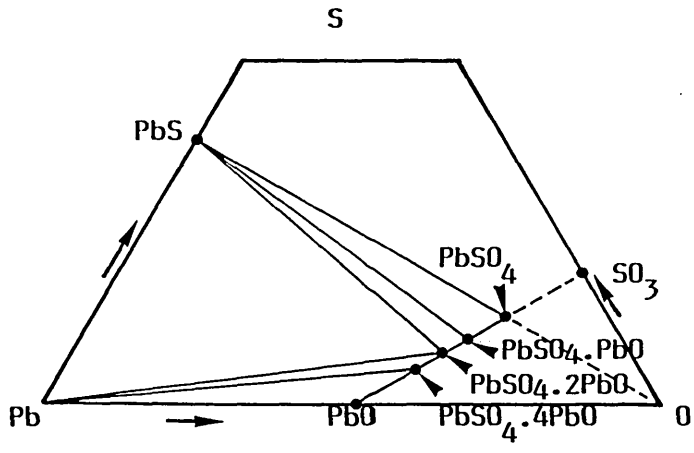

FIGURE A1.3

Composition Diagram for the Pb-S-O System
Above 733°C and Below the Melting Point [a8]

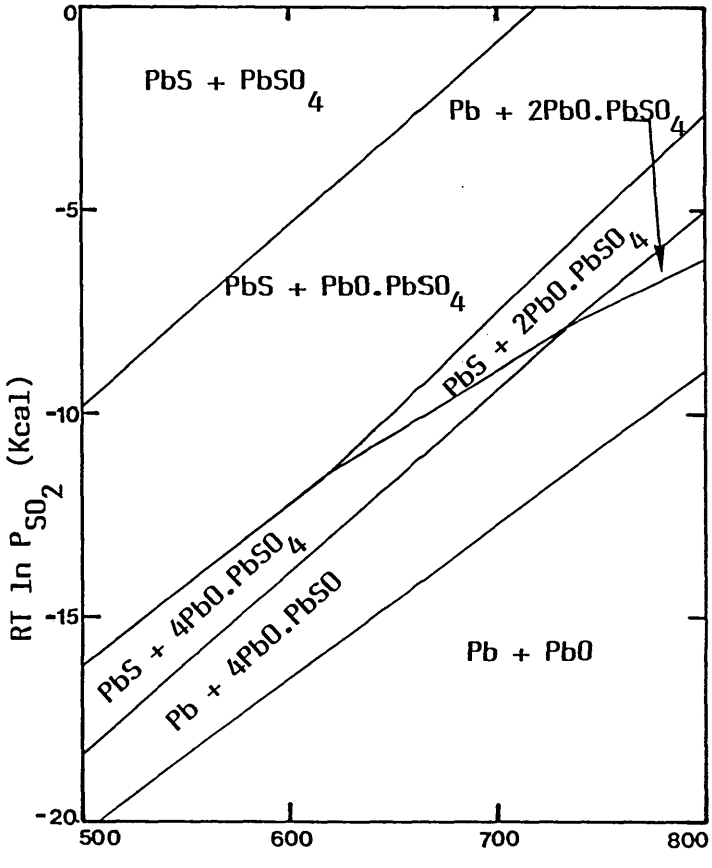

FIGURE A1.4

Thermodynamic Phase Diagram for the
Pb-S-O System [a8]

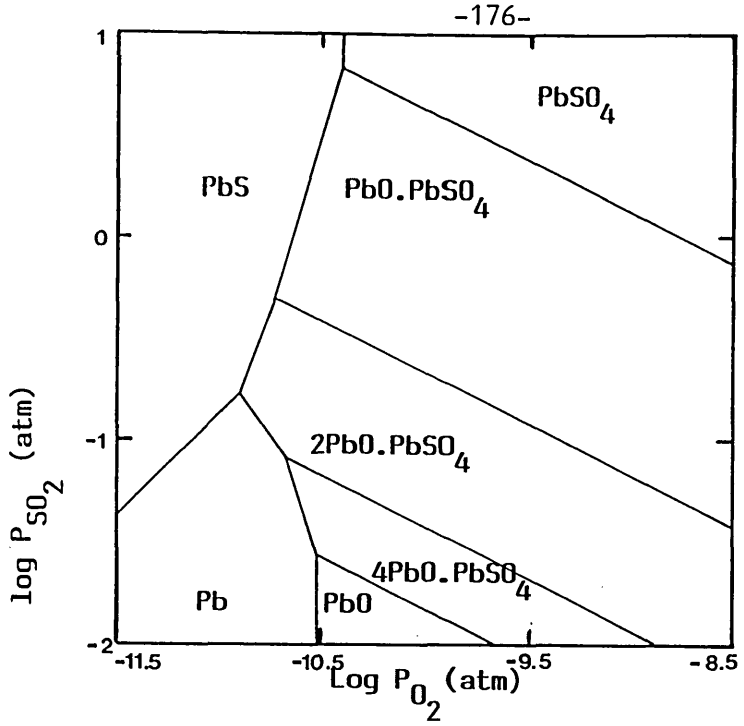

FIGURE A1.5

Bivariant Equilibria in the Ternary Pb-S-O System at 1100 K [a8]

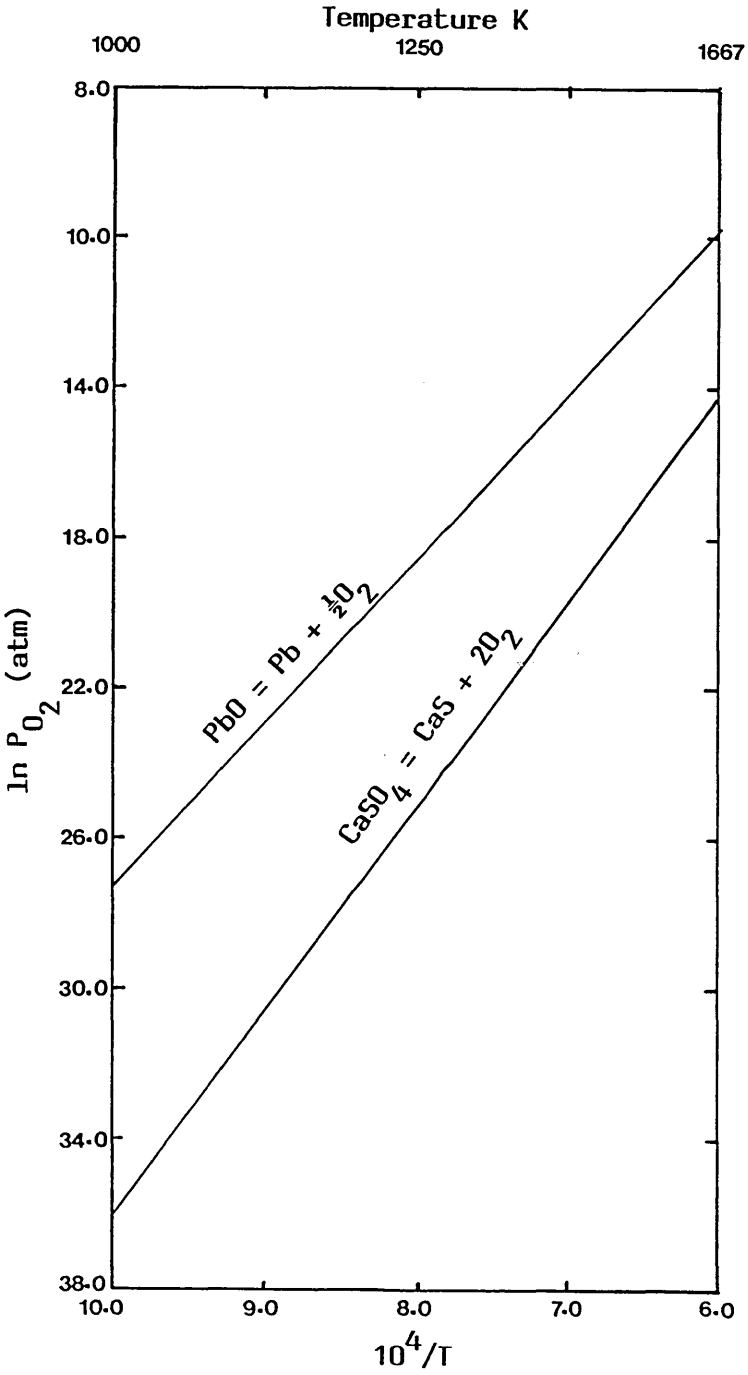

Figure A1.6

Equilibria in the Pb-O-S-Ca System

followed by:

$$2PbS_{(s)} + PbSO_4.2PbO_{(s)} = 5Pb_{(l)} + 3SO_{2(g)} \qquad [A1.7]$$

For this reaction, at 1100K, p_{SO_2} = 0.171 atm.

Reaction A1.6 consumes 2 moles of PbO and 1/3 mole of PbS, so there remains 2/3 mole of PbS to establish equilibrium A1.7. For the mixture of PbS/2PbO represented by the equilibrium

$$PbS_{(s)} + 2PbO_{(l)} = 3Pb_{(l)} + SO_{2(g)} \qquad [A1.5]$$

$$P_{SO_2} = 0.333 \text{ atm at } 1100K$$

Schenck and Borkenstein [a9] have measured a value of P_{SO_2} = 0.216 atm over a mixture of PbS and PbO at 1100K (by interpolation of their measurements at 1095K and 1103K). Their measurements are much closer to the reaction represented by equation A1.7 than that of A1.5.

Thus, the lead-sulphide-lime reaction is thought to proceed according to:-

$$6CaO_{(s)} + 7PbS_{(s)} = PbSO_4.2PbO_{(s)} + 4Pb_{(l)} + 6CaS_{(s)} \qquad [A1.8]$$

$$PbSO_4.2PbO_{(s)} + 2PbS_{(s)} = 5Pb_{(l)} + 3SO_{2(g)} \qquad [A1.9]$$

The detection of the basic lead sulphate phase ($PbSO_4.2PbO$) in the PbS/2CaO reaction product conforms with this reaction scheme.

Thus, from established thermodynamic relationships and experimental observations, it can be concluded that the carbothermic reduction of lead sulphide proceeds via a mechanism involving the formation of basic lead sulphate rather than through the COS gas-intermediate mechanism as has been suggested by Rao and El-Rahaiby [a5] and discussed in Section 4.6.

Figure A1.6 illustrates the conditions under which Pb and $CaSO_4$ can exist in a stable equilibrium. It can be observed that this would require very low oxygen potentials for example pressures of $P_{O_2} = 10^{-18.5}$ atm will be necessary at 1250K. In order to determine the possibility of the recovery of liquid lead from lead sulphide by reaction with lime without the formation of SO_2 (fixation of sulphur as $CaSO_4$), the equilibrium between $PbS/PbSO_4.2PbO/Pb/CaSO_4$ must be studied since the PbS/PbO/Pb reaction system has been shown to be metastable.

An extensive investigation of the PbS-CaO-Carbon system must be conducted in order to understand the precise mechanism by which the carbothermic reduction of lead sulphide occurs. It is also suggested that appropriate research should be undertaken to determine the conditions under which lead sulphide could be reacted with lime to produce liquid lead and calcium sulphate in a process that does not generate SO_2.

Binary Copper-Antimony Alloys Diffraction Data [a10]

TABLE A2.1 (i)
γ-Phase Cu_2Sb (66.70 at% Cu)

Structure - simple tetragonal

a = 4.02Å

b = 6.13Å

c/a = 1.52

	d(hkl)		
Indices (hkl)	Calculated	Observed	Intensity
(111)	3.3260	3.3168	W
(002)	3.0373	3.0486	W
(200)	2.8105	2.8171	S
(102)	2.6688	2.6650	W
(201)	2.5507	2.5566	S
(112)	2.4133	2.4112	VW
$(202)_\beta$	2.0628	2.0628	M
$(220)_\beta$	1.9873	1.9893	VW
(202)	2.0650	2.0628	VS
(003)	2.0249	2.0249	W
(220)	1.9873	1.9893	S
(311)	1.7060	1.7057	W
(222)	1.6030	1.6614	W
(320)	1.5589	1.5617	W
$(114)(223)_\beta$	1.4185	1.4142	W
(004)	1.5186	1.5190	W
(114)	1.4186	1.4185	VS
(223)	1.4183	1.4185	VS
(400)	1.4052	1.4057	S
(410)	1.3632	1.3634	W
$(421)_\beta$	1.2307	1.2309	W
(402)	1.2754	1.2762	S
(420)	1.2568	1.2577	M
(421)	1.2307	1.2309	S

(continued ...)

Indices (hkl)	d(hkl) Calculated	Observed	Intensity
$(205)_{\beta}$	1.1152	1.1133	S
(332)	1.2144	1.2142	W
(224)	1.2067	1.2074	S
(115)	1.1619	1.1625	VS
(422)	1.1613	1.1625	VS
(314)	1.1546	1.1547	S
(403)	1.1545	1.1547	S
(205)	1.1152	1.1151	VS
(510)	1.1023	1.1024	VW
(511)	1.0846	1.0847	M
(423)	1.0678	1.0683	M
(225)	1.0366	1.0380	M
(512)	1.3062	1.0380	M
(404)	1.0315	1.0322	VS

Intensity

VS - Very Strong S - Strong MS - Medium Strong

M - Medium MW - Medium Weak W - Weak

VW - Very Weak VVW- Very Very Weak

TABLE A2.1(ii)

ε-Phase $Cu_{4.5}Sb$ (81.35 at% Cu) [a10]

Structure - close packed hexagonal

a = 2.709Å

c = 4.305Å

c/a = 1.589

	d(hkl)		
Indices (hkl)	Calculated	Observed	Intensity
$(300)_\beta$	3.1280	3.0457	VW
(211)	3.2791	3.2703	MW
(202)	3.1734	3.1830	VW
(300)	3.1281	3.1265	M
(310)	2.6029	2.5751	M
$(400)_\beta$	2.3460	2.3344	M
$(320),(004)_\beta$	2.1532	2.1374	VW
(400)	2.3600	2.3486	S
(222)	2.2936	2.2930	W
(401)	2.2634	2.2651	S
$(402)_\beta$	2.0602	2.0541	S
(213)	2.2311	2.2200	VVW
(312)	2.2277	2.2200	VVW
(320),(004)	2.1532	2.1502	S
(104)	2.0984	2.0901	VW
(321)	2.0888	2.0901	VW
(402)	2.0602	2.0593	VS
(114)	2.0004	2.0170	VW
(501)	1.8337	1.8322	VW
$(404)_\beta$	1.5863	1.5809	W
(332)	1.6655	1.6685	W
(404)	1.5863	1.5863	S
(600)	1.5642	1.5621	VW
(305)	1.5088	1.5141	VW
(431)	1.5188	1.5141	VW
(440)	1.3545	1.3548	S

(continued ...)

Indices	d(hkl) Calculated	Observed	Intensity
(415)	1.3197	1.3182	W
(530)	1.3407	1.3430	VW
$(406)_{\beta}$	1.2243	1.2254	VW
(702),(532)	1.2802	1.2784	VW
(316)	1.2569	1.2595	M
$(444)_{\beta}$	1.1466	1.1421	M
(622)	1.2458	1.2437	W
$(802)_{\beta}$	1.1319	1.1278	W
(406)	1.2243	1.2245	S
(710)	1.2225	1.2245	S
(207)	1.1901	1.1901	VW
(800)	1.1731	1.1720	M
(631)	1.1741	1.1720	M
(720),(444)	1.1466	1.1458	VS
(802)	1.1319	1.1314	VS
(426)	1.1157	1.1177	VW
(810)	1.0984	1.0974	VW
(008)	1.0765	1.0768	S
(812)	1.0644	1.0638	W
(804)	1.0302	1.0302	S
(408)	0.9784	0.9784	S
(912),(652)	0.9591	0.9588	M
(710)	0.9307	0.9308	S
(338),(824)	0.9247	0.9240	S
(806)	0.9083	0.9072	S
(608),(840)	0.8868	0.8857	W
(842)	0.8685	0.8678	S
(448)	0.8427	0.8425	S
(844)	0.8200	0.8206	M

Intensity

VS - Very Strong S - Strong MS - Medium Strong

M - Medium MW - Medium Weak W - Weak

VW - Very Weak VVW- Very Very Weak

TABLE A2.1(ii) (continuation)

Structure - tetragonal$_o$
a = 3.728 Å
c = 5.898 Å
c/a = 1.582

Indices (hkl)	d(hkl) Calculated	Observed	Intensity
(001)	5.89	5.92	7
(101)	3.15	3.15	6
(002)	2.95	2.95	29
(110)	2.64	2.62	18
(111)	2.41	2.40	31
(102)	2.31	2.31	7
(003)	1.966	1.962	100
(112)	1.965	1.962	100
(200)	1.864	1.858	35
(201)	1.777	-	-
(103)	1.739	1.739	20
(211)	1.604	1.600	3
(202),(113)	1.576	1.572	7
(004)	1.474	1.473	11
(212)	1.451	-	-
(104)	1.371	-	-
(203)	1.353	1.352	13
(220)	1.318	1.313	6
(213)	1.272	1.271	5
(301)	1.216	-	-
(222)	1.203	-	-
(310)	1.179	-	-
(311),(204)	1.156	1.156	7
(302)	1.145	-	-
(105)	1.125	1.126	12
(214)	1.104	-	-
(223),(312)	1.095	1.093	14
(115)	1.077	1.077	12
(303)	1.050	-	-

TABLE A2.2

Copper-Iron-Arsenic $(Fe,Cu)_2As$ Diffraction Data [iii]

REFERENCES

a1) **Yarygin, V.I., Kopylov, N.I., Novoselova, V.N., Larin, V.F., Pestunova, N.P.**
Izvest. Akad. Nauk SSSR Metally, 6, 64 (1975)

a2) **Yargin, V.I., Shokarev, M.M., Mamayev, V.E., Kolganov, I.M., Kopylov, N.I.**
Izvest. Akad. Nauk. SSSR Metally, 2, 104 (1977)

a3) CRC Handbook of Chemistry and Physics, CRC press, Florida, 1978

a4) **Jha, A.**
Ph.D. Thesis, Imperial College, London 1984

a5) **Rao, Y.K., El-Rahaiby, S.K.**
Met. Trans., B, 16B, 465(1985)

a6) **Rao, Y.K., El-Rahaiby, S.K.**
AIchE. J., 31, 918 (1985)

a7) **El-Rahaiby, S.K., Rao, Y.K.**
Met. Trans. B, 13B, 633, (1982)

a8) **Kellog, H.H., Basu, S.K.**
Trans. AIME, 218, 70 (1960)

a9) **Schenck, R., Borkenstein, W.**
Z. anorg. chem., 142, 143 (1925)

a10) **Osawa, A., Shibata, N.**
Sci. repts., Tohoku Imp. Univer., Japan, 28, 1 (1939)

a11) **Henning, U., Pawlek, F.**
Z. Erz. Metall., 18, 293 (1965)